

EXPERIMENTAL AND NUMERICAL STUDIES ON REPLACEABLE LINKS
FOR ECCENTRICALLY BRACED FRAMES

A THESIS SUBMITTED TO
THE GRADUATE SCHOOL OF NATURAL AND APPLIED SCIENCES
OF
MIDDLE EAST TECHNICAL UNIVERSITY

BY

YASİN ONURALP ÖZKILIÇ

IN PARTIAL FULFILLMENT OF THE REQUIREMENTS
FOR
THE DEGREE OF DOCTOR OF PHILOSOPHY
IN
CIVIL ENGINEERING

SEPTEMBER 2020

Approval of the thesis:

**EXPERIMENTAL AND NUMERICAL STUDIES ON REPLACEABLE
LINKS FOR ECCENTRICALLY BRACED FRAMES**

submitted by **YASİN ONURALP ÖZKILIÇ** in partial fulfillment of the requirements for the degree of **Doctor of Philosophy in Civil Engineering, Middle East Technical University** by,

Prof. Dr. Halil Kalıpçılar
Dean, Graduate School of **Natural and Applied Sciences**

Prof. Dr. Ahmet Türier
Head of the Department, **Civil Engineering**

Prof. Dr. Cem Topkaya
Supervisor, **Civil Engineering**

Examining Committee Members:

Prof. Dr. Murat Altuğ Erberik
Civil Engineering, METU

Prof. Dr. Cem Topkaya
Civil Engineering, METU

Prof. Dr. Eray Baran
Civil Engineering, METU

Assoc. Prof. Dr. Alper Aldemir
Civil Engineering, Hacettepe University

Assist. Prof. Dr. Burcu Güldür Erkal
Civil Engineering, Hacettepe University

Date: 02.09.2020

I hereby declare that all information in this document has been obtained and presented in accordance with academic rules and ethical conduct. I also declare that, as required by these rules and conduct, I have fully cited and referenced all material and results that are not original to this work.

Name, Last name : Yasin Onuralp Özkılıç

Signature :

ABSTRACT

EXPERIMENTAL AND NUMERICAL STUDIES ON REPLACEABLE LINKS FOR ECCENTRICALLY BRACED FRAMES

Özkılıç, Yasin Onuralp
Doctor of Philosophy, Civil Engineering
Supervisor : Prof. Dr. Cem Topkaya

September 2020, 128 pages

Eccentrically braced frames (EBFs) are extensively used as a steel lateral load resisting systems in high seismic regions since EBFs simulate ductility and high energy absorption capacity of moment resisting frames (MRFs) and high stiffness of concentrically braced frames (CBFs). High stiffness and high ductility of EBFs are obtained from diagonal braces and yielding of link element, respectively. This thesis reports findings of a three phase experimental and numerical research program on replaceable links for EBFs.

The first research program was conducted to investigate four-bolt extended end-plate connections for replaceable shear links. Extended end-plate moment connections are used in a number of applications including the beam-to-column connections in seismic moment resisting frames (MRFs) and replaceable link-to-frame connections in eccentrically braced frames (EBFs). While the extended end-plate connections have been extensively studied for MRF applications, little is known about their performance in EBFs. The loading conditions and the acceptance criterion are different for the same connection when used in MRFs or EBFs. An experimental and numerical study has been undertaken to investigate the

performance of four-bolt extended unstiffened and stiffened end-plate connections used for replaceable shear links. Pursuant to this goal, 10 nearly full-scale EBF tests were conducted where the thickness, width and stiffening of the end-plate were considered as the variables. The results showed that the design recommendations given in AISC guidelines and Eurocode provisions provide conservative estimates of the end-plate thickness. Finite element simulations were conducted to investigate the bending strains for different plate thicknesses and to determine the sources of conservatism in the capacities determined using the design guidelines. Modifications to the AISC design guidelines were proposed to more accurately determine the required end-plate thickness.

The second research program was performed to develop novel detachable links for eccentrically braced frames. Post-earthquake replacement of links enables the use of eccentrically braced frames (EBFs) after a seismic event. Recent years have witnessed the development of numerous replaceable links. The extended end-plated replaceable links are the most efficient among the developed details. The use of these links enables to minimize the size and the weight of the part to be replaced. In addition, the performance of end-plated links is similar to the conventional links. Research reported to date showed that these links have disadvantages in terms of removal and replacement. Large axial forces can develop within the link member which may require using hydraulic jacks for the removal operation. More importantly is the difficulties associated with the link replacement under residual frame drifts. A novel detachable replaceable link is proposed in this study which employs a splice connection at the mid-length of the link. The splice connection consists of saw cut I-sections welded to both parts of the replaceable link. The detail provides an erection tolerance which facilitates easy removal and enables replacement under residual frame drifts. Proof-of-concept testing of the proposed links was performed on 3 specimens where the type of force transfer in the splice connection was considered as the prime variable. All specimens failed at link rotation angles that are significantly higher than the link rotation angle required by

AISC341 and demonstrated the potential of the proposed link concept. Complementary finite element parametric studies were conducted to validate the design procedure developed for the proposed replaceable link concept.

The third research program was carried out to enhance replaceable links by introducing frictional dampers. The main target was to extend the low-cycle fatigue life of the replaceable links by dissipating energy through the link yielding and frictional resistance provided faying surfaces of the side plates. Pursuant to this goal, brass shims were placed between saw cut I-sections and side plates which were drilled with slotted holes, and bearing type connection was utilized to promote bolt slippage. The proposed frictional mid-spliced connection was validated through a comprehensive experimental study. A total of eight specimens with proposed connection were tested considering slot size, the number of bolts and the number of slotted holes as the primary parameters. Moreover, three specimens with extended end plated connection were tested to compare low-cycle fatigue life with the link having the proposed mid-spliced connection. The link with proposed frictional mid-spliced connections exhibited significantly higher rotation capacity than the required link rotation. Furthermore, the link with the proposed connection excessively increased low-cycle fatigue life and energy dissipation capacity of links.

Keywords: Eccentrically Braced Frame, End Plate, Replaceable Link, Detachable, Residual Drift

ÖZ

DIŞMERKEZ ÇELİK ÇAPRAZLI PERDELERDE DEĞİŞTİRİLEBİLİR BAĞ KİRİŞLERİ İÇİN DENEYSEL VE NUMERİK ÇALIŞMALAR

Özkılıç, Yasin Onuralp
Doktora, İnşaat Mühendisliği
Tez Yöneticisi: Prof. Dr. Cem Topkaya

Eylül 2020, 128 sayfa

Dışmerkez çelik çaprazlı perdeler (DMÇÇP'ler) yüksek sismik bölgelerde çelik yatay yük direnç sistemi olarak yaygın olarak kullanılmaktadır, çünkü DMÇÇP'ler moment aktaran çerçevelerin (MAÇ'lerin) sünekliği ile yüksek enerji emme kapasitesini ve merkezi çaprazlı çerçevelerin (MÇÇ'lerin) yüksek rijitliğini simüle eder. DMÇÇP'lerin yüksek rijitliği ve sünekliği çaprazlardan ve bağ kiriş elemanının akmasıyla elde edilir. Bu tez DMÇÇP'lerde değiştirilebilir bağ kirişleri için üç aşamalı deneysel ve numerik çalışmaların bulgularını sunmaktadır.

Birinci araştırma programı değiştirilebilir kesme bağ kirişleri için dört bulonlu uzatılmış alın levhasını incelemek için gerçekleştirilmiştir. Uzatılmış alın plakalı moment bağlantıları, MAÇ'lerdeki kiriş-kolon bağlantıları ve DMÇÇP'lerdeki değiştirilebilir bağ kirişi-çerçeve bağlantıları dahil olmak üzere bir dizi uygulamada kullanılır. Uzatılmış alın levhalı bağlantılar MAÇ uygulamaları için kapsamlı bir şekilde incelenmiş olsa da, DMÇÇP'lerdeki performansları hakkında çok az şey bilinmektedir. MAÇ'lerde veya DMÇÇP 'lerde kullanıldığında aynı bağlantı için yükleme koşulları ve kabul kriteri farklıdır. Değiştirilebilir kesme bağ kirişleri için kullanılan dört bulonlu uzatılmış rijitlik levhalı ve rijitlik levhasız alın levhası

bağlantılarının performansını araştırmak için deneysel ve numerik bir çalışma yapılmıştır. Bu amaç doğrultusunda, alın levhasının kalınlığı, genişliği ve rijitlik levhası değişken olarak kabul edildiği 10 neredeyse tam ölçekli DMÇÇP testi yapılmıştır. Sonuçlar, AISC yönergelerinde ve Eurocode şartnamesinde verilen tasarım önerilerinin alın levhası kalınlığı için konservatif tahminler sağladığını göstermiştir. Farklı plaka kalınlıkları için bükülme gerinimleri araştırmak ve tasarım kılavuzları kullanılarak belirlenen kapasitelerde muhafazakârlığın kaynaklarını belirlemek için sonlu eleman simülasyonları yapılmıştır. Gerekli alın levhası kalınlığını daha doğru bir şekilde belirlemek için AISC tasarım kılavuzlarında değişiklikler önerilmiştir.

İkinci araştırma programı, DMÇÇP'ler için yeni değiştirilebilir bağ kirişleri geliştirmek için gerçekleştirilmiştir. Bağ kirişlerinin deprem sonrası değiştirilmesi, sismik bir olaydan sonra DMÇÇP'lerin kullanılmasını sağlar. Son yıllar çok sayıda değiştirilebilir bağ kirişlerinin gelişimine tanık olunmuştur. Uzatılmış alın levhalı değiştirilebilir bağ kirişler, geliştirilen detaylar arasında en verimli olanıdır. Bu bağ kirişlerinin kullanılması, değiştirilecek parçanın boyutunu ve ağırlığını en aza indirmeyi sağlar. Ek olarak, alın levhalı bağ kirişlerin performansı geleneksel bağ kirişlerin performansına benzerdir. Bugüne kadar raporlanan araştırmalar, bu bağ kirişlerinin çıkarılması ve değiştirilmesi açısından dezavantajları olduğunu göstermiştir. Bağ kiriş elemanın içinde, çıkarma işlemi için hidrolik krikoların kullanılmasını gerektirebilecek kadar büyük eksenel kuvvetler gelişebilir. Daha da önemlisi, artık ötelenme altında bağ kirişlerinin değiştirmesi ile ilgili zorluklardır. Bu çalışmada, bağ kirişinin orta uzunluğunda ayrılabilir bir ek bağlantısı kullanan yeni bir değiştirilebilir bağlantı önerilmiştir. Ek yeri bağlantısı, değiştirilebilir bağ kirişin her iki parçasına kaynaklanmış testere ile kesilmiş I kesitlerden oluşur. Detay, kolay sökülmeyle kolaylaştıran ve artık ötelenme altında değiştirmeyi sağlayan bir montaj toleransı sağlamaktadır. Önerilen bağ kirişlerinin kavram kanıt testi, ek bağlantısındaki kuvvet aktarım türünün ana değişken olarak kabul edildiği 3 numune üzerinde gerçekleştirilmiştir. Tüm numuneler, AISC341'in gerektirdiği

bağ kiriş dönme açısından önemli ölçüde daha yüksek olan bağ kiriş dönme açılarında göçmüştür ve önerilen bağ kiriş konseptinin potansiyelini göstermiştir. Önerilen değiştirilebilir bağ kiriş konsepti için geliştirilen tasarım prosedürünü doğrulamak için tamamlayıcı sonlu elemanlar parametrik çalışmaları yapılmıştır.

Üçüncü araştırma programı, sürtünmeli sönümleyiciler ekleyerek değiştirilebilir bağ kirişlerini geliştirmek için gerçekleştirilmiştir. Ana hedef, değiştirilebilir bağ kirişlerinin düşük çevrimsel yorulma ömrünü, bağ kirişinin akmasıyla ve yan plakaların yüzeylerinin sağladığı sürtünme direnci ile enerji sönümleyerek uzatmaktır. Bu amaç doğrultusunda, testere ile kesilmiş I-profiller ile oval delikler açılmış yan plakalar arasına pirinç levhalar yerleştirilmiş ve bulon kaymasını sağlamak için ezilme etkili bağlantı kullanılmıştır. Önerilen sürtünmeli orta ekli bağlantı, kapsamlı bir deneysel çalışma ile doğrulanmıştır. Ana parametreler olarak oval delik boyutu, bulon sayısı ve oval delik sayısı dikkate alınarak önerilen bağlantıya sahip toplam sekiz numune test edilmiştir. Ayrıca, düşük çevrimsel yorulma ömrünü önerilen orta ekli bağlantıya sahip bağ kirişleri ile karşılaştırmak için uzatılmış alın levhalı bağlantıya sahip üç numune test edilmiştir. Önerilen orta uçlu sürtünmeli bağlantılara sahip bağ kirişi, gerekli bağ kiriş dönme kapasitesinden önemli ölçüde daha yüksek dönme kapasitesi sergilemiştir. Ayrıca, önerilen bağlantıyla olan bağ kirişi, bağ kirişlerinin düşük çevrimsel yorulma ömrünü ve enerji dağıtma kapasitesini önemli derecede artırmıştır.

Anahtar Kelimeler: Dışmerkez Çelik Çarpazlı Perde, Alın Levhası, Değiştirilebilir Bağ Kirişi, Ayrılabilir, Artık Ötelenme

To My Family

ACKNOWLEDGMENTS

The author wishes to express his deepest gratitude to his supervisor Prof. Dr. Cem Topkaya for his guidance, advice, criticism, encouragements and insight throughout the research.

I would also like to express my thanks to Prof. Dr. Murat Altuğ Erberik, Prof. Dr. Eray Baran, Assoc. Prof. Dr. Alper Aldemir and Assist. Prof. Dr. Burcu Güldür Erkal for their valuable advice and constructive comments.

The author would like to thank Assist. Prof. Dr. Mehmet Bakır Bozkurt and Dr. Özer Zeybek for their contribution. The author would also like to thank Mr. Sina Kazemzadeh Azad who helped him with the numerical analyses. The technical staff of Mr. Salim Azak is gratefully acknowledged.

The author wishes to express his gratitude to Prof. Dr. Hakan Musa Arslan, Assoc. Prof. Dr. Lokman Gemi, Assist. Prof. Dr. Emrah Madenci and Dr. Ceyhun Aksoylu for their emotional support.

This study presented herein was made possible through the funds from the College of Engineering of the Middle East Technical University (BAP-03-03-2017-004 and GAP-303-2018-2858) and from the Scientific and Technological Research Council of Turkey (114M251).

Last but not least, I would like to thank my wife for always being there for me.

TABLE OF CONTENTS

ABSTRACT.....	v
ÖZ	viii
ACKNOWLEDGMENTS	xii
TABLE OF CONTENTS.....	xiii
LIST OF TABLES	xvi
LIST OF FIGURES	xvii
1 INTRODUCTION	1
1.1 Background of Eccentrically Braced Frames	1
1.2 Background of Replaceable Links	2
1.3 Objectives and Scope	8
1.4 Organization of Thesis	9
2 FOUR-BOLT EXTENDED END-PLATE CONNECTIONS FOR REPLACEABLE SHEAR LINKS	11
2.1 Background	11
2.2 Design Recommendations for End-Plate Moment Connections	13
2.2.1 The US Guidelines	13
2.2.2 The European Provisions	17
2.3 Experimental Program	20
2.3.1 Test Setup and Instrumentation	20
2.3.2 Details of Specimens	23
2.4 Experimental Results	27
2.5 Assessment of US Guidelines and European Provisions	32

2.6	Finite Element Studies.....	36
2.7	Proposed Modifications to AISC Guidelines	41
3	MID-SPLICED END-PLATED REPLACEABLE LINKS	47
3.1	Background.....	47
3.2	Mid-Spliced End-plated Replaceable Link Concept	48
3.3	Mid-Spliced End-plated Replaceable Link Concept	50
3.4	Proof-of-concept Testing of the Proposed Link Detail	54
3.4.1	Test Setup and Instrumentation	54
3.4.2	Test Specimens	55
3.4.3	Experimental Results	59
3.5	Numerical Study.....	66
3.5.1	Finite Element Modeling Details and Verification.....	67
3.5.2	Prediction of Design Axial Force	69
3.5.3	Stiffening of Saw Cut I-sections.....	70
3.5.4	Investigation of Larger Links	73
4	FRICTIONAL MID-SPLICED END-PLATED REPLACEABLE LINKS	77
4.1	Background.....	77
4.2	Frictional Mid-Spliced Link Concept and Design.....	78
4.3	Experimental Program.....	79
4.4	Experimental Results.....	85
5	SUMMARY AND CONCLUSIONS.....	109
5.1	Summary.....	109
5.2	Conclusions About Four-Bolt Extended End-Plate Connections for Replaceable Shear Links	109

5.3	Conclusions About Mid-Spliced End-Plated Replaceable Links	111
5.4	Conclusions About Frictional Mid-Spliced End-Plated Replaceable Links.	112
	REFERENCES	115
	CURRICULUM VITAE	123

LIST OF TABLES

TABLES

Table 2.1 Details of specimens.....	24
Table 2.2 Nominal and measured dimensions of IPE240 sections	25
Table 2.3 Material properties of the IPE240 sections	25
Table 2.4 Material properties of the end-plates.....	25
Table 2.5 Summary of experimental results.....	28
Table 2.6 Summary of experimental results.....	33
Table 2.7 Ratios of capacities and modes of failure for bolt rows according to European provisions	34
Table 3.1 Details of specimens.....	56
Table 3.2 Nominal and measured dimensions of IPE240 section	56
Table 3.3 Material properties of the IPE240 sections	59
Table 3.4 Summary of experimental results.....	60
Table 3.5 Properties of detachable links used to study behavior of larger links	75
Table 4.1 Nominal and measured dimensions of IPE240 sections	80
Table 4.2 Material properties of the IPE240 and HEA200 sections	80
Table 4.3 Material properties of the side plate	80
Table 4.4 Details of specimens and applied loading protocol.....	82
Table 4.5 Summary of experimental results of specimens LCF1-LCF3	87
Table 4.6 Summary of experimental results of specimens FR1-FR8.....	94
Table 4.7 Energy dissipated by specimens FR1-FR8.....	103

LIST OF FIGURES

FIGURES

Figure 1.1. EBF configurations (Kazemzadeh Azad and Topkaya, (2017)).....	1
Figure 1.2. EBFs applications (Engelhardt (2007))	2
Figure 1.3. (a) bolted flush end-plated, (b) bolted extended end-plated, (c) web connected, (d) bolted flange and web, (e) direct brace attachment, (f) gusset brace attachment replaceable link.....	5
Figure 1.4. Detachable replaceable link proposed by Bozkurt et al. (2019).....	8
Figure 2.1. Yield lines according to the AISC guideline and the parameters used in the end-plate design according to European provisions	14
Figure 2.2. T-Stub failure modes	18
Figure 2.3. Yield line patterns according to EN1993-1-8.....	19
Figure 2.4. Details of the test setup.....	21
Figure 2.5. Details of the instrumentation	22
Figure 2.6. Details of end-plated replaceable links.....	26
Figure 2.7. Deformation patterns of an unstiffened end-plate (Specimen 6).....	28
Figure 2.8. Deformation patterns of a stiffened end-plate (Specimen 10).....	28
Figure 2.9. Failure modes of specimens	29
Figure 2.10. Hysteretic responses of specimens 1 though 5	30
Figure 2.11. Hysteretic responses of specimens 6 though 10	31
Figure 2.12. A typical finite element mesh and plastic equivalent strain contours	37
Figure 2.13. A variation of strains along a path; (a) unstiffened end-plates, (b) stiffened end-plates	38
Figure 2.14. Strain versus link rotation angle response; (a) unstiffened end-plates, (b) stiffened end-plates.....	39
Figure 2.15. Normalized link shear versus link rotation angle response for end- plated with different widths	40
Figure 2.16. Variation of strains along a path for wide and narrow end-plates; (a) unstiffened end-plates, (b) stiffened end-plates	41

Figure 2.17. Finite element models of T-stubs.....	42
Figure 2.18. Load versus displacement response of t-stub models; (a) unstiffened T-stub, (b) stiffened T-stub.....	42
Figure 2.19. Proposed yield patterns	43
Figure 3.1. Detachable end-plated replaceable link	48
Figure 3.2. Isometric view of the proposed mid-splice detachable link.....	49
Figure 3.3. Variation stress resultants within the detachable link.....	51
Figure 3.4. Flowchart for design of bolted connections for side plates	52
Figure 3.5. Constructive details (minimum requirements).....	52
Figure 3.6. Stiffening detail for the mid-splice connection.....	53
Figure 3.7. Location of LVDTs.....	55
Figure 3.8. Details of Specimen 1	58
Figure 3.9. Details of Specimen 2	58
Figure 3.10. Details of Specimen 3	58
Figure 3.11. Hysteretic behavior of Specimen 1	61
Figure 3.12. Hysteretic behavior of Specimen 2	61
Figure 3.13. Hysteretic behavior of Specimen 3	61
Figure 3.14. Failure modes.....	62
Figure 3.15. Relative vertical movement between the two link pieces (Specimen 1)	64
Figure 3.16. Relative vertical movement between the two link pieces (Specimen 2)	64
Figure 3.17. Relative vertical movement between the two link pieces (Specimen 3)	65
Figure 3.18. Energy dissipation of specimens.....	65
Figure 3.19. In-plane rotation of side plates (Specimen 2)	65
Figure 3.20. Deformation of saw cut I-sections (Specimen 2).....	66
Figure 3.21. Mesh configurations.....	67
Figure 3.22. Axial force developed in the proposed detachable link	70

Figure 3.23. Location of the path for recording maximum principal strain variations	71
Figure 3.24. Strain variation along a path (IPE240 links)	72
Figure 3.25. Strain variation along a path (HEB300 links)	72
Figure 3.26. Strain variation along a path (HEA500 links)	72
Figure 3.27. Rupture index for experimented specimens	74
Figure 3.28. Rupture index for HEA500 links.....	76
Figure 4.1. Proposed frictional mid-spliced replaceable link concept.....	79
Figure 4.2. Technical drawings of specimens LCF1-LCF3.....	83
Figure 4.3. Technical drawings of specimens FR1 and FR2	83
Figure 4.4. Technical drawings of specimens FR3 and FR4	84
Figure 4.5. Technical drawings of specimens FR5	84
Figure 4.6. Technical drawings of specimens FR6.....	84
Figure 4.7. Technical drawings of specimens FR7	85
Figure 4.8. Technical drawings of specimens FR8.....	85
Figure 4.9. Hysteretic response of specimens LCF1-LCF3.....	88
Figure 4.10. Failure modes of specimens LCF1-LCF3	89
Figure 4.11. Hysteretic response of specimens FR1-FR4.....	91
Figure 4.12. Hysteretic response of specimens FR5-FR8.....	92
Figure 4.13. Failure modes of specimens	93
Figure 4.14. Abrasive and adhesive wear	95
Figure 4.15. Damages on washers	96
Figure 4.16. Bolt hole elongation	97
Figure 4.17. Relative vertical movement of specimens FR1-FR4.....	99
Figure 4.18. Relative vertical movement of specimens FR5-FR8.....	100
Figure 4.19. Link shear vs effective link rotation of specimens FR1-FR4.....	101
Figure 4.20. Link shear vs effective link rotation of specimens FR5-FR8.....	102
Figure 4.21. The comparison of normalized energy dissipation.....	104
Figure 4.22. Energy dissipation of specimens FR1 and FR3.....	105
Figure 4.23. The comparison of energy dissipation of specimens FR5-FR8.....	106

Figure 4.24. The comparison of energy dissipation of specimens FR2, FR4-FR6107

CHAPTER 1

INTRODUCTION

1.1 Background of Eccentrically Braced Frames

Eccentrically braced frames (EBFs) combine the advantages of moment resisting frames (MRFs) and concentrically braced frames (CBFs) to form a structural system with high elastic stiffness as well as high energy dissipation. In EBFs, links are the primary source of energy dissipation and the beam outside the link, braces and columns are designed to remain elastic during a seismic event. The most common EBFs configurations are given in Figure 1.1.

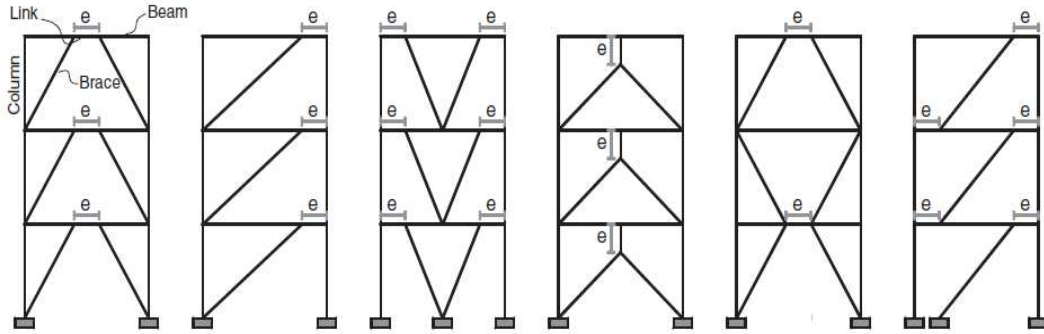


Figure 1.1. EBF configurations (Kazemzadeh Azad and Topkaya, (2017))

The link length ratio ($\rho = e/(M_p/V_p)$) is the single most important parameter that influences the behavior of links where e is the link length, and M_p and V_p are the plastic moment and plastic shear capacities of the link, respectively. The link is categorized into three categories according to the link length ratio as: short link ($\rho \leq 1.6$), intermediate link ($1.6 \leq \rho \leq 2.6$) and long link ($\rho \geq 2.6$). The links which yield under shear are called short (shear) links, the links which yield under flexure are called long (flexure) links and the links which yield under both shear and flexure are called intermediate links. Short shear yielding links are generally

preferred in practice due to their superior energy dissipation (Kazemzadeh Azad and Topkaya, (2017)).

Studies on EBFs have started in Japan in 1970s (Fujimoto et al., (1972)). EBFs are mostly used in Japan, the USA and New Zealand, and some examples of the applications are shown in Figure 1.2. Contrary to CBFs, EBFs show symmetric and stable hysteresis loops which result in high energy dissipation capacity. Therefore, EBFs are preferred in high seismic zones.



Figure 1.2. EBFs applications (Engelhardt (2007))

1.2 Background of Replaceable Links

Traditionally, the links and the beam outside of the link are designed as a continuous member having the same cross-section. This approach has two major drawbacks. First, the capacity design of the beam outside of the link is directly influenced by the forces developed in the link. A change in the size of the beam outside of the link results in a change in the link size. Second, the post-earthquake repair or replacement of the link is an onerous process if the link and the beam outside of the link are from a continuous member.

The 2010-2011 series of Christchurch earthquakes in New Zealand resulted in yielding and fracture of links in EBFs which had to be replaced with new ones (Gardiner et al. (2013)). The consequences of these earthquakes showed that the

seismic performance of the EBFs was better than expected despite developing a few link fractures (Clifton et al. (2011), Clifton et al. (2012), Gardiner et al. (2013), Macrae et al. (2011)). In order to open and reoccupy the damaged buildings, yielded or fractured links need to be replaced with the new ones. For the last fifteen years, researchers have focused on developing links that are easy to replace and fulfill the minimum link rotation capacity specified by AISC 341 (2016). The end-plated replaceable link, which is shown in Figure 1.3.a, is the first developed detail where end-plates are flush with both collector beam and link (Stratan and Dubina (2004), Stratan et al. (2003), Dubina et al. (2008), Sabau et al. (2014), Ioan et al. (2016), Dubina et al. (2011)). Although the seismic performance of the flush end-plated replaceable links was sufficient in terms of link rotation capacity, pinched cyclic response was obtained compared to conventional links due to bolt thread stripping and bending of the end-plate which led to an increase in the interstory drift of the frame and inelastic deformation demands of the link (Stratan and Dubina (2004), Stratan et al. (2003), Dubina et al. (2008), Sabau et al. (2014), Ioan et al. (2016), Dubina et al. (2011)). A dual lateral load resisting system where EBFs were utilized alongside high-strength MRFs was proposed to reduce the amount of residual drifts (Dubina et al. (2008), Sabau et al. (2014), Ioan et al. (2016), Dubina et al. (2011)). A three-story dual system with a story height of 3.5 m and a bay width of 6 m was erected in European Laboratory for Structural Assessment (ELSA) and subjected to pseudo-dynamic tests, monotonic and cyclic pushover test. After each test the residual drifts were measured and the links were removed by flame cutting, which was required due to residual stress and excessive deformation developed in the link. The residual drifts of 0.09% and 0.15% were respectively reported under the damage limitation and significant damage performance levels, which indicates re-centering capability of the dual system. Shi et al. (2020) performed experimental studies on the replaceable links with flush end-plate connection and compared these replaceable links with the traditional link with welded connection. The results revealed that the shear capacity of the replaceable link with flush end-plate connection was 24.8% lower than that of the

traditional link with welded connection while inelastic rotation capacity of the replaceable link with flush end-plate connection was 24.4% higher than that of the traditional link with welded connection. According to the numerical study conducted by Zimbru et al. (2017), the effects of different types of high strength bolts and the pretension level are limited on the behavior of the detachable link with flush end-plates. Zimbru et al. (2018) conducted a study on the replaceable links having flush end-plate connection with a continuous slab. The results revealed that the connection design of the replaceable link is not influenced by the slab since internal forces in the links with continuous slab are similar to the all-steel link without a slab.

It is recommended to limit the link length ratio with $\rho < 0.8$ to have improved behavior for the link with flush end-plate connection (Dubina et al. (2008)). In order to circumvent undesired behavior of the flush end-plate connection, the extended end-plate connection (Figure 1.3.b) based on using I-shaped steel section with a lower depth than the collector beams was proposed for the replaceable links by Mansour (2010) and Mansour et al. (2011). The bolted extended end-plated replaceable link performs similar to a conventional link and an additional limit on the link length ratio is not required. This connection detail provides a decrease in the shear and flexural demand of the link which in turn results in reducing the axial and shear force at the bolts and end-plates in the connection region. According to the test results, the extended end-plated replaceable links showed a stable cyclic hysteretic response up to 0.104 rad inelastic link rotation angle. Very short bolted extended end-plated replaceable links were also tested by Ji et al. (2016) for use as coupling beams in reinforced concrete coupled wall systems. Stephens et al. (2018) conducted experimental and numerical studies in order to improve the replaceable links with extended end-plate connection by providing additional end stiffeners that are parallel to the web. These stiffeners were placed to prevent weld fractures between the end-plate and the link by shifting strains from the connection.

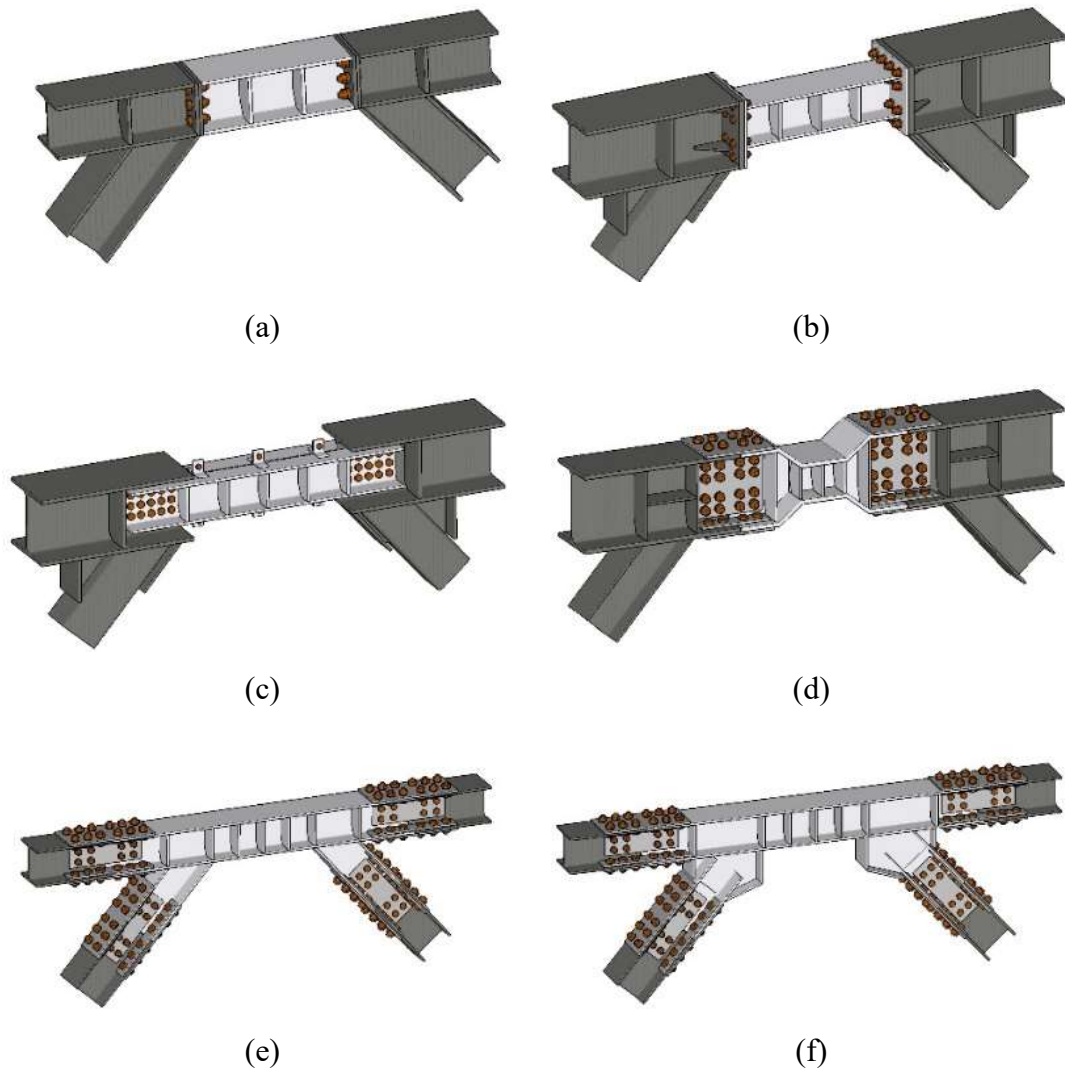


Figure 1.3. (a) bolted flush end-plated, (b) bolted extended end-plated, (c) web connected, (d) bolted flange and web, (e) direct brace attachment, (f) gusset brace attachment replaceable link

In addition to the extended end-plate connections, the bolted or welded web connections were proposed by Mansour (2010) and Mansour et al. (2011) (Figure 1.3.c). Due to localized bearing deformation around the bolt holes, pinched seismic response was obtained for the links with web connection. In order to control the bolt bearing stress, web reinforcement plates welded around the connection region were proposed. While the extended end-plated replaceable links were not tested under the residual drift, those with web connections were tested by applying the

site drilling method under 0.5% residual drift. The web-connected replaceable links were also experimentally and numerically studied by Yin et al. (2019). The performance of the links was evaluated in terms of energy dissipation capacity, stiffness degradation and angle of rotation.

As indicated in Figure 1.3.d, an innovative link detail with bolted flange and web splicing for the replaceable link was first proposed by Mansour (2010) and then examined numerically by Ashikov et al. (2016) and experimentally by Ashikov et al. (2017). Experimental results indicate that the proposed link detail is able to sustain link rotation angle of 0.063 rad which corresponds “damage limitation requirement” where the maximum frame inter-story drift is 1.5% of the frame height.

As shown in Figure 1.3.e and Figure 1.3.f, new type of replaceable links with directly connected braces (Bozkurt and Topkaya (2017), Bozkurt (2017)) and gusseted brace attachments (Bozkurt and Topkaya (2018), Bozkurt (2017)) where the splicing was employed outside of the links were investigated in Structural Mechanics Laboratory at Middle East Technical University (SML-METU). As opposed to the end-plated replaceable links, the replaceable links proposed by Bozkurt and Topkaya (2017), Bozkurt (2017), Bozkurt and Topkaya (2018) do not require the use of flame cutting for removal of the damaged links and hydraulic jack for the erection of the new ones as the splice connection provides a certain amount of gap between the connected members. According to the experimental results, both the replaceable links with directly connected brace attachments and those with gusseted brace attachments exhibit a cyclic response similar to one for conventional links.

The other challenge in the replacement process is the erection of the new links under the residual drifts that occur after the earthquake. In the end-plated connections, residual drifts were reduced by 0.15% by using a dual system (Dubina et al. (2008), Sabau et al. (2014), Ioan et al. (2016), Dubina et al. (2011)) that is lower than the construction tolerance of 0.20% recommended by AISC 360 (2010)

and EN 1090-2 (2012). The current practice requires creating a template after removal of the damaged link and manufacturing the new link accordingly (Gardiner et al. (2013)). The web-connected replaceable links, proposed by Mansour et al. (2011), were installed and tested under a residual drift of 0.5% which is the permissible limit from architectural functionality, headache and dizziness standpoint (McCormick et al. (2008)). However, the cyclic hysteretic response of these replaceable links was not as stable as the conventional links.

After the experimental studies (Bozkurt and Topkaya (2017), Bozkurt (2017), Bozkurt and Topkaya (2018)) on the replaceable links conducted at SML-METU, a research program including experimental and numerical studies have been carried out on the detachable link details that can be easily removed and reinstalled under residual drift. The replaceable link is spliced at its mid-length where end-plate connection is employed so that each separate piece can be connected to each other under a certain amount of residual drift. As shown in Figure 1.4, the standard end-plated mid-splice connection was tested under no residual drift whereas slotted and site drilled ones were tested under a residual drift of 0.5%. On the other hand, welded end-plated mid-splice connection was also tested under a residual drift of 0.7%. Moreover, finite element analyses were conducted to further validate the applicability of the proposed detachable link. Numerical and experimental studies indicated that the inelastic rotation capacity of all the specimens satisfies the requirements mandated by AISC 341 (2016), which exhibits potential use of the detachable links proposed by Bozkurt et al. (2019).

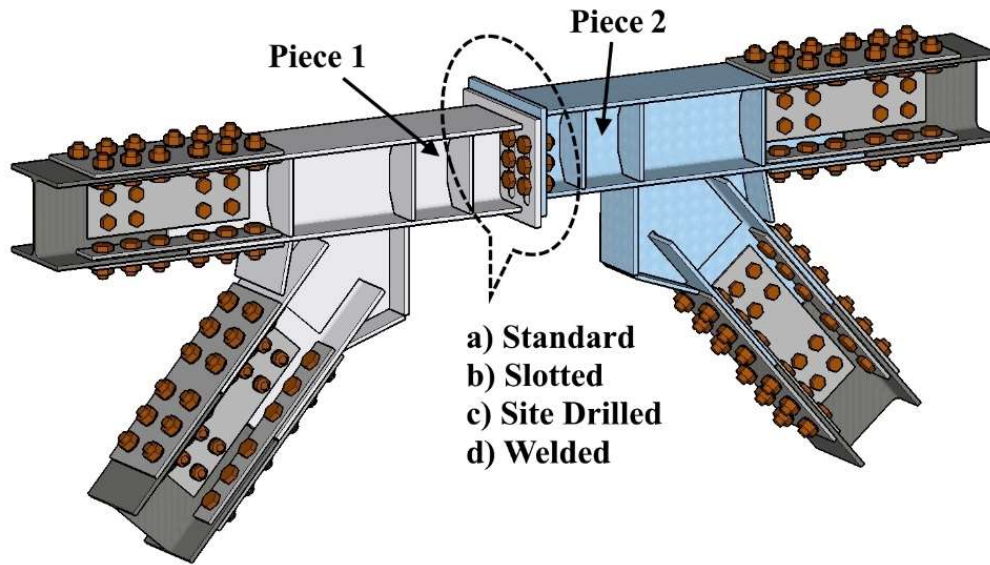


Figure 1.4. Detachable replaceable link proposed by Bozkurt et al. (2019)

1.3 Objectives and Scope

Three research programs including experimental and numerical studies on EBFs were undertaken separately in order to improve the behavior of the replaceable links.

The aim of the first research program was to examine the performance of four-bolt extended unstiffened and stiffened end-plate connections used for replaceable shear links and improve the design guidelines. Experimental and numerical studies were performed by taking into account the thickness, width and stiffening of the end-plate as the prime variables. The main target of this research program was to reduce the weight of the replaceable link by using the lightest end-plate possible.

The aim of the second research program was to develop a mid-spliced end-plated replaceable links that facilitate the replacement of the damaged links. The proposed replaceable link is designed to be also replaced under residual drift. For

experimental part the standard hole and slotted hole slip-critical and site drilled standard hole bearing type connections were considered as the variables while for numerical part different bolt configurations, the size of the links and the stiffening of the connected plate were selected as the main parameters. The main target of this research program was to extend the proposed detachable links by Bozkurt et al. (2019) to end-plated replaceable links such that these links can also be installed under residual frame drifts.

The aim of the third research program was to improve the mid-spliced end-plated replaceable links which are proposed in Chapter 3 by introducing a frictional energy dissipation mechanism. Eleven specimens were tested by taking into account slot size and the number of bolts as the primary variables. The main target of this research program was to extend the low-cycle fatigue life of mid-spliced replaceable links by dissipating energy through the link yielding and frictional resistance provided faying surfaces of the side plates.

1.4 Organization of Thesis

This thesis consists of four chapters which follow the introduction. The brief contents of these chapters can be summarized as follows:

In Chapter 2, the performance of four-bolt extended unstiffened and stiffened end-plate connections used for replaceable shear links are investigated. The experimental results of ten specimens are given. The results are compared with the design recommendations given in AISC guidelines and Eurocode provisions. The results of finite element simulations are provided to investigate the bending strains for different plate thicknesses and to determine the sources of conservatism in the capacities determined using the design guidelines. Modifications to the AISC design guidelines are proposed to more accurately determine the required end-plate thickness.

In Chapter 3, mid-spliced end-plated replaceable links are developed. The design guide for the proposed replaceable link is provided. The proposed links are verified with both experimental and numerical studies. The experimental results of three test specimens are presented in terms of hysteresis behavior, shear capacity and angle of rotation. The numerical results of the links with different bolt configurations and different link sections are compared in terms of rupture index.

In Chapter 4, the mid-spliced end-plated links that dissipate energy through friction are developed. The cyclic performance of the proposed links is provided. The low-cycle performance of the proposed links is compared with that of conventional links. The effects of the slot size and number of bolts on the behavior of the replaceable links are also presented.

Finally, Chapter 5 summarizes the outcomes of all studies performed during the course of these three research programs and offers recommendations for future research.

CHAPTER 2

FOUR-BOLT EXTENDED END-PLATE CONNECTIONS FOR REPLACEABLE SHEAR LINKS

2.1 Background

The sizing of end-plate is an important step in design of replaceable links. The end-plate and the bolts should be designed to safely transmit the forces produced in the link to the adjoining members. More importantly is that the weight of the parts to be transported and erected has a significant influence on the ease of replacement process. In conventional construction, the increase in the weight of an end-plate does not adversely affect the hoisting and maneuver of steel members. On the other hand, weight becomes the primary factor for replaceable steel members due to the constraints in the hoisting and maneuver inside existing structures. For this reason, the size of the end-plate, which determines the total weight of the part to be replaced, should be minimized to come up with weight optimized designs and facilitate the replacement process.

End-plated connections can be used in a number of applications such as beam-to-column connections or beam-to-beam connections. Research to date has mostly focused on the performance of these connections where bending was the dominant action. When used in beam-to-column connections, different design philosophies can be adopted for seismic and non-seismic applications. In the case of seismic design, the end-plate can be designed to remain essentially elastic or dissipate energy through yielding. Widely used guidelines (AISC 358) or specifications (EN 1993-1-8) can be adopted for the sizing of the end-plate connection. It should be noted that there are marked differences in the approaches given in these documents as explained in the following sections.

The end-plated beam-to-column connections for seismic applications have been extensively studied in the past (Ghobarah et al. (1992), Sumner and Murray (2002), Tsai and Popov (1990), Bu et al. (2019), ElSabbagh et al. (2019), Morrison et al. (2019), Tartaglia et al. (2018a, 2018b, 2019), Zhu et al. (2019)). On the other hand, little is known about the performance of these connections when used in replaceable shear links. The behaviors and the acceptance criterion are different for the two cases. In beam-to-column connections, the primary action is bending whereas in replaceable link connections the primary action is bending and shear. The beam-to-column connections are expected to satisfy a certain level of story drift angle when tested under the qualifying test protocol (AISC 341 (2016)). On the other hand, the EBF links should satisfy a certain level of link rotation angle when tested under a different test protocol (AISC 341 (2016)). Furthermore, parametric limitations are imposed on prequalified end-plated moment connections (AISC 358 (2016)) which were developed based on the experiments conducted to date. The size of replaceable links is smaller when compared with conventional beams used in MRF applications. Therefore, the end-plated connections for replaceable shear links have geometrical parameters that are not within the limitations given in AISC 358.

A combined experimental and numerical study has been undertaken to investigate the behavior of end-plated connections in replaceable EBF links. In this paper, the US and European design practices for the sizing of end-plates are reviewed. The details of the experimental study on 10 nearly full-scale EBFs are explained. The test results are evaluated in terms of the design recommendations provided in the US guidelines and European provisions. The test specimens are analyzed using the finite element method to investigate the bending strains developed in end-plate. Modifications to the US guidelines are developed based on finite element analysis of T-stub models.

2.2 Design Recommendations for End-Plate Moment Connections

2.2.1 The US Guidelines

In the US, Design Guide 16: Flush and Extended Multiple-Row Moment End-Plate Connections (2002), hereafter referred as DG16, provides guidelines for end-plated connections. The strength of the end-plate is calculated using assumed yield line mechanisms. Two types of end-plate behavior are defined which are named as “thick” and “thin” (Kennedy et al. (1981), Srouji et al. (1983), and Borgsmiller (1995)). In the “thin” end plate approach the full strength of the end-plate is utilized. In the “thick” end-plate design approach, 90% of the end-plate strength is used which is implemented by increasing the applied bending moment by 11%. This results in an increase of only 5% in the thickness of the end-plate. The “thin” end-plates result in prying forces to be developed which in turn results in an increase in the bolt size. In short, the “thick” end-plate design approach results in slightly thicker end-plates while the “thin” end-plate approach results in slightly larger bolt diameters.

Design Guide 04: Extended End-Plate Moment Connections - Seismic and Wind Applications (2003) forms the basis of the current AISC 358-16: Prequalified Connections for Special and Intermediate Steel Moment Frames for Seismic Applications (2016). Three end-plate moment connections namely, four-bolt unstiffened (4E), four-bolt stiffened (4ES), and eight-bolt stiffened (8ES), are recommended in the AISC 358-16 which all depend on “thick” end-plate design approach. In other words, the AISC358-16 allows for only “thick” end-plate connections to be used in seismic applications. As explained in the previous section, “thin” end-plates can be preferred for replaceable members and their use in seismic applications should be explored.

For “thin” end-plates, DG16 provides a step-by-step design procedure which is briefly explained in this section. First, the required end plate thickness ($t_{p,reqd}$) is determined as follows:

$$t_{p,reqd} = \sqrt{\frac{M_u}{\phi_b F_{py} Y}} \quad (2.1)$$

where M_u is the required flexural strength, F_{py} is yield strength of end-plate, $\phi_b = 0.9$, Y is the yield-line mechanism parameter. Yield line mechanisms for four-bolt unstiffened and stiffened extended end-plates are shown in Figure 2.1.

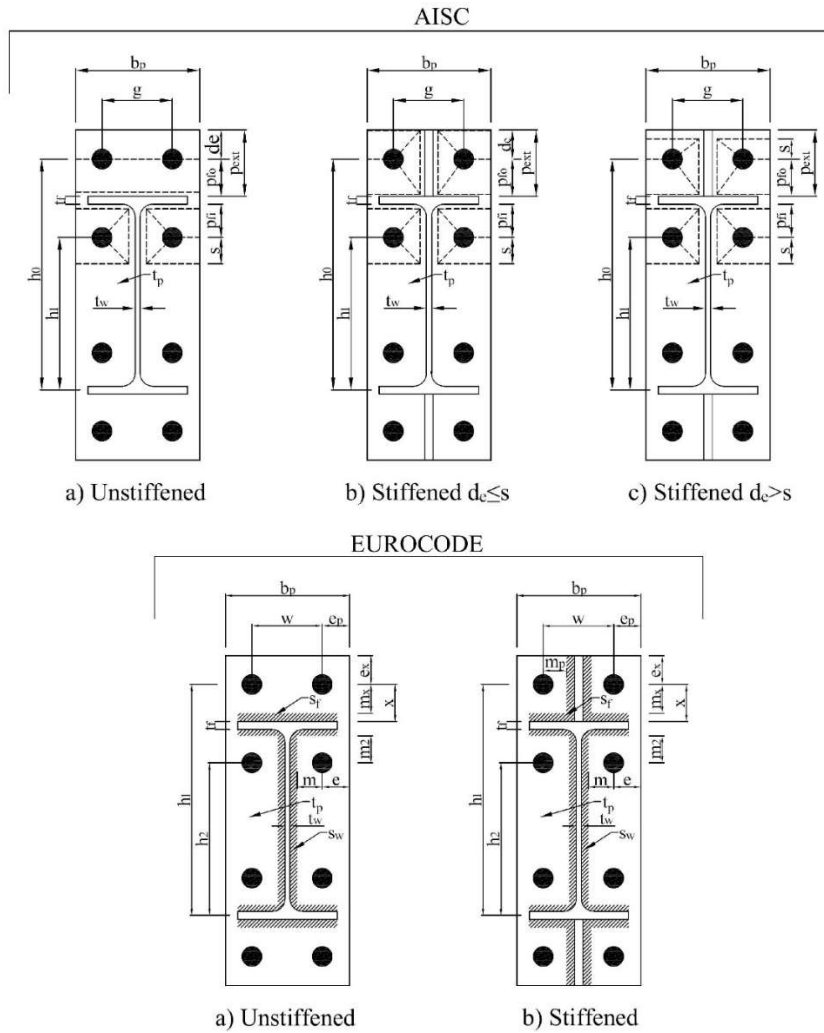


Figure 2.1. Yield lines according to the AISC guideline and the parameters used in the end-plate design according to European provisions

The calculations of the yield line mechanism parameter, Y , are given as follows:

For unstiffened case (Figure 2.1.a):

$$Y = \frac{b_p}{2} \left[h_1 \left(\frac{1}{p_{fi}} + \frac{1}{s} \right) + h_0 \left(\frac{1}{p_{fo}} \right) - \frac{1}{2} \right] + \frac{2}{g} [h_1 (p_{fi} + s)] \quad (2.2)$$

For stiffened case when $d_e \leq s$ (Figure 2.1.b):

$$Y = \frac{b_p}{2} \left[h_1 \left(\frac{1}{p_{fi}} + \frac{1}{s} \right) + h_0 \left(\frac{1}{p_{fo}} + \frac{1}{2s} \right) \right] + \frac{2}{g} [h_1 (p_{fi} + s) + h_0 (p_{fo} + d_e)] \quad (2.3)$$

For stiffened case when $d_e > s$ (Figure 2.1.c) :

$$Y = \frac{b_p}{2} \left[h_1 \left(\frac{1}{p_{fi}} + \frac{1}{s} \right) + h_0 \left(\frac{1}{p_{fo}} + \frac{1}{s} \right) \right] + \frac{2}{g} [h_1 (p_{fi} + s) + h_0 (p_{fo} + s)] \quad (2.4)$$

where h_0 is the distance from the centerline of the compression flange to the tension side outer bolt row, h_1 is the distance from the centerline of the compression flange to the tension side inner bolt row, b_p is width of end plate (shall not be taken greater than the beam flange width plus 25.4 mm in the calculations), p_{fi} is the vertical distance from inside of a beam tension flange to nearest inside bolt row, p_{fo} is the vertical distance from inside of a beam tension flange to nearest outside bolt row, g is the horizontal distance between the bolts, d_e is the vertical edge distance for outside holes and

$$s = \frac{1}{2} \sqrt{b_p g} \quad (2.5)$$

After the required plate thickness is calculated, a trial bolt diameter is selected. According to the selected bolt diameter, maximum prying forces are calculated from the following equations. Maximum possible bolt prying force in tension bolts inside, $Q_{max,i}$:

$$Q_{\max,i} = \frac{w't_p^2}{4a_i} \sqrt{F_{yp}^2 - 3 \left(\frac{F_i^2}{w't_p} \right)^2} \quad (2.6)$$

Maximum possible bolt prying force in tension bolts outside, $Q_{\max,o}$:

$$Q_{\max,o} = \frac{w't_p^2}{4a_o} \sqrt{F_{yp}^2 - 3 \left(\frac{F_o^2}{w't_p} \right)^2} \quad (2.7)$$

Where

$$w' = \frac{b_p}{2} - (d_b + 2) \quad a_i = 25.4 \left(3.682 \left(\frac{t_p}{d_b} \right)^3 - 0.085 \right) \quad a_o = \min(a_i; p_{ext} - p_{fo}) \quad (2.8)$$

$$F_i' = \frac{t_p^2 F_{yp}^2 \left(0.85 \frac{b_p}{2} + 0.80 w' \right) + \frac{\pi d_b^3 F_t}{8}}{4 p_{fi}} \quad F_o' = F_i' \left(\frac{p_{fi}}{p_{fo}} \right) \quad (2.9)$$

where t_p is thickness of end-plate, d_b is the bolt diameter, F_t is nominal tensile strength of bolts, a_i is distance from the interior bolt centerline to the prying force, a_o is distance from the outer bolt centerline to the prying force, F_i' and F_o' are flange forces per bolt at the thin plate limit when calculating Q_{\max} for end-plate configurations with large inner pitch distances. If the quantity inside the radical of Q_{\max} is calculated as negative, it means that end plate is controlled by combined flexural and shear yielding limit states and thickness of end plate is not adequate for the specified moment. The connection design strength for limit state of bolt rupture with prying action is calculated as follows:

$$M_q = \max \left[\begin{array}{l} 2(P_t - Q_{\max,o})h_0 + 2(P_t - Q_{\max,i})h_1 \\ 2(P_t - Q_{\max,o})h_0 + 2(T_b)h_1 \\ 2(P_t - Q_{\max,i})h_1 + 2(T_b)h_0 \\ 2(T_b)(h_0 + h_1) \end{array} \right] \quad (2.10)$$

where P_t is the bolt tensile strength, T_b is bolt pretension force specified in Table J3.1 of AISC360-16, M_q is nominal connection strength for the limit state of bolt fracture with prying action and

$$P_t = \frac{\pi d_b^2 F_t}{4} \quad (2.11)$$

Finally, the required moment should be compared with the design moment. The bolt diameter should be changed until the inequality of $\phi M_q > M_u$ is satisfied. If the design is controlled by bolt rupture, ϕ should be taken as 0.75 and if the design is controlled by end plate yielding, then ϕ should be taken as 0.9.

2.2.2 The European Provisions

In Europe the beam-to-column connection design provisions for seismic applications are given in EN1998-1 (2004) where dissipative semi-rigid and/or partial strength connections are permitted to be used for MRFs. The provisions of EN1993-1-8 (2003) are used to design joints of steel structures. The methods presented in EN1993-1-8 are quite general and can be applied to many different types of connections. In general, the component method is adopted in EN 1993-1-8 where strengths of individual joint components are taken into account. In bolted end-plate connections, the main source of deformability is the tension zone which can be idealized by means of equivalent T-stubs. Unlike AISC guidelines, the European provisions do not distinguish between “thick” and “thin” end-plates but rather use the same design procedure regardless of the thickness of the end-plate. Three T-stub failure modes are defined: complete flange yielding, bolt failure plus flange yielding and bolt failure as demonstrated in Figure 2.2. Multiple yield line patterns depending on the geometry of the end-plate are considered in EN1993-1-8. The detailed design procedure for end-plate moment connections can be found in the Green Book P398 (2013) and the required steps are summarized here.

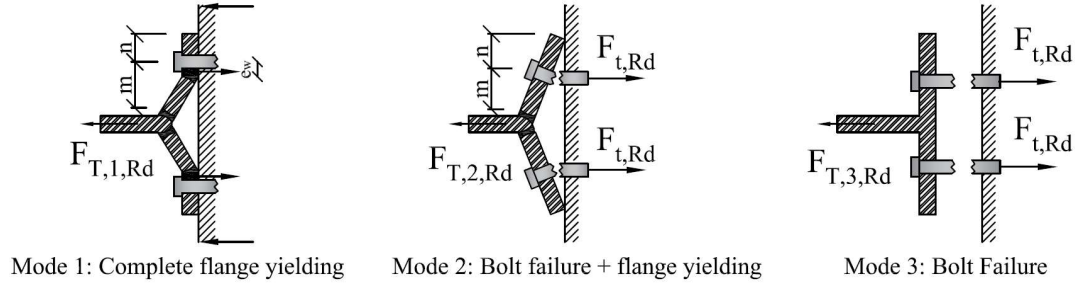


Figure 2.2. T-Stub failure modes

The EN1993-1-8 design method for an end-plate connection is an iterative procedure. First, the thickness of end-plate and diameter of bolts are selected along with configuration of bolts. After the selection, design resistance of bolt rows in tension are calculated separately. For each bolt row, effective lengths of equivalent T-stubs are determined according to yield line patterns given in EN1993-1-8. The minimum of the T-stub failure modes is taken as the design resistance of end-plate using the shortest yield line pattern which gives minimum strength. These three failure modes are calculated for each bolt row as follows:

For Failure Mode 1 two methods (Method 1 and Method 2) can be adopted as follows:

$$F_{T,1Rd} = \frac{4M_{p,1Rd}}{m} \quad \text{for Method 1} \quad (2.12)$$

$$F_{T,1Rd} = \frac{(8n - 2e_w)M_{p,1Rd}}{2mn - e_w(m + n)} \quad \text{for Method 2} \quad (2.13)$$

Where

$$e_w = d_w / 4 \quad n = \min(e_x; 1.25m) \quad M_{p,1Rd} = 0.25l_{eff,1}t_p^2F_{yp} \quad (2.14)$$

where d_w is diameter of washer, t_p is thickness of end plate, e_x is the vertical edge distance for outside holes, m is the distance from the center of a bolt to fillet weld of rolled section as shown in Figure 2.1. $l_{eff,1}$ is minimum of $l_{eff,cp}$ which is the length of the circular yield line pattern and $l_{eff,nc}$ which is the length of the non-

circular yield line pattern. $l_{eff,cp}$ and $l_{eff,nc}$ are defined differently depending on the position of bolt row and availability of the stiffener. Figure 2.3 shows the yield line patterns for bolt rows: bolts in an unstiffened end-plate extension (Figure 2.3.a), bolts on a stiffened end-plate extension (Figure 2.3.b), and bolts in end-plate below the beam flange (Figure 2.3.c).

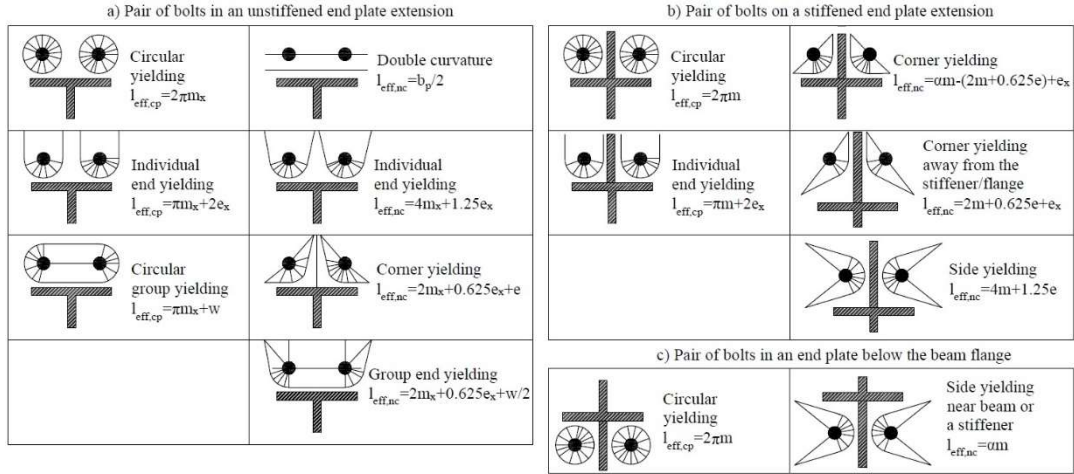


Figure 2.3. Yield line patterns according to EN1993-1-8

For Failure Mode 2:

$$F_{T,2Rd} = \frac{2M_{p,2Rd} + n2F_{t,Rd}}{m + n} \quad (2.15)$$

Where

$$F_{t,Rd} = \frac{k_2 f_{ub} A_s}{\gamma_{M2}} \quad M_{p,2Rd} = 0.25 l_{eff,2} t_p^2 F_{yp} \quad (2.16)$$

where k_2 is taken as 0.9, γ_{M2} is taken as 1.25, A_s is tensile stress area of a bolt, f_{ub} is the nominal ultimate strength of bolt, $l_{eff,2}$ is minimum of $l_{eff,nc}$.

For Failure Mode 3:

$$F_{T,3Rd} = 2F_{t,Rd} \quad (2.17)$$

The minimum of these three failure modes is taken as the resistance of bolt row which should be calculated separately for each bolt row.

Resistance of bolt row 1 (bolt row above the top flange):

$$F_{t1,Rd} = \min(F_{T,1Rd}; F_{T,2Rd}; F_{T,3Rd}) \quad (2.18)$$

Resistance of bolt row 2 (bolt row below the top flange):

$$F_{t2,Rd} = \min(F_{T,1Rd}; F_{T,2Rd}; F_{T,3Rd}) \quad (2.19)$$

After calculating the design resistance of bolt rows, the design moment is calculated as follows:

$$M_{j,Rd} = h_r F_{tr,Rd} = h_1 F_{t1,Rd} + h_2 F_{t2,Rd} \quad (2.20)$$

where h_1 is the distance from the centerline of the compression flange to the tension side outer bolt row, h_2 is the distance from the centerline of the compression flange to the tension side inner bolt row. Finally, after calculating connection design moment, required moment should be compared with the design moment. The bolt diameter and thickness of end-plate should be changed until the inequality of $M_{j,Rd} > M_u$ is satisfied.

2.3 Experimental Program

2.3.1 Test Setup and Instrumentation

The test setup designed by Bozkurt and Topkaya (2017) was used for testing of end-plated replaceable links. As shown in Figure 2.4 the test setup consists of loading and base beams from HEA300 sections and two pin ended columns from HEA400 sections. A 1500 kN capacity hydraulic actuator which was attached to a strong wall was used to apply lateral loading. The test setup simulates a nearly full scale one-story one-bay EBF where the bay width is 5 meters and the distance

between the column pin supports is 2.7 meters. The applied force from the actuator was distributed almost uniformly to the columns with the help of a loading beam. Beams and braces were connected to columns using moment connections. The moment connections were used to distribute the moment on the link to both braces and beam. On the other hand, columns were attached to base beam and loading beam using pin connections. The EBF was tested in a V-configuration in order to facilitate the replacement procedure, monitoring, and lateral bracing of links. The out-of-plane displacements of the loading beam, columns, and link ends were controlled using the lateral restraining system and lateral braces shown in Figure 2.4.

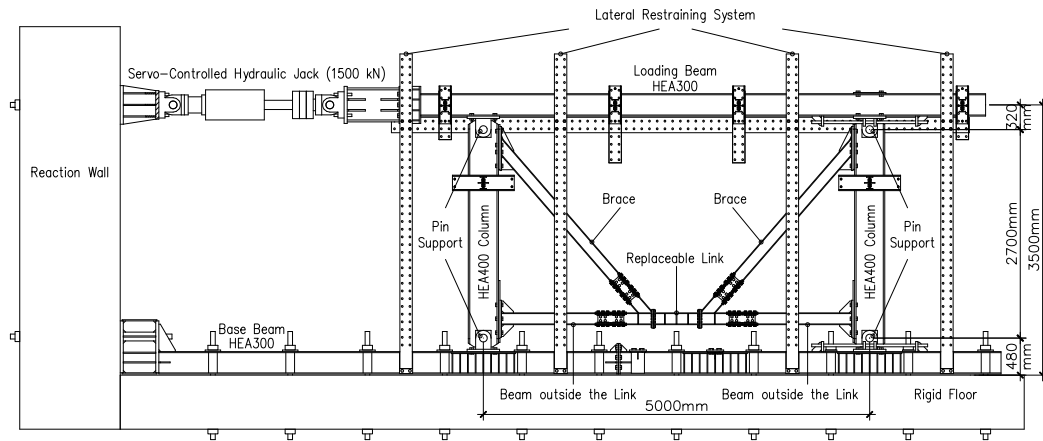


Figure 2.4. Details of the test setup

The replaceable links were attached to the HEA260 section beams using an end-plated moment connection. The HEA220 section braces were directly attached to the beams using a welded connection. In a typical experiment, the replaceable link specimen was loaded to failure. The beams and braces were reused since these members remain elastic during the experiments.

During a typical experiment, the lateral displacement of the frame and link rotation angle were monitored using Linear Variable Differential Transformers (LVDTs). Two different measurement techniques were employed to measure the link rotation angle. As shown in Figure 2.5, the vertical displacements of the link ends were

measured with respect to the stationary strong floor. In addition, the tangential deviation of one end of the link with respect to the other was also measured using an LVDT connected to an L-shaped bar. Readers are referred to Bozkurt and Topkaya (2017) for further information regarding the test setup and instrumentation.

Tests were controlled by the link rotation angle. The loading protocol recommended in AISC341-16 was used in the experimental program. Six cycles were repeated at 0.00375 rad, 0.005 rad, 0.0075 rad and 0.01 rad, then four cycles were repeated at 0.015 rad and 0.02 rad, later two cycles were repeated at 0.03 rad. Following cycles were repeated with increments of 0.02 rad. A shear link should complete 0.08 rad in order to satisfy AISC criteria.

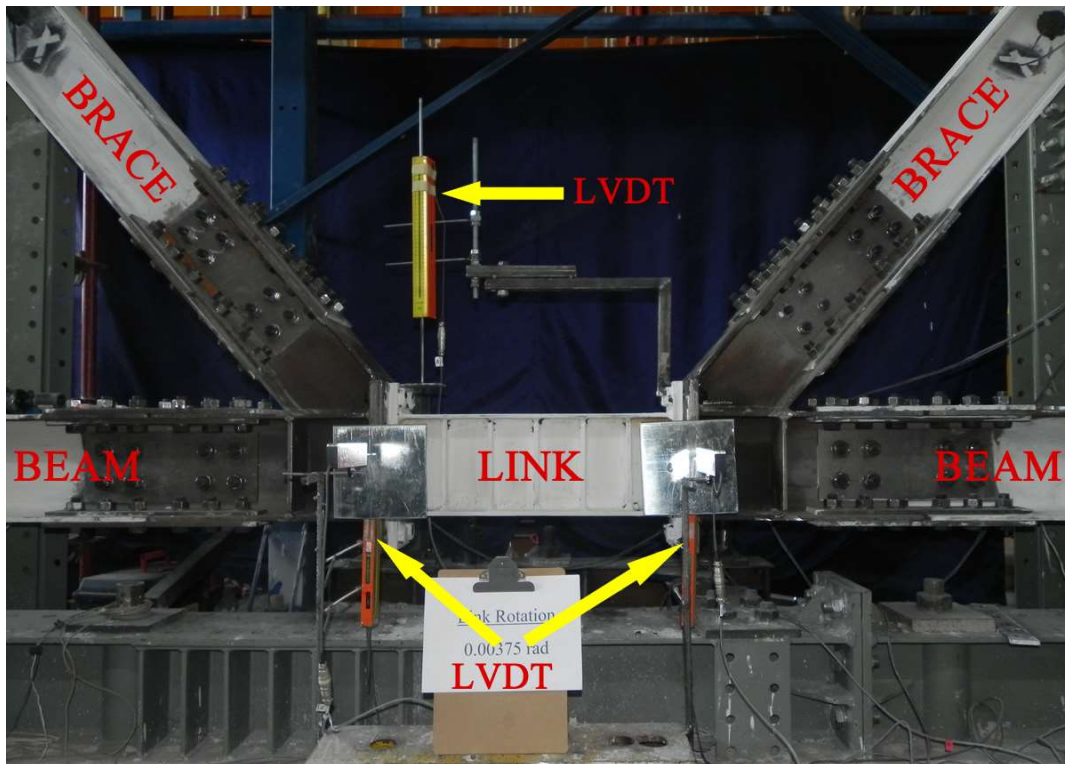


Figure 2.5. Details of the instrumentation

2.3.2 Details of Specimens

A total of 10 specimens were tested as a part of the experimental program. A European rolled I-section IPE240 was used for all replaceable links. The size of link was selected according to the capacity of the actuator. The depth of the link section is outside the parametric limitations on prequalification according to AISC 358. The length of the part to be replaced was kept constant at 700 mm. The length of the IPE240 section was varied depending on the thickness of the end-plate. The total length was determined based on the link length ratio (ρ). The aim of the study was to explore the behavior of shear links ($\rho \leq 1.6$) while maximizing the bending moment applied at the end-plate connection. Therefore, the length of the IPE240 section was adjusted to provide link length ratios that vary between 1.43 and 1.52. The width, thickness and stiffening of the end-plate were considered as the prime variables. The AISC358 Specification, which provides “thick” plate behavior, was used in the preliminary sizing of the end-plate. Using the end-plate geometry adopted in this study and considering a probable maximum moment of 190 kN-m, the end-plate thicknesses are determined as 23.3 mm and 18.9 mm for unstiffened and stiffened cases respectively for end-plates with a yield strength (F_y) of 275 MPa. The bolt configuration was kept constant throughout the testing program. European grade 10.9 bolts with an ultimate strength of 1000 MPa were used in all specimens. For the unstiffened plate thickness of 23.3 mm and a moment capacity of 190 kN-m, the minimum required bolt diameter is 22.7 mm according to DG16. For the stiffened plate thickness of 18.9 mm, the minimum required bolt diameter is 22.5 mm. The next available bolt diameter M24 was selected based on the requirements of DG16.

Geometrical details of the specimens are given in Figure 2.6 and Table 2.1. End-plate thicknesses of 30 mm, 20 mm, 15 mm, 12 mm, and 10 mm were considered. Both unstiffened and stiffened cases were studied where 4 specimens were stiffened and 6 were unstiffened. Normally the width of the end-plate does not have an influence on the capacity of the connection according to the DG16 because the

width of the end-plate is considered 25.4 mm greater than the width of the I-section in calculations. On the other hand, no such restriction is provided in EN 1993-1-8. End-plate widths of 150 mm and 285 mm were considered in the experimental program. The 150 mm width was selected according to the flange width of IPE240 and the 285 mm width was selected based on the available width provided by the HEA260 beam. The commonest European S275 steel with a yield stress of 275 MPa and ultimate stress of 430 MPa was considered in ordering of the IPE240 sections and end-plates. The specimens were ordered in two groups which resulted in two different heats for the IPE240 sections. The first 3 specimens, which employ wide end-plates, belong to the first group (Heat 1) while the others, which employ narrow end-plates, belong to the second group (Heat 2). The nominal and measured dimensions of the IPE240 sections as well as the material properties obtained from tensile coupon tests are summarized in Table 2.2 and Table 2.3. In addition, the material properties of the end-plates are reported in Table 2.4. The coupons were extracted and tested according to EN10002 (2001) and the values reported in Table 2.3 and 2.4 are the average of three coupon test results. The material test results showed that the Heat 2 for IPE240, Heat 2 for 15 mm thick, Heat 1 for 20 mm and 30 mm thick plates have considerably higher strength than standard S275 steels.

Table 2.1 Details of specimens

Sp. #	IPE240 Heat	Link Length (mm)	ρ Nom.	ρ Mes.	End Plate Thickness (mm)	End Plate Heat	End Plate Width (mm)	Stiffening	Wt. (kg)
1	1	640	1.43	1.62	30	1	285	U	76.6
2	1	670	1.50	1.70	15	1	285	U	50.7
3	1	446	1.00	1.13	15	1	285	S	52.3
4	2	660	1.48	1.46	20	1	150	U	42.3
5	2	670	1.50	1.48	15	2	150	U	37.9
6	2	676	1.51	1.49	12	1	150	U	35.3
7	2	680	1.52	1.50	10	1	150	U	33.5
8	2	446	1.00	0.99	15	2	150	S	39.5
9	2	452	1.01	1.00	12	1	150	S	36.9
10	2	456	1.02	1.01	10	1	150	S	35.1

Nom: Nominal, Mes: Measured, U: Unstiffened, S: Stiffened, Wt: Weight of specimen

Table 2.2 Nominal and measured dimensions of IPE240 sections

	d (mm)	b _f (mm)	t _w (mm)	t _f (mm)
Nominal	240.00	120.00	6.20	9.80
IPE240 Heat 1	239.37	119.56	6.58	9.31
IPE240 Heat 2	240.65	121.12	6.25	9.35

d = section depth; b_f = flange width; t_w = web thickness; t_f = flange thickness

Table 2.3 Material properties of the IPE240 sections

Section	H	Web					Flanges				
		F_{yl}	F_{yu}	$F_{y,0.2}$	F_u	EL	F_{yl}	F_{yu}	$F_{y,0.2}$	F_u	EL
		MPa	MPa	MPa	MPa		MPa	MPa	MPa	MPa	
IPE240	1	310	327	318	427	29	282	294	302	412	34
IPE240	2	387	391	391	525	21	410	422	415	546	20

H=heat; F_{yl} = lower yield stress (MPa); F_{yu} = upper yield stress (MPa); $F_{y,0.2}$ = yield stress at 0.2% permanent elongation (MPa); F_u = ultimate stress (MPa); EL = elongation (%)

Table 2.4 Material properties of the end-plates

Plate	Heat	F_{yl}	F_{yu}	$F_{y,0.2}$	F_u	EL
Thickness		(MPa)	(MPa)	(MPa)	(MPa)	
(mm)						
10	1	303	314	313	387	32
12	1	314	329	325	388	32
15	1	282	299	292	377	35
15	2	417	426	422	530	27
20	1	-	-	447	578	26
30	1	-	-	448	579	26

F_{yl} = lower yield stress (MPa); F_{yu} = upper yield stress (MPa); $F_{y,0.2}$ = yield stress at 0.2% permanent elongation (MPa); F_u = ultimate stress (MPa); EL = elongation (%)

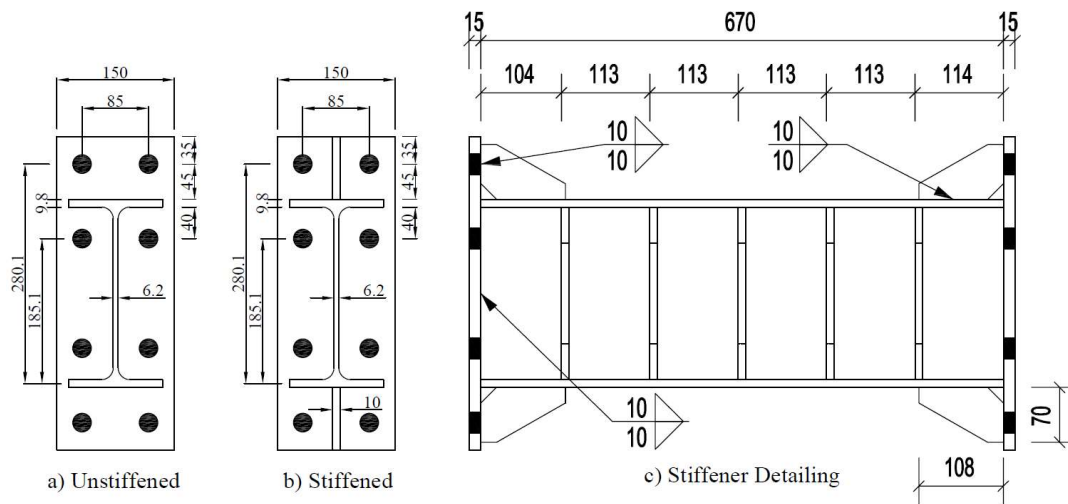


Figure 2.6. Details of end-plated replaceable links

The IPE240 links were stiffened according to the AISC341-16 provisions by using 10 mm thick stiffeners on one side. The stiffened end-plates employed 10 mm thick ribs, dimensions of which are indicated in Figure 2.6. When ribs are used, the yielding length of the IPE240 link reduces significantly. The link lengths reported in Table 2.1 for these specimens are based on the yielding length, which is equal to the clear distance between the ends of the ribs. While the length of the yielding segment reduces, the maximum amount of bending moment produced at the face of the end-plate is not influenced by the presence of the ribs. The clear length between the faces of the end-plates should be used to determine the amount of bending moment.

Welding details for all connections are indicated in Figure 2.6. In all welded connections Gas Metal Arc Welding was utilized with SG2 electrodes (similar to ER70S-6 electrodes) with a nominal tensile strength of 540 MPa. In general, all around fillet welds were used to connect the IPE240 section and ribs to the end-plates. The bolt configuration was kept constant throughout the testing program. M24 European grade 10.9 bolts with an ultimate strength of 1000 MPa were used in all specimens.

2.4 Experimental Results

All specimens were loaded to failure and sudden fractures in various forms were responsible for the failure of specimens. A summary of experimental results is given in Table 5 where plastic shear (V_p) and bending (M_p) capacities determined using the measured geometrical and material properties, the maximum shear (V_{max}) and bending (M_{max}) resistances obtained during the experiments, overstrengths, link rotation angle at failure and failure mode are reported. For properly stiffened shear links ($\rho < 1.6$) the inelastic link rotation angle should be at least 0.08 rad according to AISC341-16. If the specimen is capable of sustaining the 0.09 rad rotation cycle it should be considered to have adequate rotation capacity according to AISC341. Specimens 6 and 7 failed due to tearing of the end-plate and these were the only two specimens which could not satisfy the link rotation angle limit. Due to relatively thin end-plates adopted in this study the inelastic deformations of the end-plates were common to most specimens. Progression of end-plate deformations is indicated in Figures 2.7 and 2.8 for unstiffened and stiffened end-plates respectively. Typical failure modes observed during the experimental program are given in Figure 2.9. The values given in Table 2.5 for overstrength in shear resistance indicate that all specimens provided resistances in excess of the plastic shear capacity of the link (V_p). On the other hand, all specimens, except for specimens 6 and 7, the overstrength in bending resistance is greater than the plastic moment capacity of the link (M_p). In other words, except for two specimens the end-plate details were capable of developing M_p .

Table 2.5 Summary of experimental results

Sp. #	V_p (kN)	M_p (kN-m)	V_{max} (kN)	M_{max} (kN-m)	Overst. Shear	Overst. Bending	γ (rad)	Failure Mode
1	277	109	487	156	1.76	1.43	0.11	TFT
2	277	109	437	146	1.58	1.34	0.09	TFT
3	277	109	506	170	1.83	1.56	0.17	WF
4	325	149	532	176	1.64	1.18	0.11	BF+WF
5	325	149	514	172	1.58	1.16	0.09	TFT
6	325	149	409	138	1.26	0.93	0.07	EPT
7	325	149	342	116	1.05	0.78	0.05	EPT
8	325	149	563	189	1.73	1.27	0.13	WF
9	325	149	564	191	1.74	1.28	0.13	BF
10	325	149	495	168	1.52	1.13	0.11	EPT+RT

TFT: Top flange tearing; WF: web fracture; EPT: end-plate tearing; BF: bolt failure; RT: rib tearing

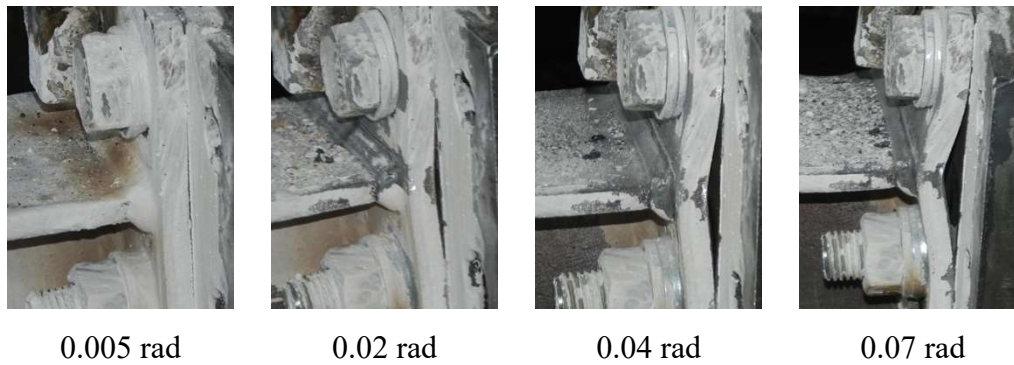


Figure 2.7. Deformation patterns of an unstiffened end-plate (Specimen 6)

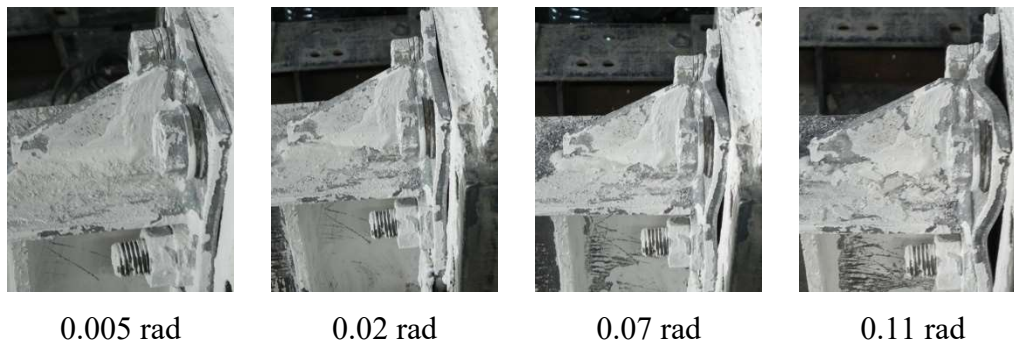


Figure 2.8. Deformation patterns of a stiffened end-plate (Specimen 10)

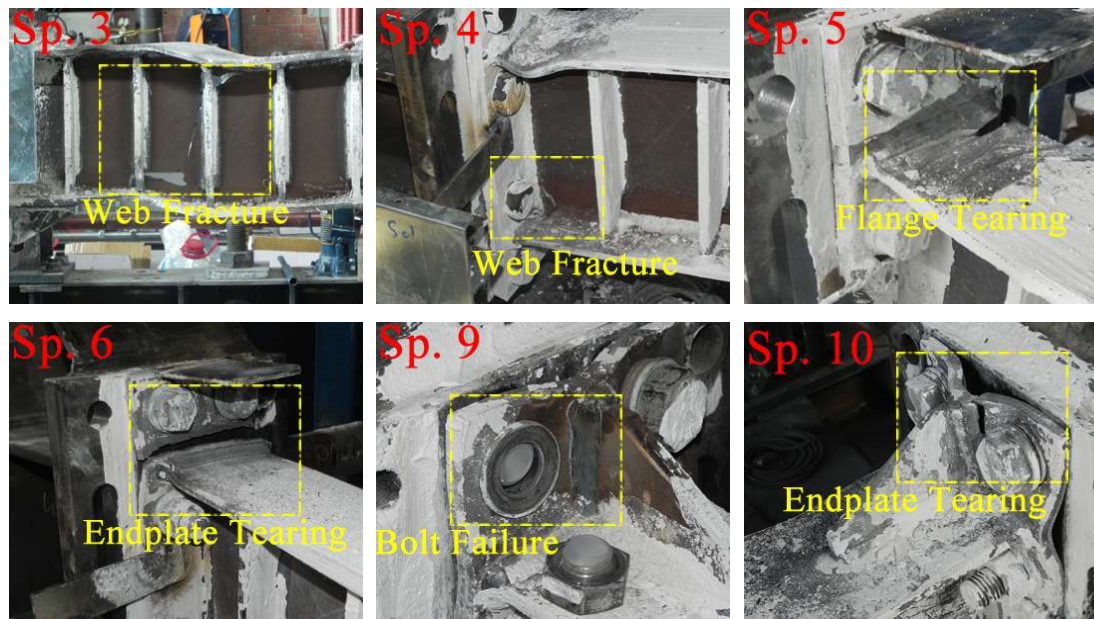


Figure 2.9. Failure modes of specimens

The hysteretic link rotation versus link bending moment response for all specimens is given in Figures 2.10 and 2.11. In general, all specimens, except specimens 6 and 7, exhibited a stable hysteretic response until failure. Specimens 6 and 7 exhibited a pinched response due to excessive deformations that took place in the unstiffened end-plates. The results show that adopting a “thin plate” design for replaceable EBF links in seismic regions can be a viable option. Controlled yielding of the end-plate contributes to energy dissipation and can also allow for shear and flexural yielding of the replaceable link.

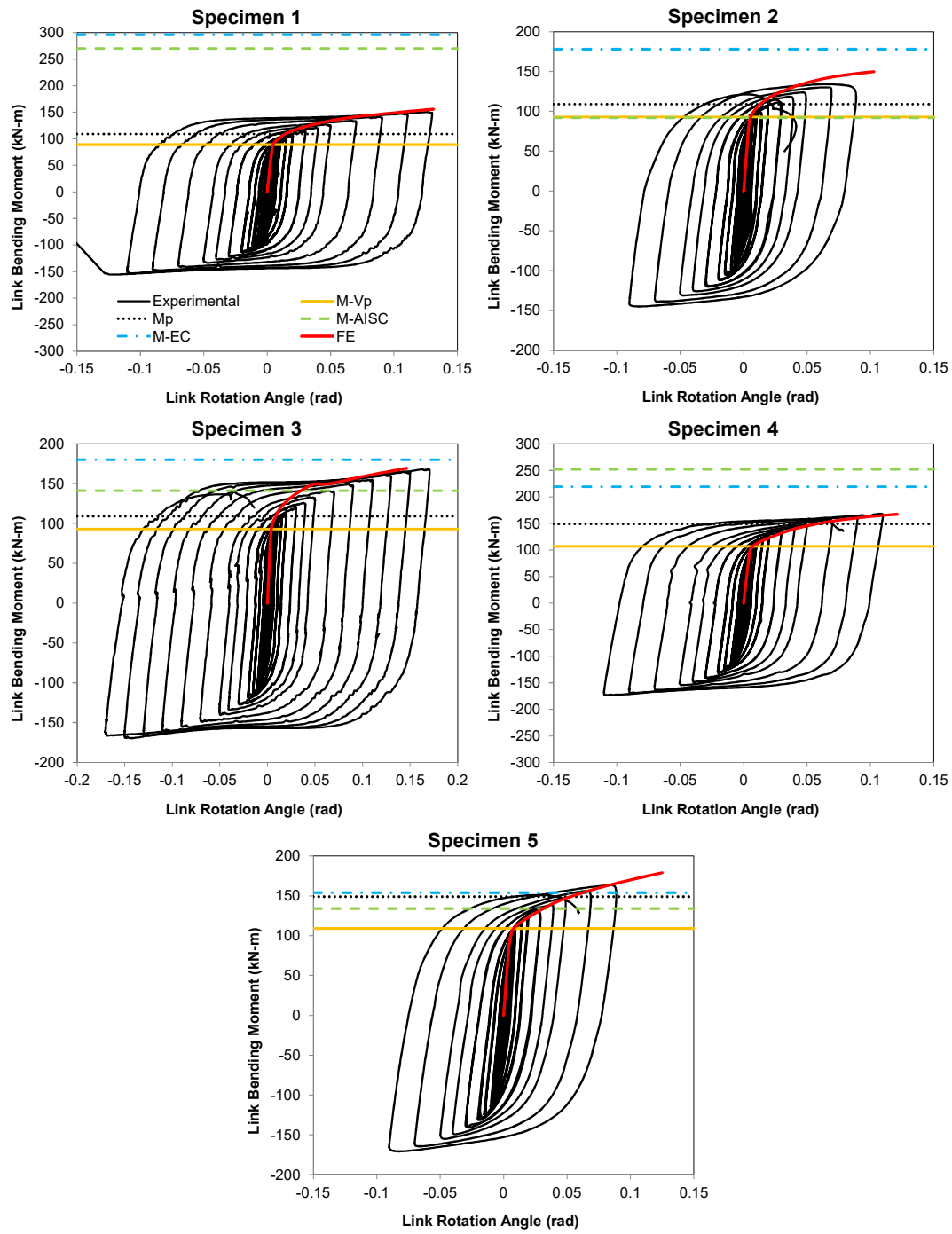


Figure 2.10. Hysteretic responses of specimens 1 though 5

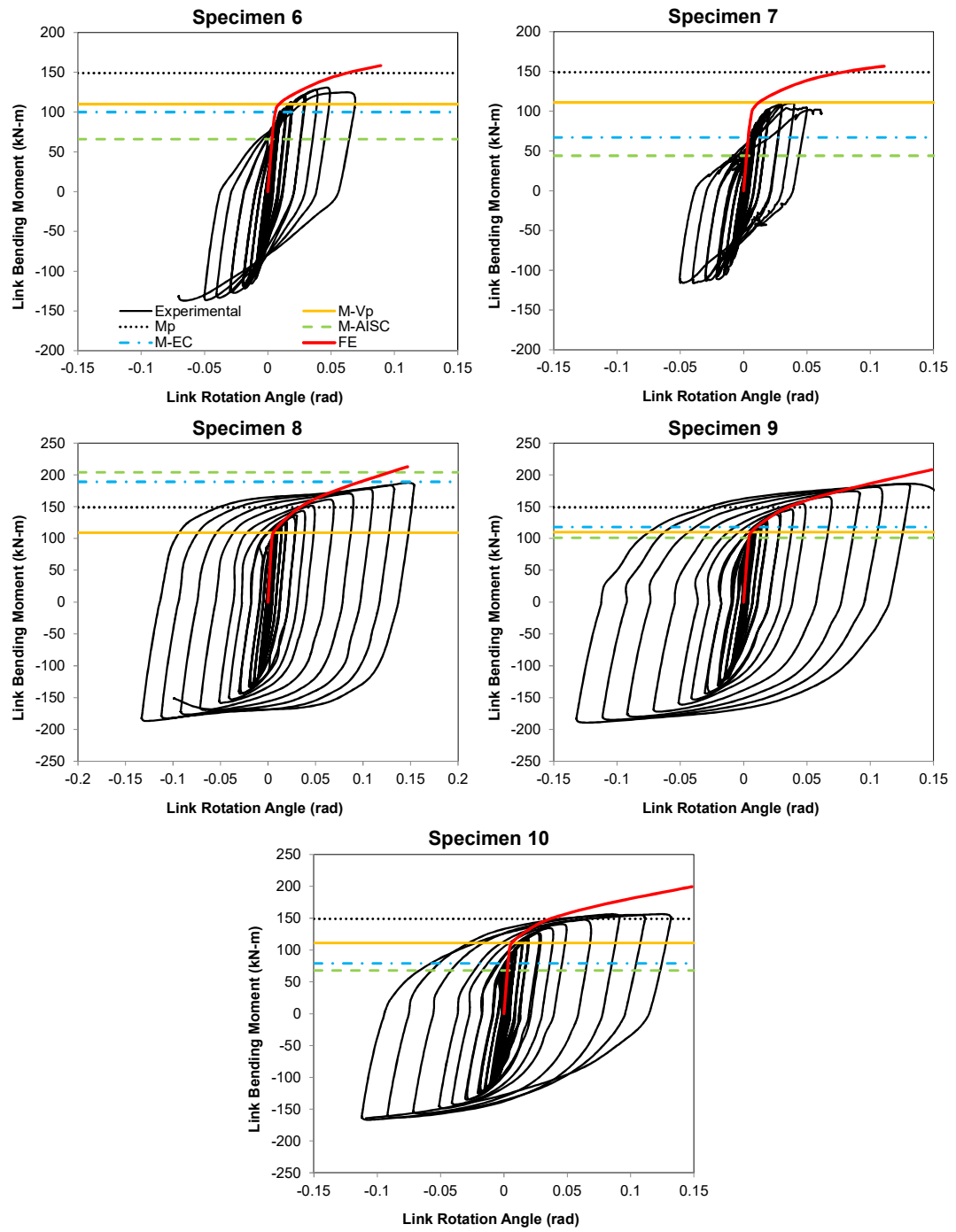


Figure 2.11. Hysteretic responses of specimens 6 though 10

One of the bolts above the bottom flange of specimen 4 ruptured during the positive excursion of the 0.13 rad cycle. The loading was reversed after bolt rupture and web fracture was observed during the negative excursion of the 0.13 rad cycle. Tensile testing of the bolts used for specimen 4 revealed that the ultimate strength was only 665 MPa which is lower than the nominal value of 1000 MPa. Bolts used for specimens 5 through 10 were from the same batch and tensile testing showed that the ultimate strength of these bolts was 1041 MPa which is slightly above the nominal value. Failure of specimen 9 was also triggered by bolt rupture. Significant amount of bending was observed in the end-plate of this specimen which resulted in an increase in the bolt forces due to the prying action.

2.5 Assessment of US Guidelines and European Provisions

The resistances of the end-plates were calculated using the DG16 and EN 1993-1-8 and these resistances were compared with the maximum bending strength of the link measured during a typical experiment. In order to make a fair comparison, the measured material properties were used for the end-plate material and the resistance factors and material factors were assumed equal to unity ($\phi=1.0$ and $\gamma_M=1.0$) for all limit states. The calculated resistances are given in Table 2.6 where M_{AISC} and M_{EC} denote the bending moment resistances calculated according to DG16 and EN 1993-1-8 respectively. In calculating M_{EC} the two methods (Eqns 2.12 and 2.13) were considered separately and the strengths were indicated as $M_{EC,1}$ and $M_{EC,2}$ for Methods 1 and 2 respectively. In general, Method 2 (“the alternative method” according to EN 1993-1-8) gives strengths that are in average 20% more than the strengths calculated according to Method 1. The calculated resistances are indicated in Figures 2.10 and 2.11 to make a direct comparison with the experimental results and $M_{EC,2}$ values were considered to represent the estimates of EN 1993-1-8. In these figures, two other bending moment capacities are also indicated. These are the plastic flexural strength of the link (M_p) and the bending moment resistance ($M-V_p$) that corresponds to the development of plastic shear

resistance (V_p) of the link section. The provisions of AISC341 for nominal shear resistance were used in calculating V_p .

Table 2.6 Summary of experimental results

Sp	M_{max}	AISC		EC Method 1		EC Method 2		Proposed	
		M_{AISC}	M_{max}/M_{AISC}	$M_{EC,1}$	$M_{max}/M_{EC,1}$	$M_{EC,2}$	$M_{max}/M_{EC,2}$	$M_{AISC,M}$	$M_{max}/M_{AISC,M}$
1	156	270	N.A	296	N.A	296	N.A	206	N.A
2	146	92	1.59	145	1.01	178	N.A	149	N.A
3	170	141	1.20	150	1.13	180	N.A	215	N.A
4	176	252	N.A	208	N.A	219	N.A	206	N.A
5	172	134	1.29	138	1.25	154	1.12	203	N.A
6	138	66	2.11	76	1.82	100	1.38	106	1.30
7	116	44	2.62	50.8	2.29	67	1.74	71	1.64
8	189	204	N.A	167	1.13	189	N.A	212	N.A
9	191	101	1.89	89.9	2.12	118	1.62	157	1.21
10	168	68	2.49	60.1	2.80	79	2.13	105	1.60
Av.			1.88		1.69		1.60		1.44

Sp: specimen number; M_{AISC} : end-plate resistance according to AISC Guidelines (kN-m); M_{EC} : end-plate resistance according to European provisions ($M_{EC,1}$ using Method 1, $M_{EC,2}$ using Method 2) (kN-m); $M_{AISC,M}$: end-plate resistance according to modified AISC Guidelines (kN-m). N.A.: not applicable (cases where the strength is governed by the ultimate strength of the link not by the end-plate strength i.e. $M_{AISC} > M_{max}$ or $M_{EC} > M_{max}$)

For all the specimens, the bending resistances calculated according to EN 1993-1-8 $M_{EC,1}$ and $M_{EC,2}$ are in average 5% and 26% greater than the ones calculated using DG16 respectively. Only for specimens 4 and 8 the M_{AISC} values are greater than $M_{EC,2}$. The M_{AISC} and $M_{EC,2}$ capacities were normalized by $M-V_p$ and M_p and the ratios are reported in Table 2.7. The $M_{AISC}/M-V_p$ ratios indicate that specimens 2, 6, 7, 9 and 10 should not be capable of developing the plastic shear resistance of the link due to the resistance being governed by the end-plate strength. The $M_{EC,2}/M-V_p$ ratios indicate that strength of specimens 6, 7 and 10 should be governed by the end-plate strength. When bending resistance of the link is considered, M_{AISC}/M_p ratios indicate that specimens 2, 5, 6, 7, 9 and 10 should not be capable of developing the plastic moment capacity of the link due to the resistance being governed by the end-plate strength. Similarly $M_{EC,2}/M_p$ ratios indicate that strength of specimens 6, 7, 9 and 10 should be governed by the end-plate strength. The

specimens 1, 3, 4, and 8 are expected to develop plastic shear and flexural resistance of the link when assessed according to either DG16 or EN 1993-1-8. These specimens belong to cases with wide 30 mm thick (Specimen 1) or narrow 20 mm thick (Specimen 4) unstiffened end-plates and 15 mm thick stiffened end-plates (Specimens 3 and 8). The modes of failure according to EN 1993-1-8 and considering Method 2 (Eqn 2.13) are reported in Table 7 for the two bolt rows where row 1 is for the bolts above the top flange and row 2 is for the bolts below the top flange. Mode 1 type of failure dominates for most of the cases for bolt row 1, while Mode 1 and 2 types of failure are expected for bolt row 2.

Table 2.7 Ratios of capacities and modes of failure for bolt rows according to European provisions

Sp.	$M_{AISC}/M-V_p$	$M_{EC,2}/M-V_p$	M_{AISC}/M_p	$M_{EC,2}/M_p$	EN1993-1-8	
					Row 1	Row 2
1	3.05	3.34	2.48	2.72	3	3
2	0.99	1.92	0.84	1.63	1	2
3	1.52	1.94	1.29	1.65	1	2
4	2.35	2.04	1.69	1.47	2	2
5	1.23	1.41	0.90	1.03	1	2
6	0.60	0.91	0.44	0.67	1	1
7	0.40	0.61	0.30	0.45	1	1
8	1.87	1.74	1.37	1.27	1	2
9	0.92	1.07	0.68	0.79	1	1
10	0.61	0.71	0.45	0.53	1	1

The experimental results showed that thinner plates than the required ones can also provide satisfactory performance. Specimens 2 and 5 employing 15 mm thick unstiffened end-plates were capable of satisfying the link rotation limit by a slight margin. On the other hand, Specimens 9 and 10 employing 12 mm or 10 mm thick stiffened end plates were capable of satisfying the link rotation limit by a wide margin. The results indicate that both the DG16 and EN 1993-1-8 provide conservative estimates of the end-plate strength. In order to quantify the level of conservatism, the ratio of the measured-to-predicted bending strengths were considered (M_{max}/M_{AISC} or M_{max}/M_{EC}). Cases where the end-plate strength is

expected to govern the design were taken into account (i.e. $M_{AISC} < M_{max}$ or $M_{EC} < M_{max}$) in order to make a fair comparison (Table 2.6).

The ratios of measured-to-predicted strengths show that the approach given in DG16 provides in average 88% conservative estimates of the end-plate strength. This ratio modifies to 69% and 60% for Methods 1 and 2 respectively, when EN 1993-1-8 is considered indicating that the DG16 is more conservative than EN 1993-1-8 for end-plate design.

Another important observation is on the relationship between the plate thickness and the measured-to-predicted strength ratios. The level of conservatism is more pronounced as the plate thickness reduces. For example, the M_{max}/M_{AISC} ratios are 1.89 and 2.49 according to DG16 for specimens 9 and 10 which employ 12 and 10 mm thick stiffened end-plates respectively. This high level of conservatism provided in the design codes result in relatively thicker plates to be used while thinner ones can also perform quite satisfactorily. A set of modifications is proposed in later sections of this paper to reduce the level of conservatism. Another important observation from the test results is associated with the shear failure of the end-plates. AISC-358 requires checks of yielding and shear rupture of the extended portion of the end-plate in extended unstiffened end-plate connections. Half of the force delivered by the connected beam flange is considered as the shear demand. Accordingly the shear demand on end-plates of Specimens 6 and 7 are determined as 300 kN and 252 kN, respectively. The yielding and shear rupture capacities without resistance factors are determined as 339 kN and 254 kN for Specimen 6 and 272 kN and 211 kN for Specimen 7, respectively. The shear yielding capacities of both the end-plates are slightly above the shear demand indicating that the shear yielding is not a controlling failure mode. On the other hand, the shear rupture capacities are lower than the demands indicating that shear rupture through the net area should be controlling failure mode. However, as shown in Figure 9 both the specimens failed though the gross section of the end-plate, not through the net section. These failures are due to excessive bending of the end-plates associated with low-cycle fatigue effects. The comparisons show that AISC-358 is

conservative in a sense that the net section is used to calculate the shear resistance. Due to the concentrated forces produced by the bolts, the net section is subjected to a demand less than the demand estimated by AISC-358. In other words, the maximum demand is produced at the gross cross section between the toe of the fillet weld and the edge of the bolts. The net section that passes through the bolt holes is subjected to lesser amounts of the shear force demand.

2.6 Finite Element Studies

Finite element analyses were conducted to investigate the amount of yielding in the end-plates and also to study the effect of end-plate width on the response. The specimens investigated in the experimental program were not instrumented with strain gages and the finite element analysis results provide further information into the level of yielding that takes place in end-plates with different thicknesses and widths. Three-dimensional nonlinear finite element analyses were conducted by using a commercially available software ABAQUS (2012).

Isolated models which include link and end-plated connections were modeled to reduce the computational time. The study conducted by Bozkurt et al. (2019) revealed that the isolated model was capable of simulating link behavior performed in the experiments and a negligible difference was observed between the results of the full model and the isolated model. The reduced integration eight-node brick elements with hourglass control (C3D8R) were used for meshing all elements. Six layers of elements were used through the thickness of the web while four layers of elements were used through the thickness of flanges and stiffeners. Ten layers of elements were employed through the thickness of the end plate to be able accurately represent bending of this member. Figure 2.12 shows a typical finite element mesh and plastic equivalent strain contours obtained after an analysis.

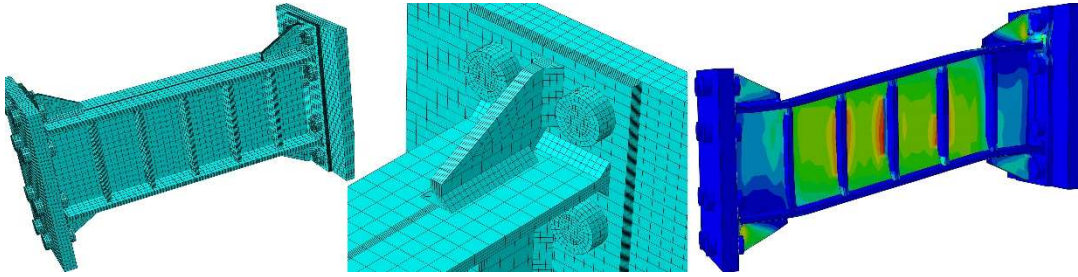


Figure 2.12. A typical finite element mesh and plastic equivalent strain contours

The finite sliding surface-to-surface contact was defined to model contact between surfaces. Tangential contact behavior was considered and the friction coefficient was taken equal to 0.3. Boundary conditions of numerical models were determined to replicate full-scale experimental setup. Axial and rotational restraints were applied to end-plates of the beam in order to simulate link behavior in frame system. Material properties of link and end plate were modeled using stabilized cyclic stress strain curve proposed by Della Corte et al. (2013). In order to obtain a stabilized cyclic curve, the equation given by Kaufmann et al. (2001) was adopted up to 0.04 strain and the curve was extrapolated from 0.04 strain to the strain corresponding to ultimate stress obtained from coupon test. The accuracy of this approach was also proved by Bozkurt et al. (2019).

More than three layers of elements were also utilized through thickness of bolt head, nut and shank to prevent shear locking and hourglass (D'Aniello et al (2017)). Elastic perfectly plastic material properties were used to model the bolts with yield and ultimate strength of 800 MPa and 1000 MPa, respectively. Proper mesh detailing was employed to the bolts and around the bolt holes to eliminate possible convergence problems (Özkılıç (2020)). Pretension loads amounting to 70% of the bolt tensile strength were given to bolts using Bolt Load option in ABAQUS (2012). Geometrical and material nonlinearity were implemented in the model.

Finite element models of all specimens were prepared and analyzed under monotonic loading. The link bending moment versus link rotation responses obtained from finite element analyses are given in Figures 2.10 and 2.11. The

comparisons with experimental results indicate that the finite element models are capable of accurately representing the behavior of the experimented specimens.

The finite element analysis results were chiefly used to examine the amount of yielding that takes place in the end-plates due to bending. For this purpose, a path was defined on the surface of the end-plate between the bolt rows above and below the top flange, which pass through the center of the end-plate (through the half-width). The strain parallel to the path (i.e. bending strain) was extracted from finite element results and was normalized with the yield strain (ϵ_y). The variation of strains along the path is given in Figure 2.13 for all specimens. These strains were obtained at link rotation angles that correspond to the maximum link rotation angle that was observed in the experimental program. The location of maximum strain is 12 mm away from the center of flange for both the unstiffened and stiffened end-plates. The variation of this maximum strain as a function of the link rotation angle is presented in Figure 2.14. The responses until the link rotation angle at failure observed in the experimental program are shown in this figure.

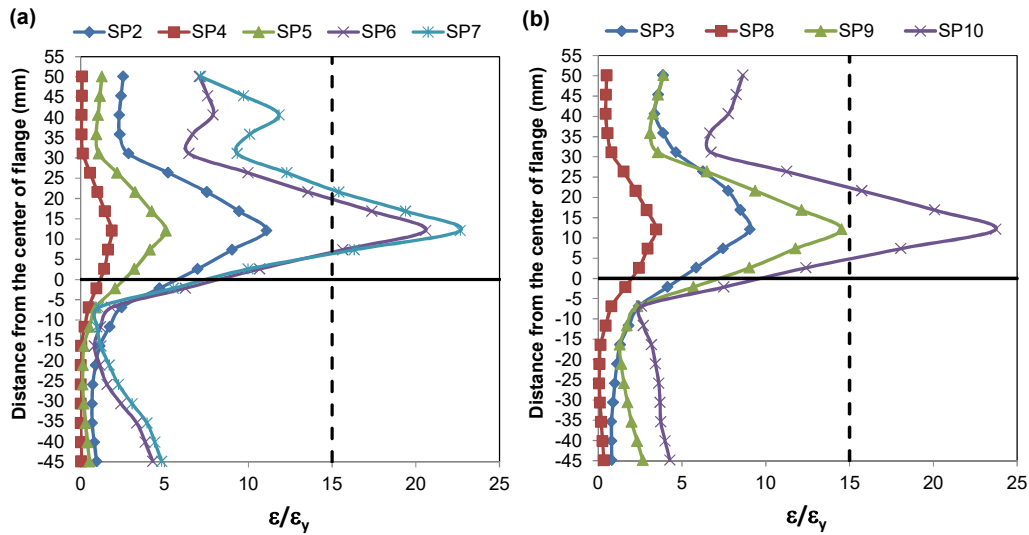


Figure 2.13. A variation of strains along a path; (a) unstiffened end-plates, (b) stiffened end-plates

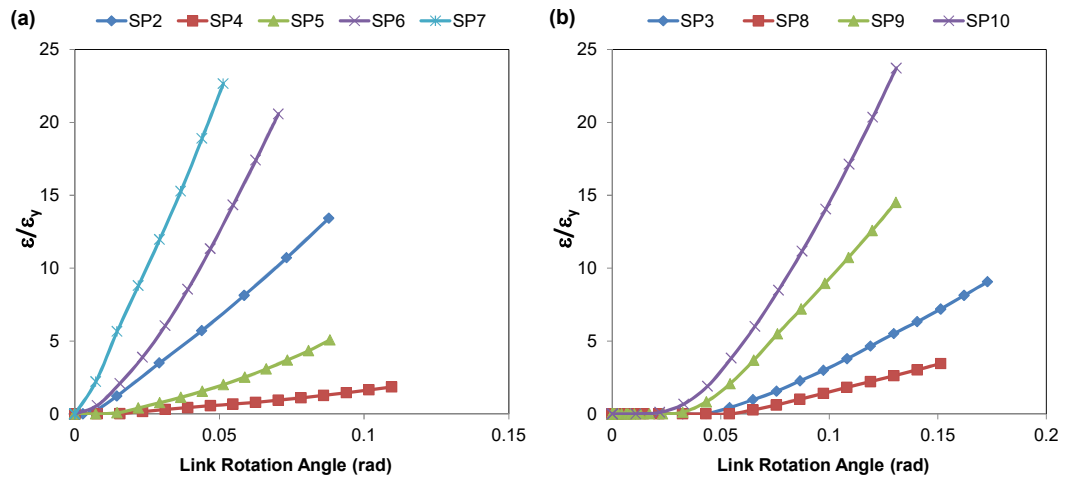


Figure 2.14. Strain versus link rotation angle response; (a) unstiffened end-plates, (b) stiffened end-plates

The maximum strains reached at the onset of end-plate failure are consistent for specimens 6 and 7, where the normalized strains (ϵ/ϵ_y) are reported as 20.6 and 22.6. For the stiffened end-plates, specimen 10 experienced a normalized strain (ϵ/ϵ_y) of 23.7 at failure. The fracture of end-plates is a complex phenomenon and depends on the cyclic history of loading. In the absence of more detailed finite element studies, a conservative normalized strain (ϵ/ϵ_y) limit of 15 can be recommended to evaluate the performance of an end-plated shear link. As shown in Figure 2.13, all of the specimens that showed satisfactory performance have maximum strains less than this limiting value. End-plate geometries that are different than the ones studied here can be evaluated by finite element analysis and the recommended strain limit can provide a starting point for the assessment of the end-plate connection.

Experimental results do not provide an opportunity to derive direct conclusions about the effect of plate width because of the type of failure observed in the specimens and the differences in yield strengths. Specimens 2 and 5 with unstiffened end-plates and specimens 3 and 8 with stiffened end-plates were geometrically identical except for the width of end-plates where specimens 2 and 3 employed wide (285 mm) and specimens 5 and 8 employed narrow (150 mm) end-

plates. The yield strengths of the link sections and the end-plates for the companion specimens are different. In order to make a fair comparison the link shear resistance was normalized by the plastic resistance of the link (V_p) and the responses are indicated in Figure 2.15. According to this figure the link shear versus link rotation responses obtained using wide and narrow plates are almost identical. For the stiffened end-plates slightly more pinching is observed for the narrow end-plate (Specimen 8) when compared with the wide end-plate. Specimens 2, 5, 3 and 8 did not fail through end-plate fracture and therefore additional finite element studies were needed to study the response of wide end-plates. For this purpose the width of specimens was increased from 150 mm to 285 mm by keeping all the other geometrical and material variables the same. The specimens were subjected to link rotation angles that are identical to the ones observed in the experimental program. The variations of normalized strains along a path are given in Figure 2.16 for both the plate widths. The results indicate that the width of the end-plate does not have a pronounced effect on the level of maximum strain observed along the path. By increasing the plate width from 150 mm to 285 mm the normalized strain decreased from 20.6 to 15.1 for specimen 6 from 22.7 to 18.7 for specimen 7. The decrease in strains is not directly proportional to the increase in the plate width. Therefore, the recommended calculation method of DG16, which limits the plate width to flange width plus 25.4 mm, is reasonable.

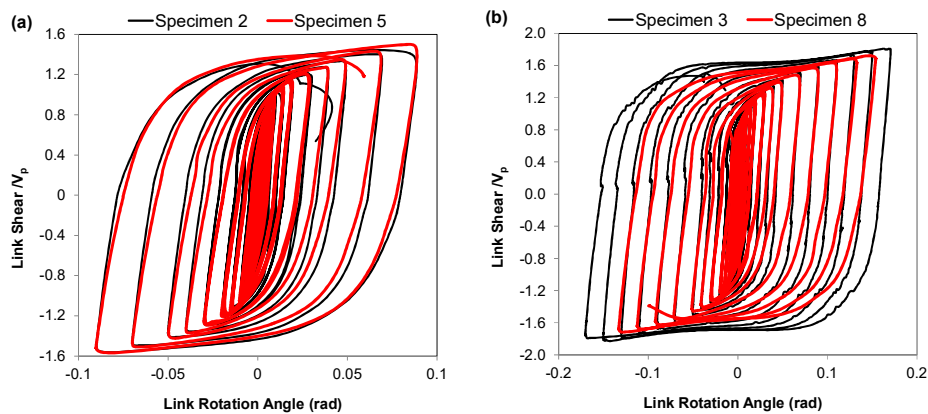


Figure 2.15. Normalized link shear versus link rotation angle response for end-plated with different widths

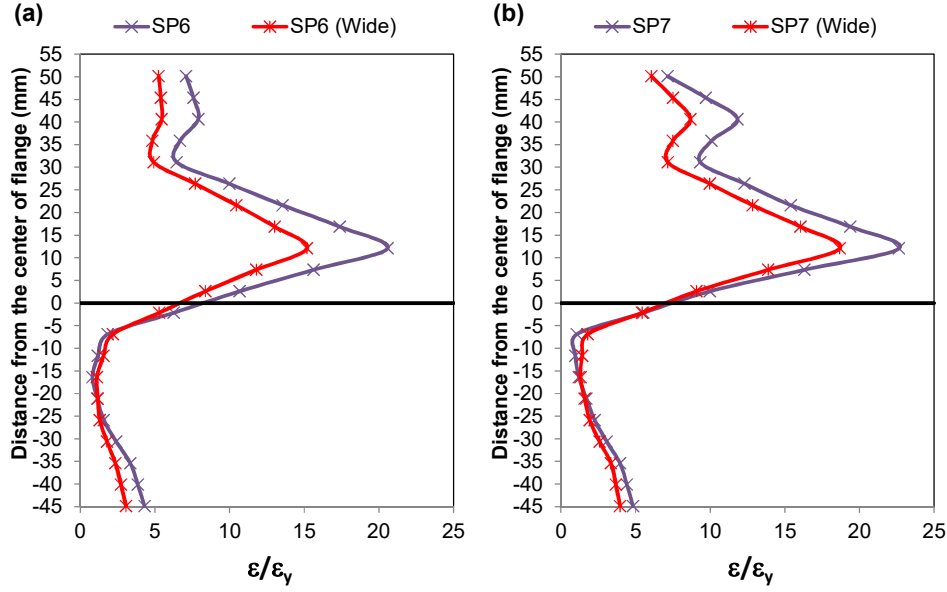


Figure 2.16. Variation of strains along a path for wide and narrow end-plates; (a) unstiffened end-plates, (b) stiffened end-plates

2.7 Proposed Modifications to AISC Guidelines

Recommendations were developed to improve DG16 and AISC358 in regard to calculating the bending capacity of end-plates. The yield line mechanisms can be independently studied using unstiffened and stiffened T-stub models. For this purpose, the strength of T-stubs was studied using finite element analysis. End-plates having a width of 145 mm were analyzed. The largest differences between experiments and code estimates are for Specimens 7 and 10 which employ 10 mm thick end-plates. Based on this observation, 10 mm thick plates with a yield strength (F_y) of 313 MPa were analyzed. A symmetrical bolt configuration was considered with $p_{fo}=45$ mm, $g=85$ mm and $d_e=35$ mm, which is identical to the geometry of the test specimens. Typical finite element models for unstiffened and stiffened cases are given in Figure 2.17. A rigid plate was defined under the T-stub connection. Boundary conditions were assigned to this rigid plate. All degrees of freedom were restrained. Pretension loads were defined to the bolts and welds were modeled explicitly.

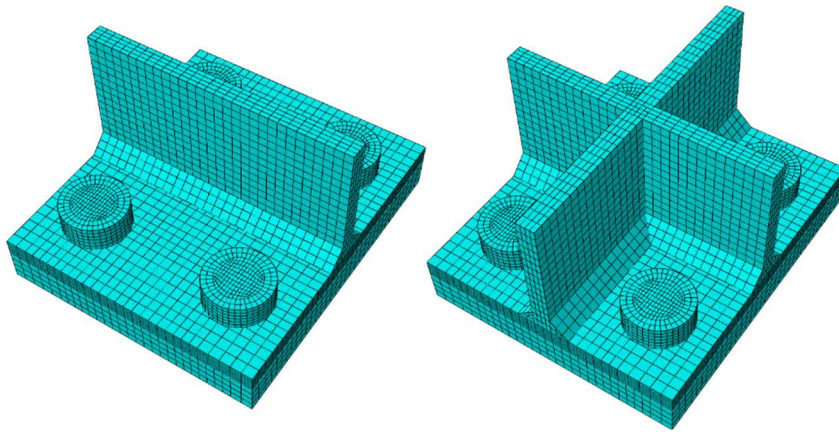


Figure 2.17. Finite element models of T-stubs

The results from the finite element analysis are given in Figure 2.18, where the applied load versus displacement response is shown. The failure loads based on the yield line mechanism adopted by DG16 are also indicated in this figure. The comparisons reveal that the capacities according to DG16 are very conservative. For the unstiffened case, the AISC Guideline provides a capacity of 100.8 kN whereas the model exhibits stiffness reduction around 250 kN. For the stiffened case, the AISC Guideline capacity is 259.6 kN whereas stiffness reduction is observed around 450 kN.

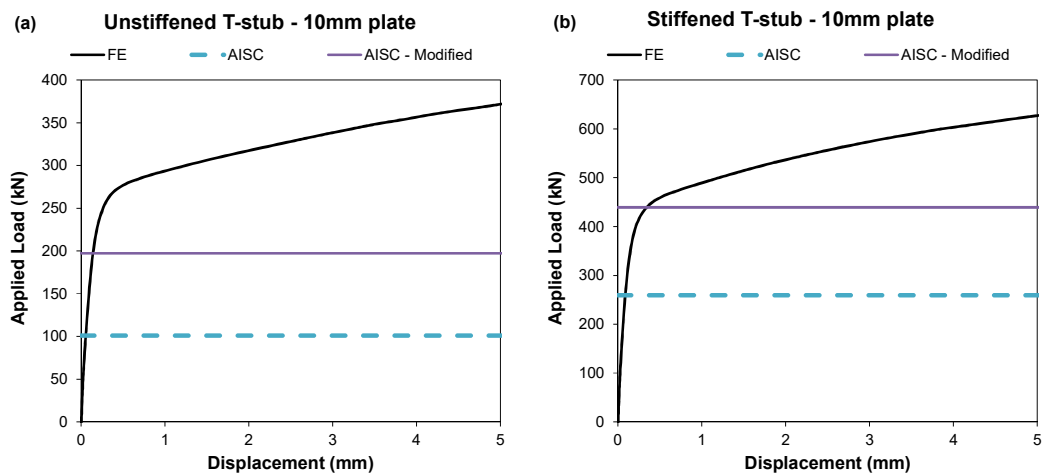


Figure 2.18. Load versus displacement response of t-stub models; (a) unstiffened T-stub, (b) stiffened T-stub

The sources of discrepancies can be attributed to the lengths used in the calculations and the yield line patterns. The proposed yield line patterns and the lengths to be used in calculations are indicated in Figure 2.19. In general, DG16 utilizes the before welded length and does not take into account the reduction due to the diameter of the bolts. Therefore, it is recommended to use the after welded length and also take into account the reduction due to the bolt diameter. In other words, more accurate estimates can be obtained by using the net length between the toe of the fillet weld and the edge of the bolt. By considering this reduced length, the capacity calculated for the unstiffened case increases from 100.8 kN to 197.3 kN which is indicated in Figure 2.18.

While similar reductions in the lengths are required for the stiffened case, the yield line pattern also requires a modification. To this end, the yield line pattern recommended by Shi et al. (2007) can be adopted. By applying these modifications the capacity calculated for the stiffened case can be increased from 259.6 kN to 439.2 kN as shown in Figure 2.18.

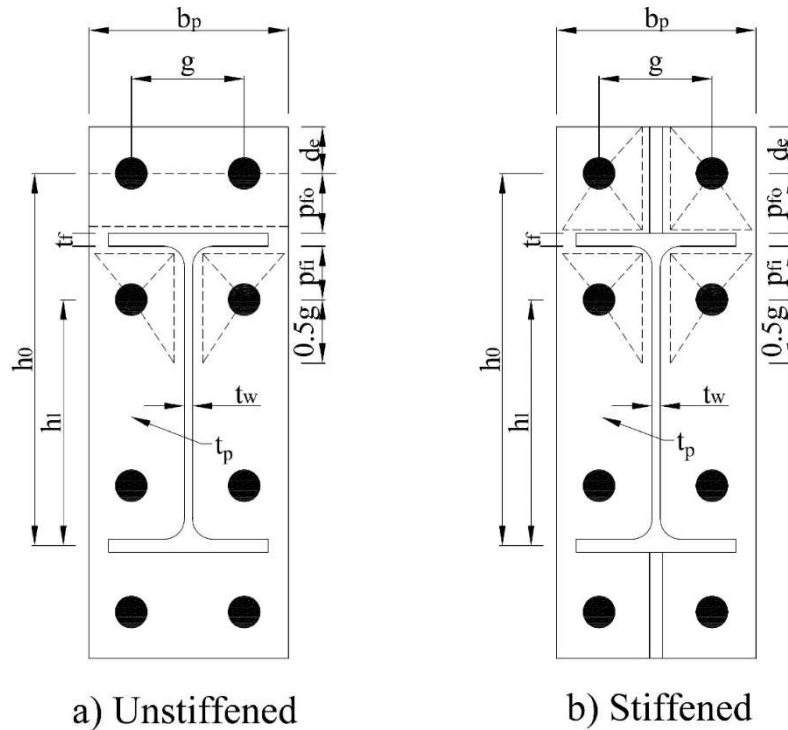


Figure 2.19. Proposed yield patterns

The modifications can be implemented into the AISC Guideline by modifying the yield line mechanism parameter as follows:

For unstiffened end plates:

$$Y = h_o \left[\frac{b_p}{2} \frac{1}{p_{fo} - 0.5d_b - t_{w,f}} \right] + 2h_1 \left[\frac{b_p - t_{web} - 2t_{w,w}}{4(p_{fi} - 0.5d_b - t_{w,f})} + \frac{p_{fi} - t_{w,f} + 0.5g}{g - t_{web} - 2t_{w,w} - d_b} \right] \quad (2.21)$$

For stiffened end plates:

$$Y = 2h_o \left[\frac{b_p - t_{rib} - 2t_{w,r}}{4(p_{fo} - 0.5d_b - t_{w,f})} + \frac{p_{fo} - t_{w,f} + d_e}{g - t_{rib} - 2t_{w,r} - d_b} \right] + 2h_1 \left[\frac{b_p - t_{web} - 2t_{w,w}}{4(p_{fi} - 0.5d_b - t_{w,f})} + \frac{p_{fi} - t_{w,f} + 0.5g}{g - t_{web} - 2t_{w,w} - d_b} \right] \quad (2.22)$$

Where t_{rib} and t_{web} are the thickness of the rib and web, respectively, d_b is the diameter of the bolt, $t_{w,f}$, $t_{w,w}$, and $t_{w,r}$ are the leg thicknesses of the flange, web and rib welds, respectively.

The end-plate capacities were recalculated using the modified yield line mechanism parameter and the results are indicated in Table 2.6. The modifications provide end-plate capacities that are greater than the maximum link bending moment for 6 cases. For specimens 6, 7, 9, and 10 the modified expressions provide conservative estimates of the capacity but the level of conservatism reduced significantly. It should be mentioned that for end-plated connections with bolts that are placed very close the flanges and the rib, the use of net lengths result in a significant change in the capacity. Further increases in the capacity can be obtained by considering the effect of the washer and bolt head.

The selection of an end-plate thickness requires an accurate estimation of the maximum link bending moment which in turn requires accurate determination of the link overstrength. The source of the overstrength arises mainly due to the strain hardening of the steel under cyclic loading. The following formulation, with a link overstrength of $\Omega=2.0$, is recommended based on the overstrengths observed in this

and the past experimental studies (Kazemzadeh Azad and Topkaya (2017), Bozkurt and Topkaya (2017))

$$M_{link} = \frac{\Omega R_y V_p e}{2} \quad (2.23)$$

where R_y is the ratio of the expected yield stress to the specified minimum yield stress determined according to AISC341.

CHAPTER 3

MID-SPLICED END-PLATED REPLACEABLE LINKS

3.1 Background

The second research program focused on developing a mid-spliced end-plated replaceable link. As mentioned in Chapter 1, post-earthquake installment of end-plated links can be accomplished if the residual frame drifts are quite low. The frame needs to be re-straightened if the residual drifts are high. In addition, the end-plated replaceable links may need to be removed by making use of hydraulic jacks due to the excessively high axial forces developed in the link after a seismic event.

The detachable link concept proposed by Bozkurt et al. (2019) can be extended to end-plated links as shown in Figure 3.1. In this type of a replaceable link, an end-plated connection is provided at the mid-length similar to the one adopted in Figure 1.4. By making use of this mid-splice detail, the link can be installed under residual drift. However, this type of a replaceable link does not have an erection tolerance and therefore, the replacement operation will most likely require hydraulic jacks for link removal.

A different type of mid-splice detail was developed and investigated as a part of this research program. The following sections outline the details of the proposed link detail and associated investigations.

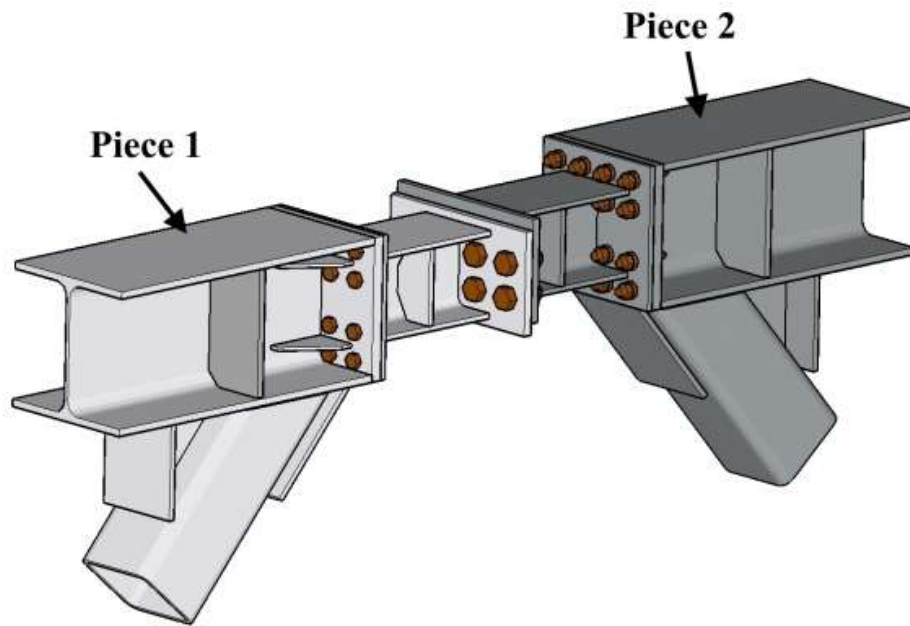


Figure 3.1. Detachable end-plated replaceable link

3.2 Mid-Spliced End-plated Replaceable Link Concept

Bozkurt et al. (2019) developed a detachable link which enables the links to be replaced under residual frame drifts. In this detail, the replaceable link is divided into two symmetrical pieces where each piece is connected to each other by making use of an end-plated connection at the mid-length of the link. The detachable link concept was applied to replaceable links with braces where erection tolerances already exist. Almost the same concept can be utilized for end-plated links as shown in Figure 3.1; however, this detail does not provide an erection tolerance. The proposed link concept, given in Figure 3.2, builds upon the detachable link concept developed by Bozkurt et al. (2019). The idea here is to attach saw cut I-sections to the ends of each piece such that a gap can be provided in between the ends. This gap facilitates easy removal and replacement of the links. The saw cut I-sections should be welded to the I-section links by making use of either all around fillet welds or groove welds. The two link pieces are connected to each other by using side plates bolted to the flanges of the saw cut I-sections. Depending on the

type of application, the bolted connection used for the side plates can be bearing type or slip critical type. In addition, slotted holes can be introduced into the side plates so that replacement under residual drift conditions can be possible. Channel sections can also be used instead of saw cut I-sections but the depth and flange sizes of channel sections are limited compared to saw cut I-sections and the flanges of channel sections are usually tapered which makes the bolting operation little more difficult.

It should be noted that axial forces are developed in the links due to the frame geometry and also due to the axial restraining effect of the connecting members as the link undergoes large rotations. These axial forces on the link produce axial forces on the bolts when the end-plated connection detail shown in Figure 3.1 is employed at the mid-length. The change in the bolt axial force results in a change in the slip resistance at the faying surfaces. In the proposed link detail, the axial forces produced in the link do not create axial forces in the bolts and the bolts are primarily under shearing actions. The next section outlines the steps to be undertaken to design the mid-splice detail with the side plate connections.

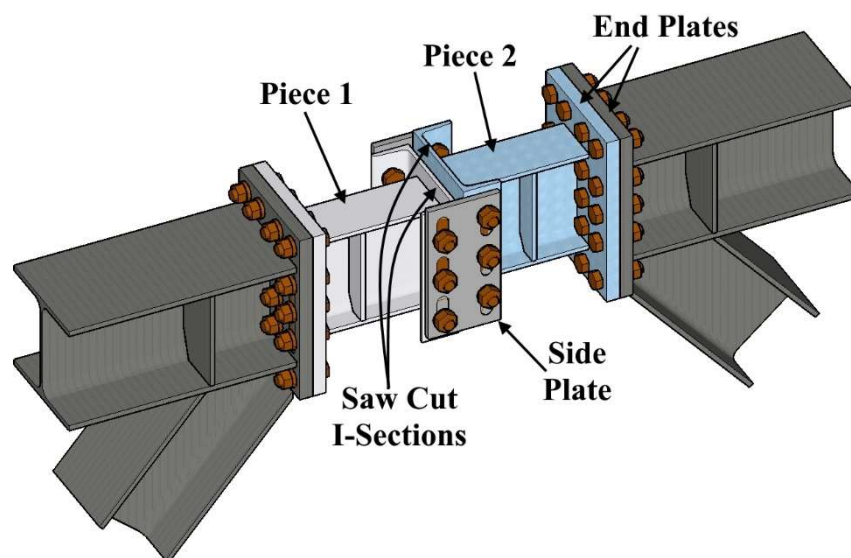


Figure 3.2. Isometric view of the proposed mid-splice detachable link

3.3 Mid-Spliced End-plated Replaceable Link Concept

The bolted connection between the flanges of the saw cut I-section and side plates should be able to transfer the forces developed in the link pieces. Either bearing type or slip critical type connections can be utilized depending on the amount of relative movement allowed between the flanges and the side plates. The use of bearing type connections is expected to result in relative slip between the flanges and the side plates, which in turn cause a slightly pinched behavior. The use of slip critical connection can alleviate the slip problem but this type of a connection can require more number of bolts.

The variation of stress resultants developed in the mid-spliced end-plated replaceable link is given in Figure 3.3. At mid-length the bending moment developed in the link is theoretically zero and the mid-splice connection should be designed for the shear and axial forces developed in the link. In addition, the eccentricity between the centroid of the bolt group on one side and the centroid of the side plate should be considered. Torsional moments are developed on the bolt group, which in turn result in additional shearing forces on the bolts. A flowchart for the design of bolt groups is indicated in Figure 3.4. The bolted connection design rules mandated by the AISC Specification for Structural Steel Buildings (AISC360, 2016) has been adopted. The amount of additional axial force developed in the link due to the axial restraining effect of the connecting members is considered equal to 10% of the axial yield strength of the link (P_y). This value was selected based on the finite element parametric studies, details of which are explained in the following sections.

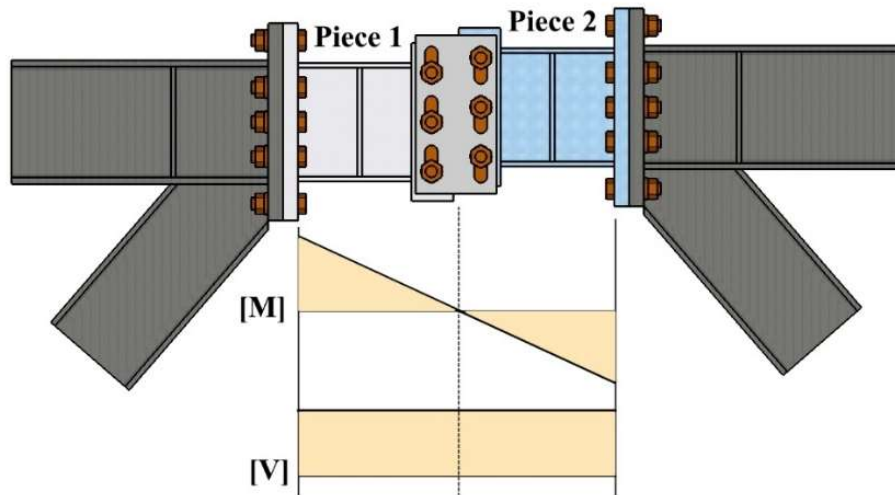


Figure 3.3. Variation stress resultants within the detachable link

As shown in Figure 3.4, the connection design starts with the decision on bolt pattern, which could be single row, double row, or staggered. Then, the design is continued by the type of holes, which could be standard site drilled holes or slotted holes, bolt grade and the number of bolts. During post-earthquake replacement, the side plates can be drilled on site using the bolt hole pattern on the flanges of the saw cut I-section as a template. These standard site drilled holes can be used in a bearing type connection or a slip-critical connection. On the other hand, if drilling the holes on site is not preferred, then slotted holes can be drilled on the side plates at the fabrication shop. The size of the slotted holes is determined according to the residual frame drifts. However, the connection must be designed as slip-critical to prevent excessive amount of slip that may take place in the slotted holes. While the resistance factor, ϕ , is taken as 1.00 for standard size holes, it is taken as 0.7 for long-slotted holes according to AISC360. Regardless of the type of connection, the design should consider plate bearing and tear-out strength at bolt holes. The constructive details given in Figure 3.5 should also be followed, which depend on the minimum requirements given in AISC360.

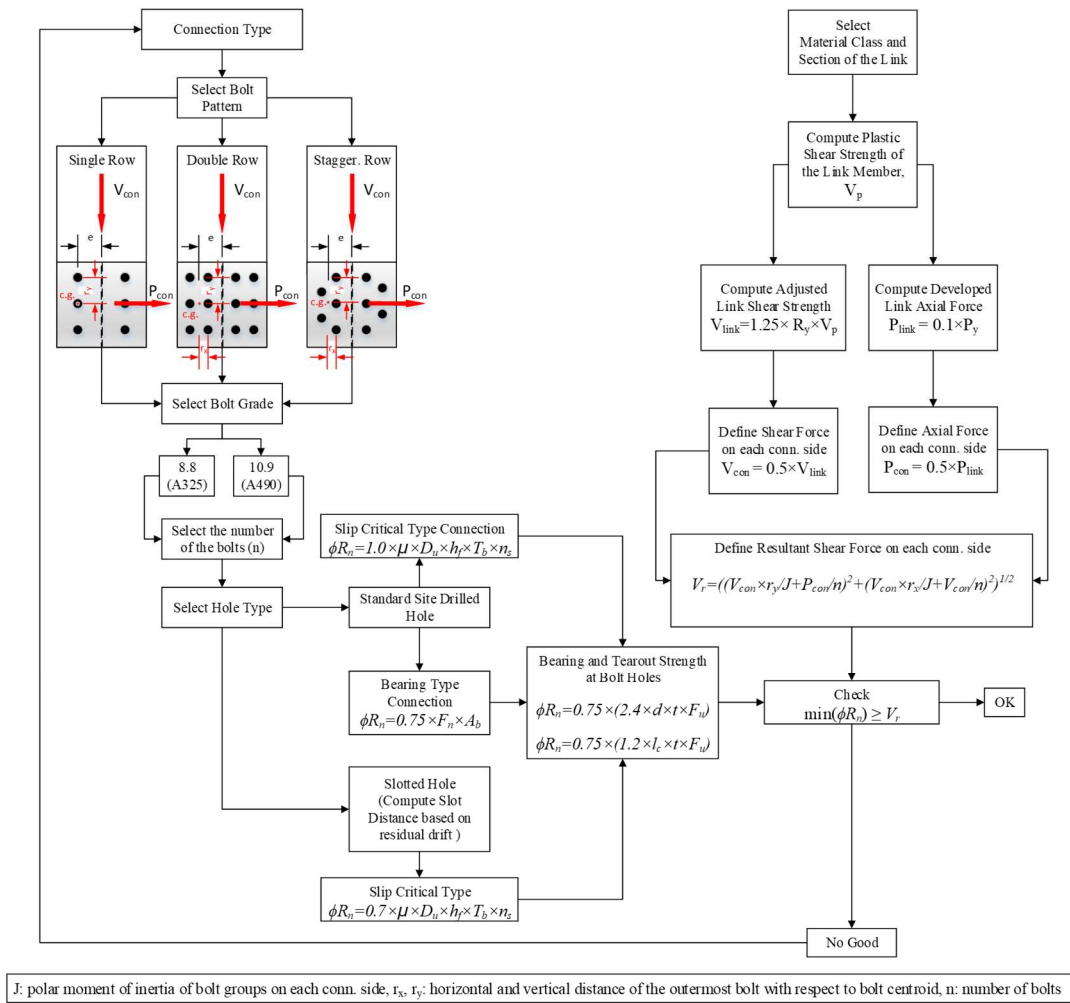


Figure 3.4. Flowchart for design of bolted connections for side plates

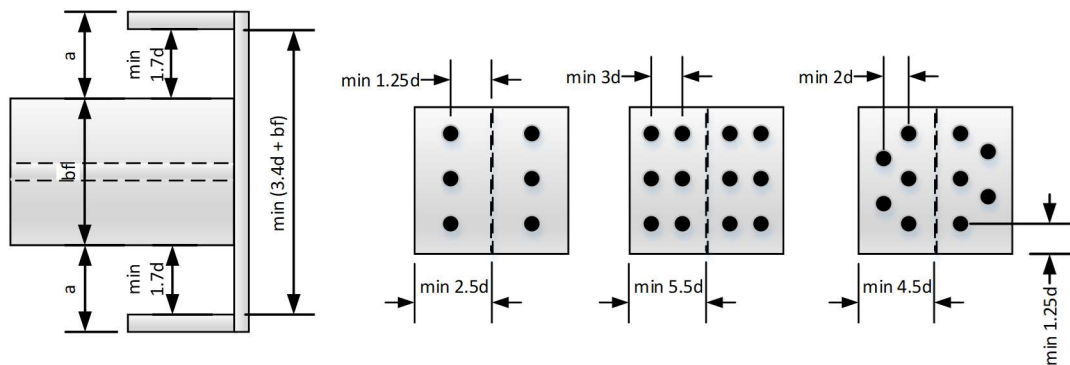


Figure 3.5. Constructive details (minimum requirements)

In order to provide easy access to the bolts, a clearance of $1.7d$ is preferred between the flange of the saw cut I-section and the link flange, where d is the bolt diameter (Figure 3.5). Due to this clearance, the saw cut I-sections cantilever out from the sides of the link. The web of the saw cut I-section is subjected to bending due to the eccentricity between the plane of the bolts and edge of the link section flange. The web may experience yielding and fracture due to excessive bending and this aspect should be considered at the design stage. A rapid remedy to this problem is to use additional stiffener plates between the flanges of the saw cut I-section as shown in Figure 3.6. Finite element studies on the local behavior of saw cut I-sections are given in the following sections.

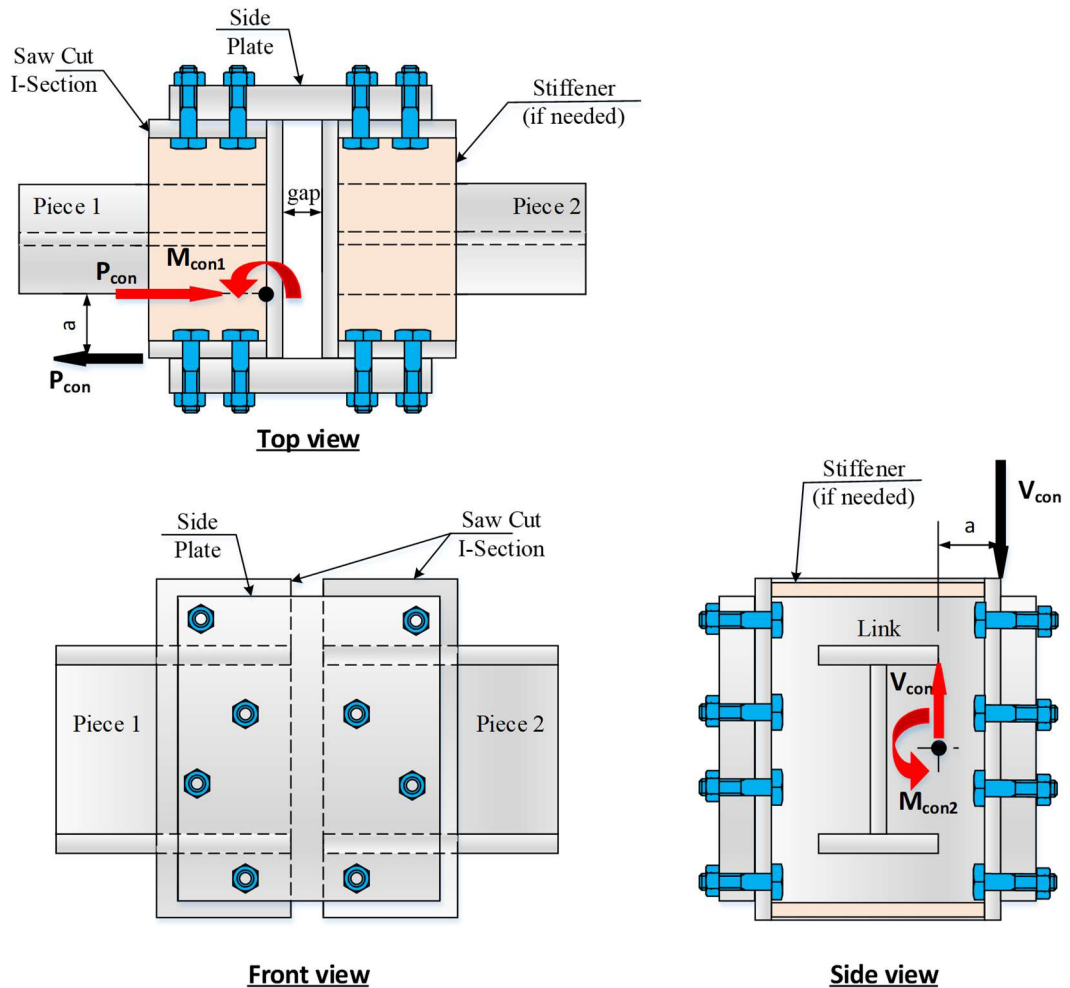


Figure 3.6. Stiffening detail for the mid-splice connection

3.4 Proof-of-concept Testing of the Proposed Link Detail

3.4.1 Test Setup and Instrumentation

The experimental program was carried out by using the test setup shown in Figure 8, which was previously employed for the research series conducted by Bozkurt et al. (2017, 2018, 2019). The height and width of the test setup were 3.5 m and 5 m, respectively. The lateral load was provided by making use of the servo-controlled hydraulic jack with 1500 kN capacity. One end of the jack was mounted to the reaction wall whereas the other was connected to the loading beam providing even lateral displacement to both the columns of the EBF. Both ends of the columns were connected to the base beam and the loading beam with pin connections. During the experiments, out-of-plane movement of the EBF was restricted by the lateral frame system installed around the EBF. In addition, the out-of-plane movements of link ends were prevented by making use of lateral restraining system. Further details of the test setup are provided in Bozkurt et al. (2017, 2018, 2019).

The link was subjected to a constant shear force (V_{link}) which can be determined from the following expression:

$$V_{link} = F_{actuator} \frac{H}{L} \quad (3.1)$$

where $F_{actuator}$ is the force applied by the actuator, h is the distance between the pin supports at column ends which is equal to 2.7 m, L is the frame width measured between the pinned column bases which is equal to 5 m.

Lateral frame displacements, the link rotation angle (γ) and relative vertical movement between the two link pieces were measured using LVDTs. The locations of LVDTs in the test setup are indicated in Figure 3.7. The link rotation angle was monitored using two methods: the vertical movement of the link ends with respect to the strong stationary floor and the tangential deviation of one of the link ends

with respect to the other was monitored by attaching an LVDT to an L-shaped frame which was welded to one of the brace-to-link joints. The detailed differences between these two measurement methods are provided in Bozkurt and Topkaya (2017). The specimens were subjected to a cyclic loading based on the AISC 341 (2016) loading protocol which is controlled by the link rotation angle.

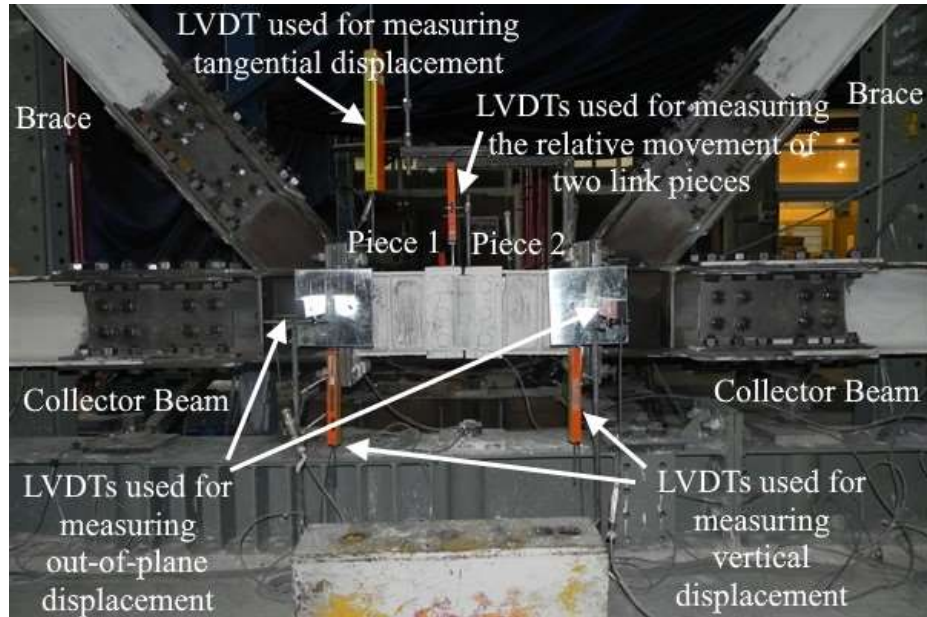


Figure 3.7. Location of LVDTs

3.4.2 Test Specimens

Three specimens were tested for the validation of the proposed replaceable link concept. The type of connection employed for the mid-splice connection was considered as the prime variable. The links were made from an IPE240 section with a total link length of 640 mm. Nominal and measured dimensions of IPE240 section are given in Table 1. The design of the links was performed by considering the material properties of the links as a European steel grade S275 with a nominal yield strength (F_y) of 275 MPa and ultimate strength (F_u) of 430 MPa. Tensile tests were conducted on the coupons extracted from the I-shapes according to EN 10002 (2001). The measured material properties are indicated in Table 2. According to the

material test results, the yield stress at 0.2% permanent elongation ($F_{y,0.2}$) is 10 and 16 percent higher than the nominal yield stress for the flanges and web, respectively. Link length ratio $\rho=e/(M_p/V_p)$, where e is the link length, M_p and V_p are respectively the plastic moment and shear capacity of the link, was kept constant throughout the experiments. The links were stiffened according to the requirements of AISC 341 with single sided stiffeners having a thickness of 10 mm. End-plated connections were utilized to attach the two replaceable link pieces to the beam-brace joint. The end-plated connections utilized 30mm thick end plates and 20 M24 bolts.

Table 3.1 Details of specimens

Sp. #	ρ Nom.	ρ Mes.	Connection Type	Res. Drift	Bolts
1	1.43	1.62	Slip Critical	-	20 M24
2	1.43	1.62	Bearing	-	12 M24
3	1.43	1.62	Slip Critical	0.5%	20 M24

Nom: Nominal, Mes: Measured, Res. Drift: Residual Drift

Table 3.2 Nominal and measured dimensions of IPE240 section

d (mm)		b_f (mm)		t_w (mm)		t_f (mm)	
Nom.	Mes.	Nom.	Mes.	Nom.	Mes.	Nom.	Mes.
240	239.37	120	119.56	6.2	6.58	9.8	9.31

d = section depth; b_f = flange width; t_w = web thickness; t_f = flange thickness; Nom: Nominal; Mes: Measured

Saw cut HEA200 sections were used for the mid-splice connection. The flanges on one side of the HEA200 were removed. The HEA200 section was welded to the IPE240 link with all around fillet welding with throat sizes of 3 mm and 7 mm for the web and flanges, respectively. Gas Metal Arc Welding (GMAW) with SG2 electrodes (similar to ER70S-6 electrodes) with a nominal tensile strength of 540 MPa was used. A gap of 10 mm was used in between the saw cut I-sections.

Specimens 1 and 2 were tested to investigate the behavior of mid-splice connection with standard holes. These specimens represent cases where the holes are drilled on site based on the positions of the holes on the flanges of the saw cut I-section. In other words, the ends of the link pieces may not perfectly align after a seismic event due to residual frame drifts. In this case, the standard holes on the side plates must be drilled on site to match the hole geometry of the saw cut I-sections. Specimen 1 was designed as a slip critical connection whereas Specimen 2 was designed as a bearing type connection. M24 European grade 8.8 bolts with an ultimate strength of 800 MPa were used for mid-splice connections. The design flowchart given in Section 3 was used to determine the number of bolts and the bolt configuration. Specimens 1 and 2 had a single bolt row with 5 and 3 bolts per flange, respectively. The coefficient of friction (μ) between the faying surfaces was considered equal to 0.3. The details of Specimens 1 and 2 are indicated in Figures 3.8 and 3.9 together with the side plate geometry.

Specimen 3 was tested to investigate the behavior of mid-splice connection with slotted holes. This specimen utilized slotted holes in both the flanges of the saw cut I-section and the side plates. Normally vertical slotted holes on the side plates should allow for installation under residual frame drifts. In order to facilitate replacement, horizontal slotted holes can also be introduced into the flanges of saw cut I-sections. In this specimen, horizontal slotted holes were also introduced. Geometrical details of Specimen 3 with its side plates are indicated in Figure 3.10. This specimen was installed under a residual frame drift of 0.5%. The details of specimens are given in Table 3.3.

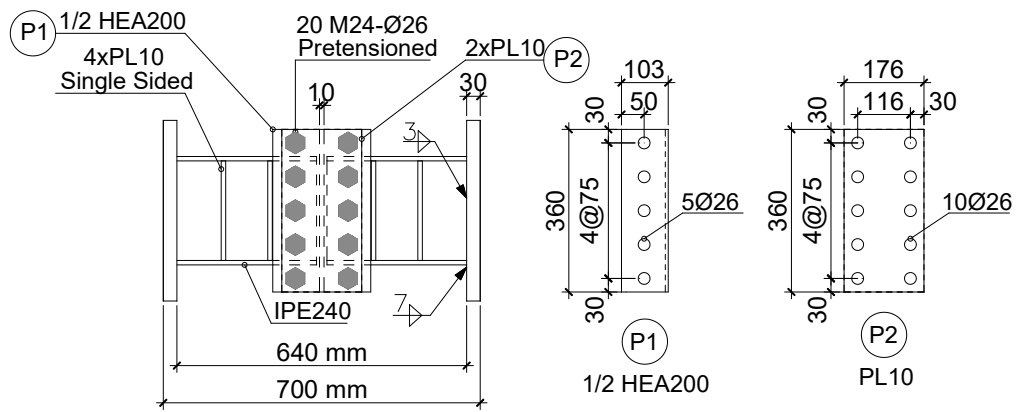


Figure 3.8. Details of Specimen 1

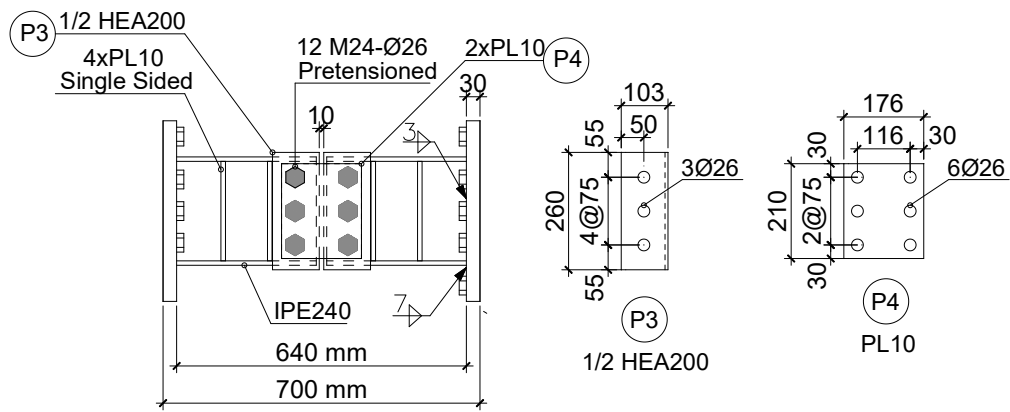


Figure 3.9. Details of Specimen 2

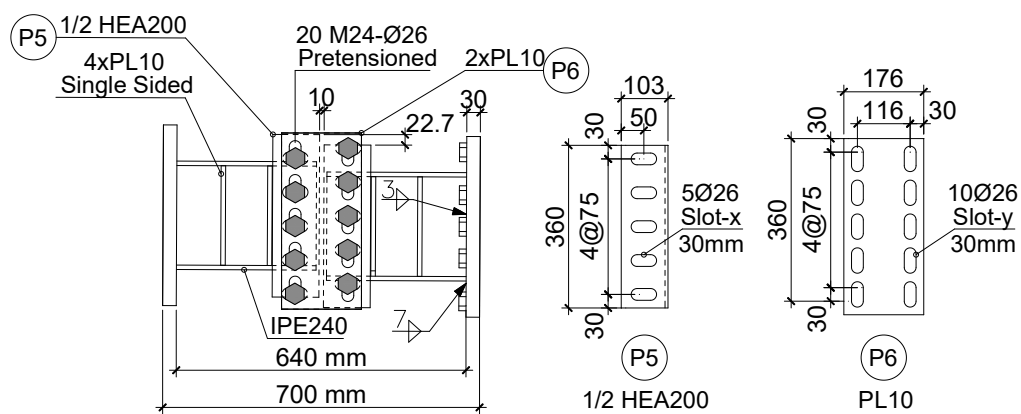


Figure 3.10. Details of Specimen 3

Table 3.3 Material properties of the IPE240 sections

Web					Flanges				
F_{yl}	F_{yu}	$F_{y,0.2}$	F_u	EL	F_{yl}	F_{yu}	$F_{y,0.2}$	F_u	EL
(MPa)	(MPa)	(MPa)	(MPa)		(MPa)	(MPa)	(MPa)	(MPa)	
310	327	318	427	29	282	294	302	412	34

F_{yl} = lower yield stress (MPa); F_{yu} = upper yield stress (MPa); $F_{y,0.2}$ = yield stress at 0.2% permanent elongation (MPa); F_u = ultimate stress (MPa); EL = elongation (%)

3.4.3 Experimental Results

The nominal and measured link length ratios of the specimens are 1.43 and 1.62, respectively. The measured link length ratio exceeded the limit for shear links ($\rho < 1.6$) by a slight margin. According to AISC341 the inelastic link rotation angle capacity should be at least 0.08 radians under the qualifying cyclic test protocol. All specimens successfully completed the 0.13 rad rotation cycle. Specimens 1 and 3 failed at positive excursion of 0.15 rad rotation and while Specimen 2 failed at negative excursion of 0.15 rad rotation. A summary of experimental results is given in Table 3.4 where plastic shear capacity, V_p determined using the measured geometrical and material properties, the maximum shear resistance (V_{max}) obtained during the experiments, overstrength, link rotation angle at failure, inelastic link rotation, inelastic story drift angle and failure mode are reported. The following expressions were used to calculate the inelastic link rotation (γ_p) and story drift angle (θ_p):

$$\gamma_p = \gamma - \frac{V_{link}}{K_{link}} \quad \theta_p = \theta - \frac{F_{actuator}}{K_{frame}} \quad (3.2)$$

where γ_p is inelastic link rotation, θ_p is inelastic story drift angle, θ is total story drift angle, K_{link} is elastic stiffness of the link, K_{frame} is elastic stiffness of the frame.

The hysteric responses of the specimens given in Figures 3.11, 3.12, and 3.13 demonstrate that all specimens exhibited stable hysteresis behavior. The failure modes observed at the end of each experiment are depicted in Figure 3.14. Specimens 1 and 3 failed due to web fracture at the left corner of the first stiffener whereas Specimen 2 failed due to flange fracture at the right bottom flange.

Table 3.4 Summary of experimental results

Sp. #	V_p (kN)	V_{max} (kN)	Link Overst.	K_{link} (kN/rad)	K_{frame} (kN/rad)	γ (rad)	γ_p (rad)	θ_p (rad)	Failure Mode
1	277	480	1.73	60299	177896	0.13	0.122	0.010	WF
2	277	480	1.73	49662	179238	0.13	0.120	0.007	TFT
3	277	476	1.72	56886	182525	0.13	0.122	0.009	WF

V_p : Measured shear strength, V_{max} : the maximum shear resistance, γ : Rotation Capacity, γ_p : Inelastic Rotation Capacity, θ_p : Inelastic Story Drift Angle, TFT: Top flange tearing; WF: web fracture

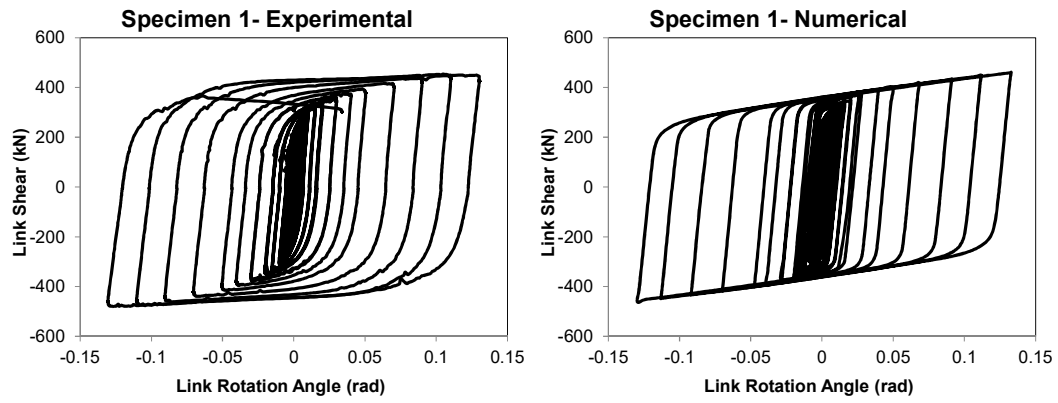


Figure 3.11. Hysteretic behavior of Specimen 1

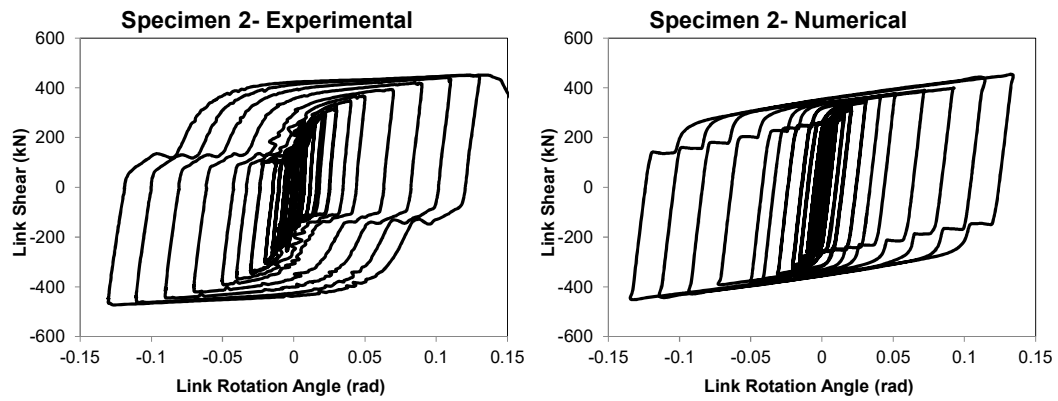


Figure 3.12. Hysteretic behavior of Specimen 2

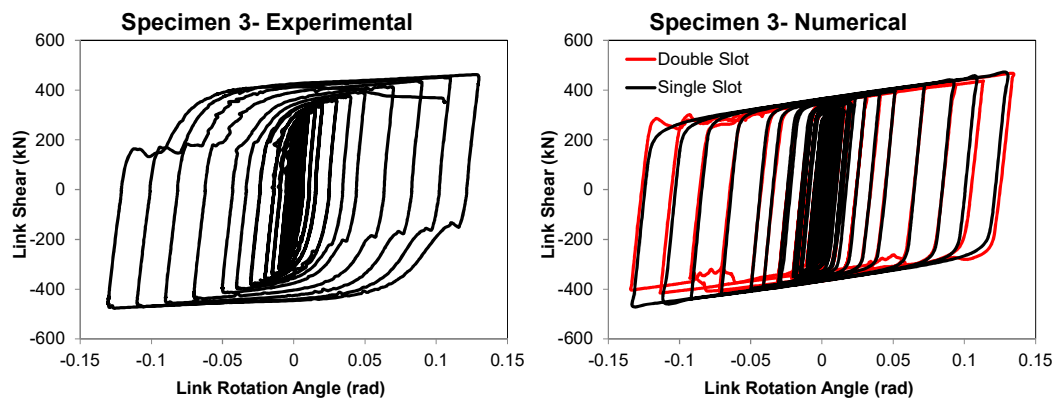


Figure 3.13. Hysteretic behavior of Specimen 3

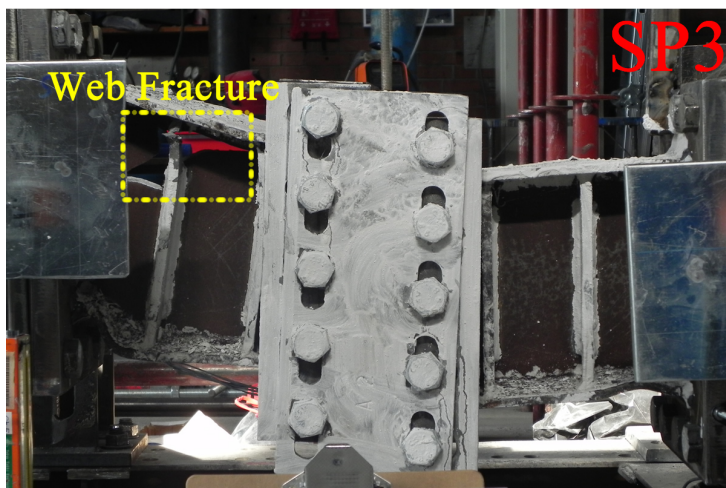
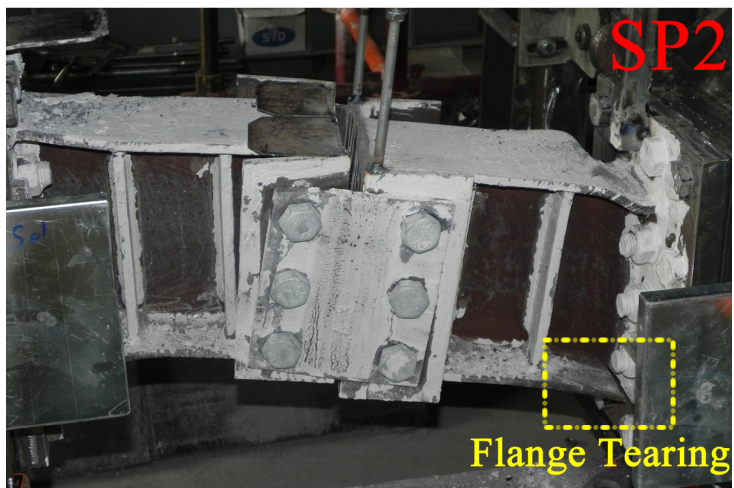
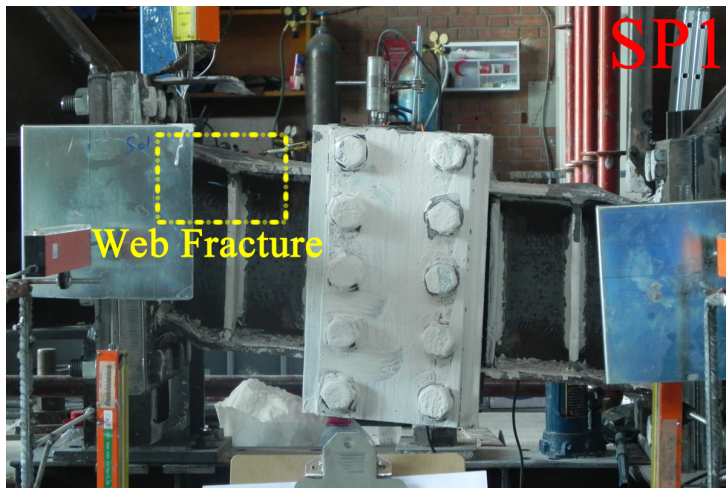


Figure 3.14. Failure modes

The variation of the relative vertical movement between the two link pieces are given in Figures 3.15, 3.16, and 3.17. The mid-splice connection in Specimen 1 was designed as a slip critical connection and the maximum relative moment between the pieces was only 1.01 mm indicating that the two pieces were almost perfectly connected to each other at mid-length. The hysteretic behavior given in Figure 3.11 consists of full cycles with no indication of sudden increase in the link rotation angle which can be due to slip at the faying surfaces. The mid-splice connection in Specimen 2 was designed as a bearing type connection and the maximum relative moment between the pieces was 15.29 mm. The hysteretic behavior, given in Figure 3.12, shows sudden increases in link rotation angle with a slight increase in the applied link shear. These are attributable to the slip that took place in the faying surfaces. The sign of slip was first evident in the 0.0075 rad rotation cycle. The slip resulted in a decreased energy dissipation capacity for Specimen 2 when compared with those of Specimen 1. The energy dissipated at each rotation cycle is reported in Figure 3.18 for all specimens. In addition, the energy dissipated by Specimens 2 and 3 were normalized with the energy dissipated by Specimen 1 to make a comparison. The normalized energy dissipation is also given in Figure 3.18. According to the results, the decrease in energy dissipation is very limited. In the last complete cycle with 0.13 rad rotation, the energy dissipation decreased by only 11% due to slip at the connections. Although the mid-splice connection in Specimen 3 was designed as a slip critical connection and the maximum relative moment between the pieces was 16.75 mm. As shown in Figure 3.13 the specimen experienced slip at the faying surfaces. The overall behavior is similar to the behavior of Specimen 2. The sign of slip was evident during the cycle with 0.05 rad rotation. The unexpected slip at the faying surfaces can be attributable to the use of double slotted holes, one vertical and one horizontal for each bolt. In general, only one plate has a slotted hole and the other employs a standard hole. In this particular specimen, a horizontal slotted hole is introduced which resulted in a significant loss in the contact area and in turn resulted in slip at lower force levels. Nevertheless, the specimen was capable of

successfully completing the cycles and fulfilled the testing requirements of AISC341. The decrease in energy dissipation was less than that of Specimen 2. When compared with Specimen 1, the energy dissipation decreased by only 5% in the last complete cycle with 0.13 rad rotation. It should be noted that the relative movement between the pieces is a result of the rotation of the side plates as shown in Figure 3.19.

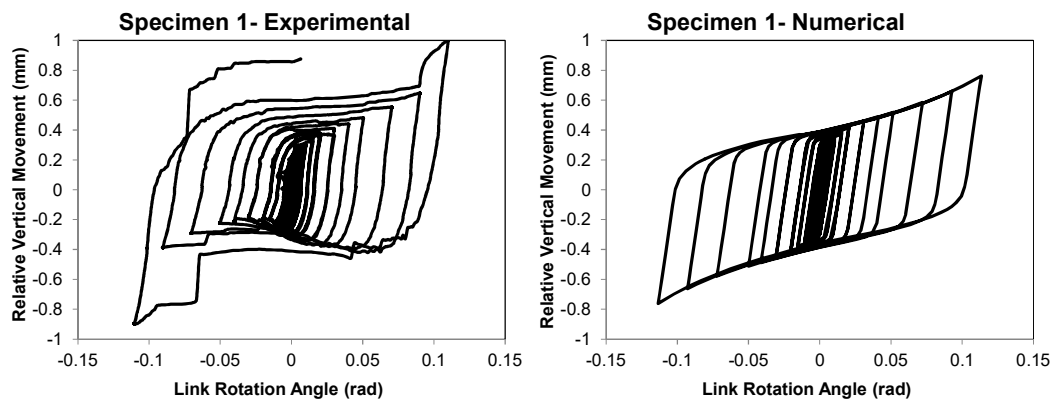


Figure 3.15. Relative vertical movement between the two link pieces (Specimen 1)

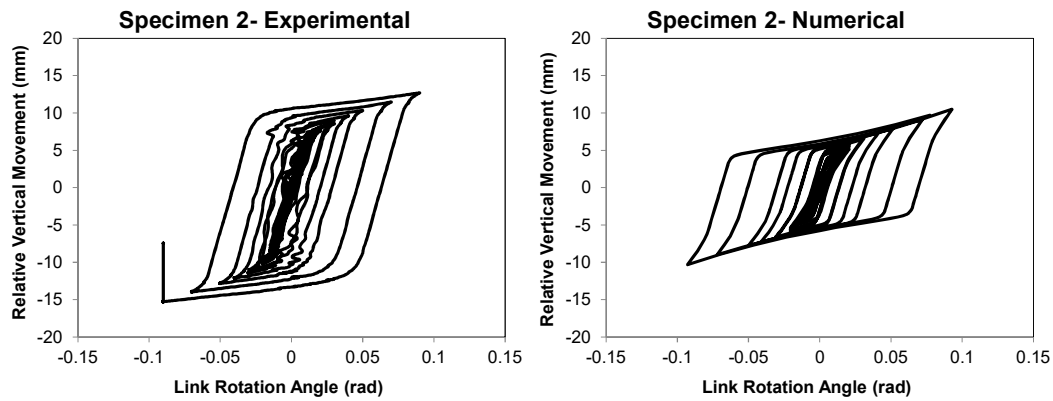


Figure 3.16. Relative vertical movement between the two link pieces (Specimen 2)

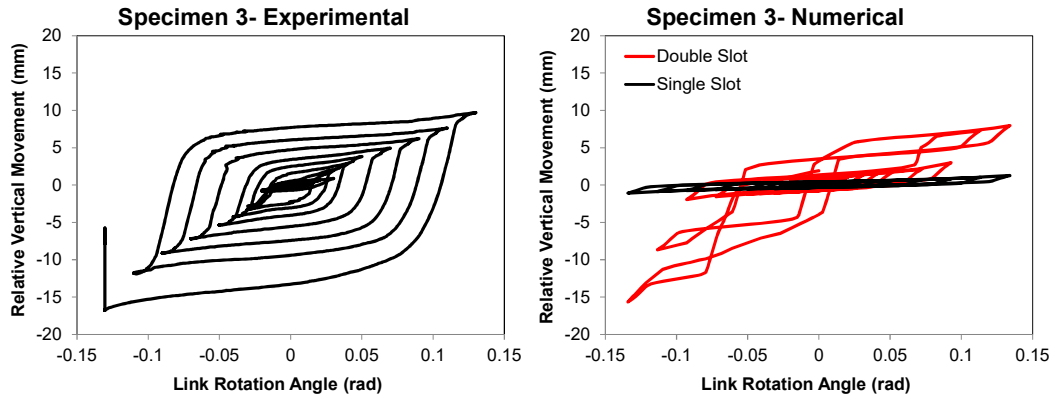


Figure 3.17. Relative vertical movement between the two link pieces (Specimen 3)

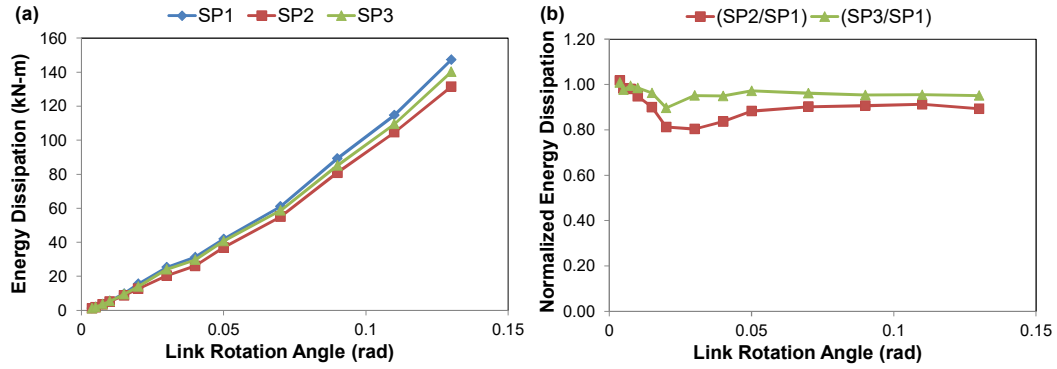


Figure 3.18. Energy dissipation of specimens

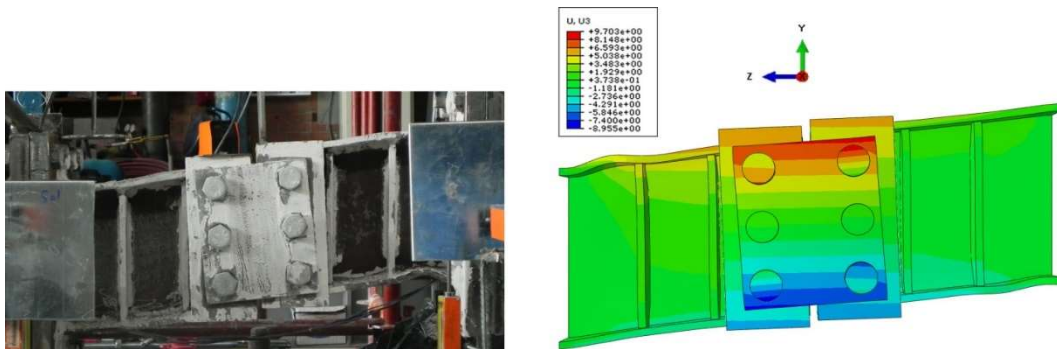


Figure 3.19. In-plane rotation of side plates (Specimen 2)

The clear distance between the flanges of the saw cut I-section was observed to change due to bending of the web. As discussed in Section 3.3, the web is subjected to bending moments due to the eccentricity between the outer face of the saw cut I-section and the edge of link flange. The specimens experimented as a part

of this study did not employ stiffeners to circumvent the bending problem and should therefore be considered as the most vulnerable design detail. A representative deformed shape of the saw cut I-sections during the last cycles of testing is given in Figure 3.20 for Specimen 2. Among all specimens, the amount of bending deformation was the highest for this specimen.

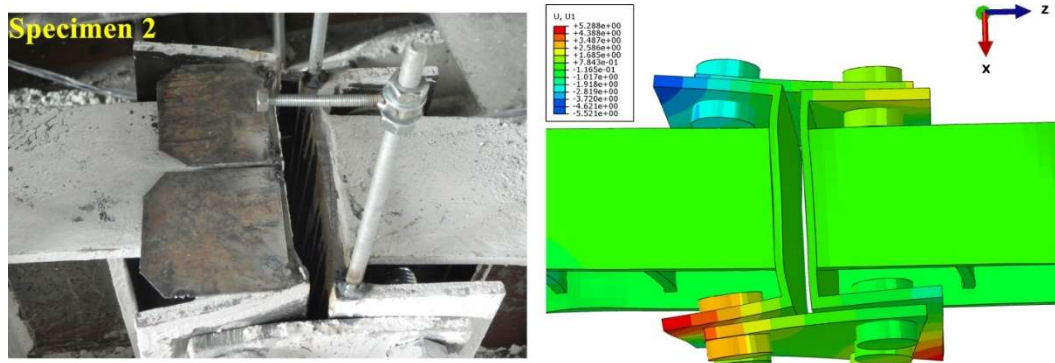


Figure 3.20. Deformation of saw cut I-sections (Specimen 2)

It should be emphasized that the proposed replaceable link connections which were exposed to excessive deformations were easily demounted after cyclic loading due to the presence of a 10 mm gap. The proposed new replaceable link connections were also easily assembled without the need for a hydraulic jack. The experimental program demonstrated the potential of the proposed link concept. The following section presents details of a complementary numerical study.

3.5 Numerical Study

A complementary finite element parametric study has been conducted to investigate issues that were not addressed in the proof-of-concept testing. The specific topics include quantifying the axial force developed in the links as a result of the axial restraining effect of the connecting members, stiffening of saw cut I-sections, and verification of the proposed link concept on larger links than tested.

3.5.1 Finite Element Modeling Details and Verification

A commercially available finite element package Abaqus 6.12-1 was employed for numerical analysis. In order to reduce computational time, only isolated links were modeled. No significant difference was reported for the results of between isolated and full models (Bozkurt et al., 2019). For finite element model verification cyclic analyses were conducted where the models were subjected to the loading protocol given in AISC341.

All elements including the link, stiffeners, mid-splice connection and bolts were meshed by eight-node linear brick elements with reduced integration (C3D8R). A finer mesh was utilized for the parts where contact behaviors were defined since contact simulations are quite sensitive to mesh size. On the other hand, a relatively coarser mesh size was used for the rest of the model. Typical mesh details are demonstrated in Figure 3.21. The interactions between the mid-splice connection components such as bolts and side plate or side plate and flange of the saw cut I-section were simulated by defining surface-to-surface interaction. Tangential behavior with the coefficient of friction (μ) of 0.3 was considered. A typical model consists of more than 224540 nodes and 171250 elements. A typical analysis lasts averagely for three days. Geometrical and material nonlinearities were taken into account in the numerical models.

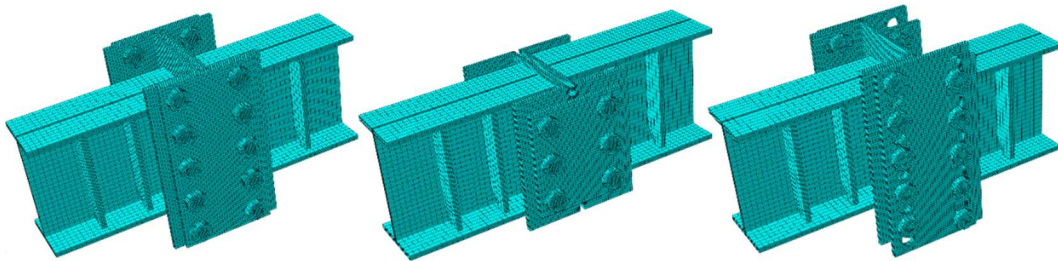


Figure 3.21. Mesh configurations

The pretension force equal to 70% of bolt tensile strength was applied to the bolts using “Bolt Load” option in Abaqus. Boundary conditions were defined to simulate actual boundary conditions of the full model of the test setup. All rotational and axial movements of the link ends were restrained. MPC constraints were defined to the ends of the link since the end-plated connections of the link were not modeled explicitly. Tie constrain was used between the welded parts instead of modeling welding explicitly. A combined kinematic and isotropic hardening model was utilized to simulate the cyclic response of the material. Since cyclic stress and strain curve is not available, stress and strain relationship obtained from monotonic loading was defined as half-cycle test data in order to simulate approximately cyclic response of the material.

The hysteretic behaviors of the specimens obtained from numerical analysis are indicated in Figures 3.11, 3.12, and 3.13. Comparisons with experimental results show that the finite element models were capable of accurately simulating the behavior. Slip at the faying surfaces can be simulated by FE models as shown in the behaviors of Specimens 2 and 3. For the third specimen, two cases were analyzed, where one case has double slots like the experimented specimen and the other has a vertical slot only. When the behaviors of these cases are compared, it is evident that introducing a second slotted hole results in slip at the connections. This observation strengthens the assertion that introducing double slotted holes has an adverse effect on the connection performance and should therefore be avoided. The simulations of relative vertical movement between the saw cut I-sections are given in Figures 3.15, 3.16, and 3.17. The general trend and the maximum amplitude of the vertical movement are accurately represented by the FE models. Deformed shapes given in Figures 3.19 and 3.20 indicate that deformation patterns can also be accurately predicted by the numerical models. The in-plane rotation of the side plates and the deformation of the saw cut I-sections can be simulated using numerical analysis. The following sections outline the details of parametric studies that employed the aforementioned FE modeling details.

3.5.2 Prediction of Design Axial Force

Bozkurt et al. (2019) studied the axial force developed in a detachable link while it is being subjected to rotation. The level of axial force is important for the design of the mid-splice connection and depends on the type of connection adopted. The detachable link proposed by Bozkurt et al. (2019) employs end-plated connections for the mid-splice detail. This type of a connection provides considerable axial stiffness to the link and according to their findings the link axial force can be as high as 50 percent of the axial yielding capacity of the link (P_y). In the proposed link concept the axial stiffness of the detachable link depends significantly on the geometrical properties of the saw cut I-sections. As shown in Figure 3.20, the saw cut I-section webs are susceptible to bending deformations which results in a significant loss of axial stiffness. Therefore, the particular problem of a detachable link with saw cut I-sections at mid-length should be studied by numerical analysis.

Table 3.5 Properties of detachable links used to study axial force effect

Model	Link Section	Saw Cut I-Section	Side Plate thickness (mm)	Bolt Grade	Bolt Diameter	Friction Coefficient	Link Length Ratio	Link Length (mm)
1	IPE240	1/2HEA200	10	8.8	M24	0.3	0.5	224
2	IPE240	1/2HEA200	10	8.8	M24	0.3	1.0	447
3	IPE240	1/2HEA200	10	8.8	M24	0.3	1.6	715
4	HEB300	1/2HEA500	25	10.9	M27	0.4	0.5	541
5	HEB300	1/2HEA500	25	10.9	M27	0.4	1.0	1081
6	HEB300	1/2HEA500	25	10.9	M27	0.4	1.6	1730
7	HEA500	1/2HEA500	25	10.9	M27	0.5	0.5	618
8	HEA500	1/2HEA500	25	10.9	M27	0.5	1.0	1236
9	HEA500	1/2HEA500	25	10.9	M27	0.5	1.6	1977

Pursuant to this goal, a parametric study has been undertaken to determine the level of axial force produced in links with various sizes and link length ratios. Three different link sizes, IPE240, HEB300, HEA500, were considered where the links are from S275 steel. The parameters considered in the study are summarized in

Table 3.5. Single row bolted slip-critical connections with standard holes were considered in all models. All links were subjected to a monotonic loading up to 0.13 radians of link rotation. Two models were analyzed for each case in order to study the effects of the presence of stiffeners. One of these models had a stiffener placed in between the flanges of the saw cut I-section to reduce the amount of deformations that take place in this element whereas the other model did not have any stiffeners. The axial forces developed in the links were collected and normalized by P_y . The variation of the normalized link axial force with the link length ratio is indicated in Figure 3.22. According to the results, the level of axial force increases with an increase in the link length ratio. The stiffened cases produce slightly more axial force when compared with the unstiffened cases. Overall, the maximum axial force produced in the links reached to 10% of the axial yield strength of the link. Depending on the flexibility of the mid-splice connection and the link length ratio, the normalized axial forces can be less than 10% of P_y . From a practical standpoint, an axial force level equal to $0.1 \times P_y$ is recommended for the design of the links proposed in this study.

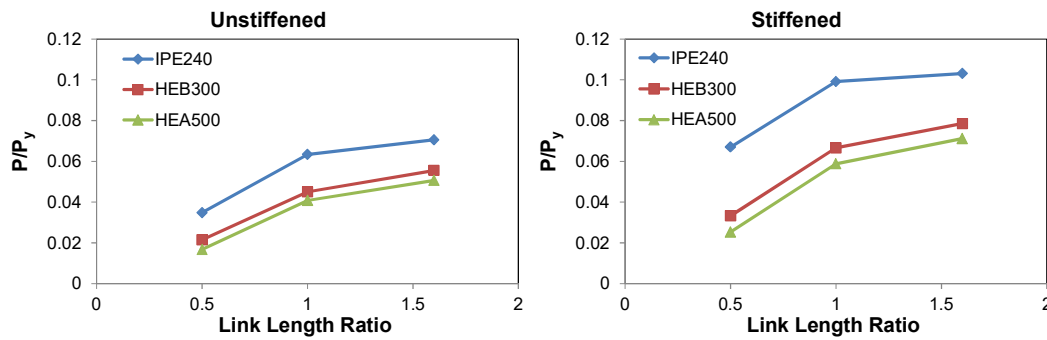


Figure 3.22. Axial force developed in the proposed detachable link

3.5.3 Stiffening of Saw Cut I-sections

The webs of saw cut I-sections are subjected to significant bending strains in the proposed replaceable link. The amount of bending strains depend significantly on the distance (a) between the edge of the link flange and the outer face of the flange

of saw cut I-section as shown in Figure 3.5. The parametric study has been extended to investigate the bending effect and the need for stiffeners to reduce the amount of bending. Pursuant to this goal, IPE240, HEB300 and HEA500 links investigated in the previous section were considered. The geometric details are identical to the ones reported in Table 3.5. The link length ratio was considered equal to unity in all models. In order to study the influence of the eccentricity of connection, “ a ” values of 50 mm, 75 mm, 100 mm, 125 mm and 150 mm were considered. The links were subjected to monotonic loading up to a link rotation angle of 0.13 radians. The results were investigated by examining the principal strains produced along a path on the web of the saw cut I-section. As shown in Figure 3.23, the path was parallel to the top flange of the link section and along the web of the saw cut I-section. The principal strains were normalized by the yield strain and reported in Figures 3.24, 3.25, and 3.26 for the cases studied. The results showed that the maximum strains occur at a point which coincides with the end of the link flange. The amount of bending strains increase with an increase in the distance (a). The maximum distance (a) should be kept below 75 mm to keep the principal bending strains less than $5 \times \epsilon_y$. In cases where this distance cannot be maintained, stiffeners can be attached to the saw cut I-section to reduce the bending effects. For each link, a model with $a=150$ mm and with stiffeners was also considered. The results shown in Figures 3.24, 3.25, and 3.26 indicate that the bending effects can be significantly reduced by stiffening of the saw cut I-section.

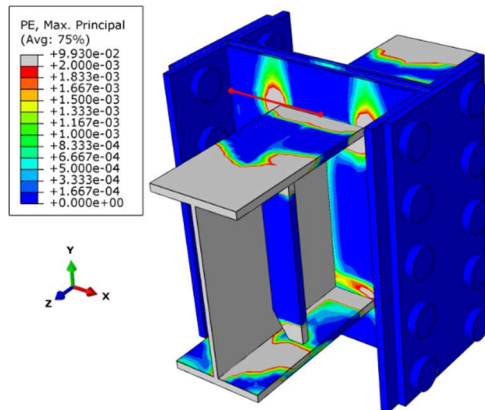


Figure 3.23. Location of the path for recording maximum principal strain variations

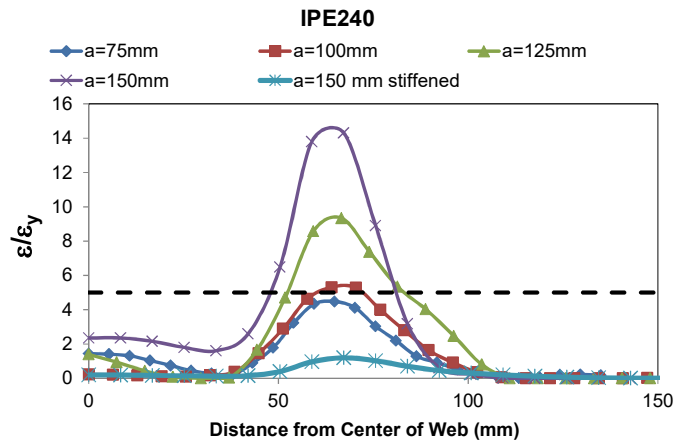


Figure 3.24. Strain variation along a path (IPE240 links)

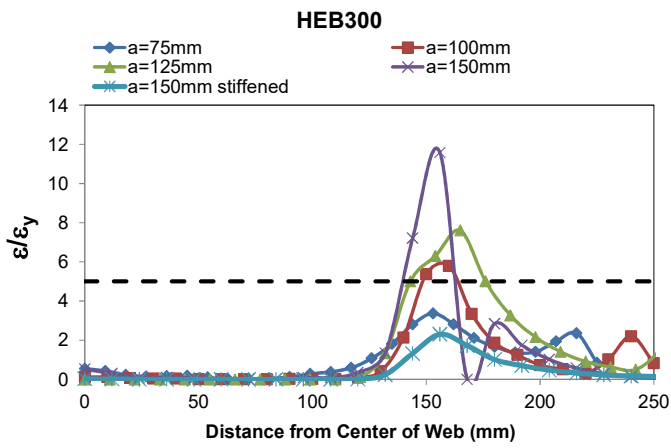


Figure 3.25. Strain variation along a path (HEB300 links)

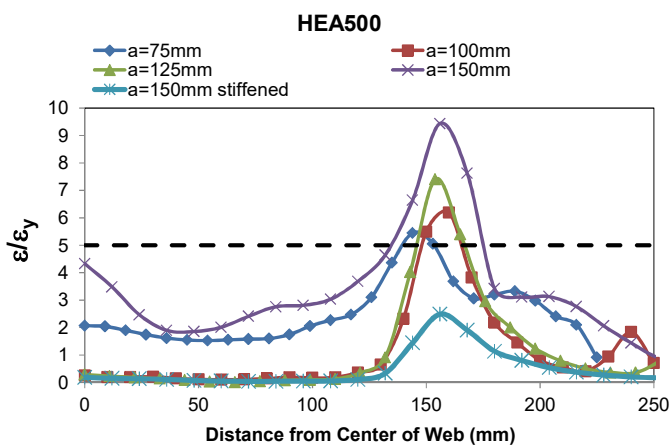


Figure 3.26. Strain variation along a path (HEA500 links)

3.5.4 Investigation of Larger Links

Fracture of steel members is a complex phenomenon and depends significantly on the loading history. The propensity of fracture for links larger than the ones studied experimentally has been investigated by making use of finite element analysis. The idea here is to compare the behavior of tested links and larger ones to demonstrate that the proposed link concept can also be applied to other link sections with higher shear capacity. The evaluations used the rupture index (RI) as a measure to quantify the propensity of link fracture. Rupture index proposed by El-Tawil et al. (1999) can be calculated as follows:

$$RI = \frac{PEEQ}{\exp\left(-1.5 \frac{p}{q}\right)} \quad (3.3)$$

where PEEQ is the plastic equivalent strain and calculated as the ratio of effective plastic strain to yield strain. PEEQ is a measure of local plastic strain demand and higher values of PEEQ indicate potential damage and vulnerability; p and q are hydrostatic pressure and von Mises stress, respectively. The calculation of PEEQ, p and q are given in following equations:

$$PEEQ = \sqrt{\frac{2}{3} \varepsilon_{ij}^p \varepsilon_{ij}^p} \quad (3.4)$$

$$p = -\frac{1}{3} tr(\sigma_{ij}) = -\frac{1}{3} \sigma_{ii} \quad (3.5)$$

$$q = \sqrt{\frac{3}{2} S_{ij} S_{ij}} \quad (3.6)$$

where ε_{ij}^p stand for the plastic strain, σ_{ij} is Cauchy stress and S_{ij} is deviatoric stress.

The RI values were calculated for the IPE240 links studied in the experimental program. The cyclic loading history was considered and the RI value after the completion of 0.13 radian cycle is reported as 3.87, 3.76 and 3.61 for specimens 1,

2, and 3, respectively. The *RI* contours for these three specimens are given in Figure 3.27.

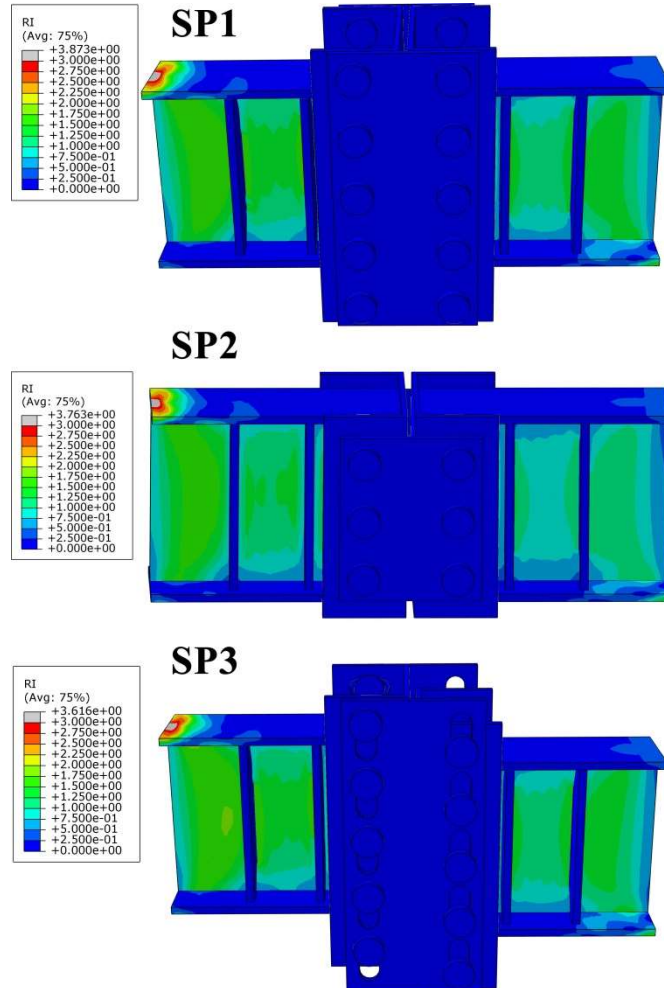


Figure 3.27. Rupture index for experimented specimens

Six models were considered with HEA500 links to study the behavior of links with higher shear capacities. The parametric details of these models are indicated in Table 3.6. In all models, 10.9 grade M27 bolts were considered. The saw cut I-section employed in the models was HEA500 as well. The AISC loading protocol was applied to these models until the end of the cycle with 0.13 radian rotation. The *RI* contours given in Figure 3.28 indicate that the maximum *RI* for these models range between 2.92 and 3.49. These values demonstrate that the proposed detachable link concept can be applied to links with higher shear capacities. The *RI*

of the parametric study models are less than their counterparts from experimented specimens. This complementary study demonstrated that the proposed mid-splice connection detail can be employed using different bolt configurations, connection types and coefficient of friction.

Table 3.5 Properties of detachable links used to study behavior of larger links

Model #	Section	Link Length	# of bolts	Bolt Pattern	Connection Type	Stiffener	Friction Coefficient
1	HEA500	1000	20	Single Row	Bearing	S	0.3
2	HEA500	1000	36	Single Row	Slip Critical	S	0.3
3	HEA500	1000	24	Single Row	Slip Critical	S	0.5
4	HEA500	1000	36	Staggered	Slip Critical	S	0.5
5	HEA500	1000	40	Double Row	Slip Critical	S	0.3
6	HEA500	1000	64	Double Row	Slip Critical	S	0.5

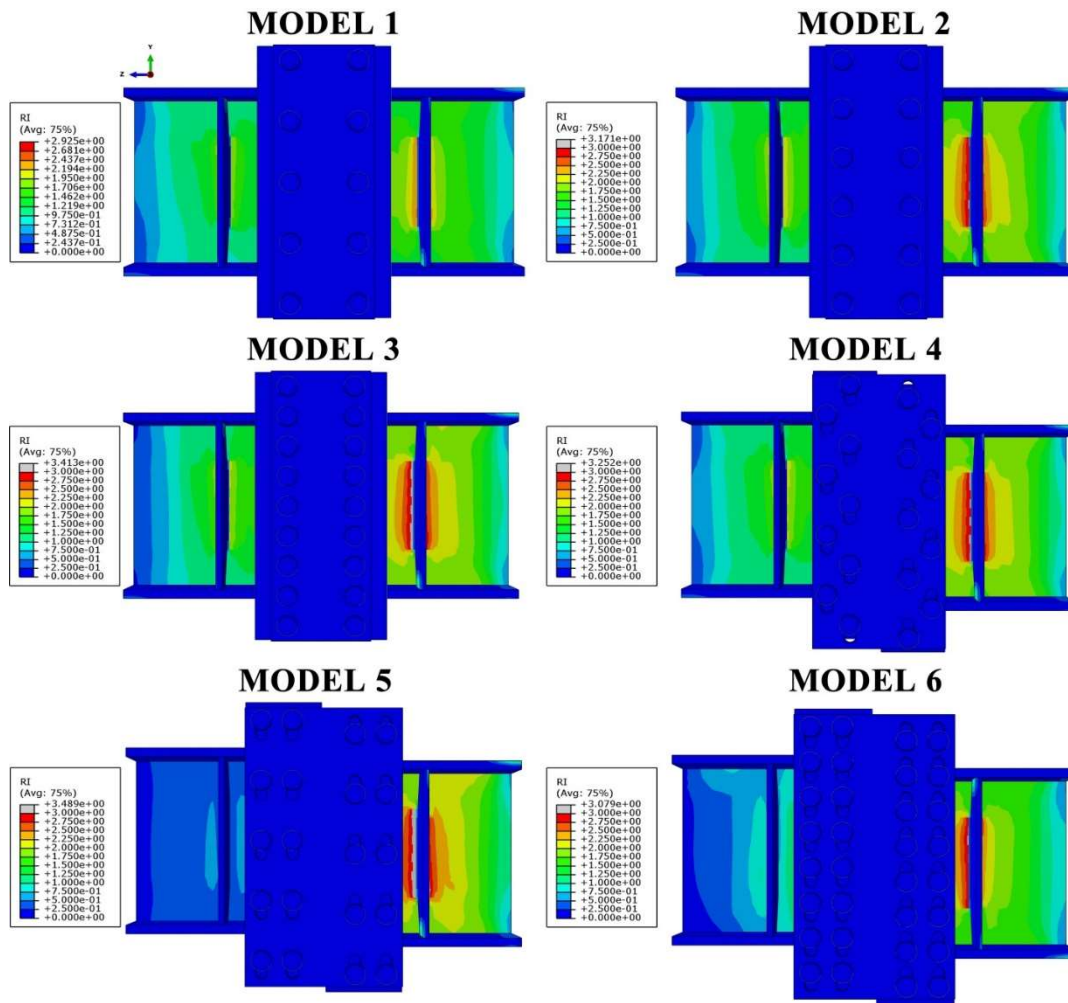


Figure 3.28. Rupture index for HEA500 links

CHAPTER 4

FRICITIONAL MID-SPLICED END-PLATED REPLACEABLE LINKS

4.1 Background

Seismic energy is generally dissipated by the structural members, which leads to severe damage to these members. Energy dissipaters have been introduced in order to enhance the energy dissipation of the structures by adding additional dampers. Friction dampers are one of the energy dissipaters that dissipate energy with a non-destructive mechanism. These friction dampers exhibit stable hysteresis behavior and enhance seismic durability (Monir and Zeynali, 2013).

Slotted bolted connection is one of the friction dampers that dissipates energy through frictional resistance between the faying surface clamped by the bolts with a predefined pretension force. The experiments were conducted by researchers (Tremblay, 1993; Grigorian and Popov, 1994) in order to investigate the effects of the different faying surfaces such as mild steel, high hardness steel, brass, brake lining pad, stainless steel, aluminum, and rubber to the hysteresis behavior. It was concluded that using the materials having the same properties as faying surfaces leads to fluctuations in hysteresis behavior. Using brass and mild steel was recommended to obtain stable hysteresis behavior (Grigorian and Popov, 1994; Petty, 1999)

In this chapter, it is aimed to increase the low-cycle fatigue life of the replaceable links by friction dampers. Slotted holes are provided in order to allow relative sliding movement, which leads to frictional energy dissipation.

4.2 Frictional Mid-Spliced Link Concept and Design

The very same mid-spliced link concept described in Chapter 3 was utilized in the proposed frictional mid-spliced replaceable links. In addition to the concept of the mid-spliced link (Chapter 3), herein brass shims were employed between side plates and saw cut I-sections (Figure 4.1) in order to take advantage of stable frictional resistance provided by faying surfaces of side plates. The proposed system dissipates energy and increases low-cycle fatigue life of the replaceable links by yielding the link as well as friction between the brass shims and side plates. The energy will be mainly dissipated by frictional surfaces until the bolts come into contact with the edge of the slotted holes. After this point on, the energy will be dissipated by the yielding of the link until the direction of the load is reversed.

The very same design described in Chapter 3 can be utilized herein except that only bearing type of connection is employed in order to allow the slip at the faying surfaces. The loads applied to the bolts should exceed the resistance of slip critical connection so that the faying surfaces slip relative to each other. Slotted holes are introduced to side plates in order to allow the relative movement between the two pieces of the replaceable link. This proposed link concept also allows the replacement under residual drift conditions.

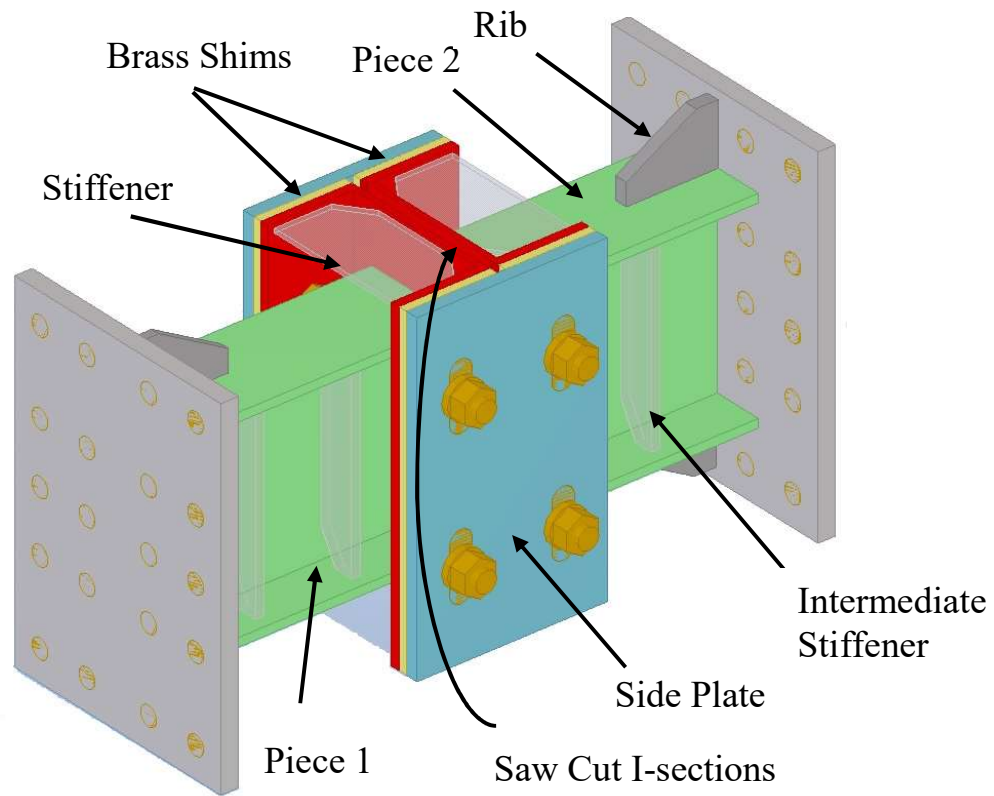


Figure 4.1. Proposed frictional mid-spliced replaceable link concept

4.3 Experimental Program

The experimental setup and instrumentations which were used in Chapter 3 were also utilized in this research program. A total of eleven links were tested as a part of this study. The first three specimens (LCF1-LCF3) were conventional extended end-plated replaceable links and these were tested to investigate the low-cycle fatigue life. The other eight specimens were the replaceable links with proposed frictional mid-spliced connection (FR1-FR8). All specimens were made from the IPE240 section. Nominal and measured dimensions of IPE240 section are given in Table 4.1. All specimens were designed considering European S275 steel with a yield stress of 275 MPa and ultimate stress of 430 MPa. In order to obtain material properties of ordered IPE240 sections, tensile tests were performed on the coupons

extracted from the links, saw cut I-section and side plate according to EN 10002. The measured material properties are indicated in Tables 4.2 and 4.3. For all specimens, the ribs were introduced to increase the rotation capacity of the link. Nominal and measured link length ratios of 1.17 and 1.23 were kept constant throughout the experiments. Intermediate stiffeners having a thickness of 10 mm were welded on one side of the links according to the requirements of AISC 341. All specimens were connected to the frame using the extended end-plated connections having 20 mm plate thickness with 20 M24 pretensioned bolts.

Table 4.1 Nominal and measured dimensions of IPE240 sections

IPE240	d (mm)	b _f (mm)	t _w (mm)	t _f (mm)
Nominal	240.00	120.00	6.20	9.80
Measured	240.83	119.63	6.36	9.49

d = section depth; b_f = flange width; t_w = web thickness; t_f = flange thickness

Table 4.2 Material properties of the IPE240 and HEA200 sections

Section	Web					Flanges				
	F_{yl}	F_{yu}	$F_{y,0.2}$	F_u	EL	F_{yl}	F_{yu}	$F_{y,0.2}$	F_u	EL
	MPa	MPa	MPa	MPa		MPa	MPa	MPa	MPa	
IPE240	399	415	406	534	24	327	343	336	495	25
HEA200	437	439	439	554	19	341	348	351	511	25

F_{yl} = lower yield stress (MPa); F_{yu} = upper yield stress (MPa); $F_{y,0.2}$ = yield stress at 0.2% permanent elongation (MPa); F_u = ultimate stress (MPa); EL = elongation(%)

Table 4.3 Material properties of the side plate

Plate Thickness	F_{yl}	F_{yu}	$F_{y,0.2}$	F_u	EL
(mm)	(MPa)	(MPa)	(MPa)	(MPa)	
15	295	300	300	396	37

The specimens can be classified into two categories. The first category includes specimens LCF1-LCF3, which were designed to investigate the low-cycle fatigue life of replaceable links with the extended end-plate connection. These specimens were subjected to constant amplitude cycles of 0.03, 0.09 and 0.15 rad rotation. On the other hand, the second category includes specimens FR1-FR8 which were designed to examine the performance of the proposed frictional mid-spliced connection detail for the replaceable links considering the slot size, the number of bolts and the number of slotted holes (double or single sided slotted holes) used in the mid-spliced connection as the main variables. Saw cut HEA200 sections were used for all specimens as described in Chapter 3. Furthermore, stiffeners were employed between the flanges and web of the saw cut I-sections in order to eliminate any possible bending of the mid-splice connection. M24 European grade 10.9 bolts with an ultimate strength of 1000 MPa were used for both mid-splice connections and extended end-plated connections. Slotted holes were introduced into the side plates to allow for slip at the faying surfaces. Two types of side plates were used depending on the hole type. For all side plates, two rows of holes were introduced where each row is used to attach the side plate to the flange of saw cut I-section. In the first type, a single row of slotted holes was used and the other row employed standard holes. In the second type, both the rows employed slotted holes. Two slot lengths of 25 mm and 50 mm were considered. Moreover, a total of eight and twelve bolts were considered for the mid-spliced connection. The details of specimens are given in Table 4.4.

Table 4.4 Details of specimens and applied loading protocol

Sp #	Slot Size (mm)	Slot #	# of bolts	Loading Protocol
LCF1	NA	NA	NA	0.03 rad*
LCF2	NA	NA	NA	0.09 rad*
LCF3	NA	NA	NA	0.15 rad*
FR1	50	SS	8	AISC+0.17 rad*
FR2	50	SS	8	0.17 rad*
FR3	50	DS	8	AISC+0.17 rad*
FR4	50	DS	8	0.17,0.2, 0.23 rad*
FR5	25	DS	8	0.17 rad*
FR6	25	SS	8	0.17 rad*
FR7	25	DS	12	0.17 rad*
FR8	25	SS	12	0.17 rad*

DS: Double Sided, SS: Single Sided, NA: Not Applicable

*constant amplitude cycles

Specimens FR1-FR2 are identical replaceable links with frictional mid-spliced connection where single sided slotted holes of 50 mm with 8 bolts were employed. The only difference is the applied loading protocol. Specimen FR1 was subjected to AISC loading protocol up to 0.15 rad and additional constant amplitude cycles of 0.17 rad whereas specimen FR2 was subjected to constant amplitude cycles of 0.17 rad. Specimens FR3 and FR4 are identical where double sided slotted holes of 50 mm with 8 bolts were employed. Similar to specimens FR1-FR2, only difference is the applied loading protocol. Specimen FR3 was subjected to AISC loading protocol up to 0.15 rad and additional constant amplitude cycles of 0.17 rad whereas specimen FR4 was subjected to constant amplitude cycles of 0.17, 0.20 and 0.23 rad.

Specimens FR5 and FR6 employed 25 mm slotted holes with 8 bolts. These specimens were subjected to constant amplitude cycles of 0.17 rad. The difference is that double sided slotted holes were utilized in specimen FR5 while single sided

slotted holes were used in specimen FR6. Slot sizes of 25 mm were also employed in specimens FR7 and FR8. For these specimens, however, 12 bolts were utilized. Both specimens were exposed to constant amplitude cycles of 0.17 rad. Similar to specimens FR5 and FR6, only difference between FR7 and FR8 is that double sided slotted holes were utilized in specimen FR7 while single sided slotted holes were used in specimen FR8. Technical drawings of the specimens are given in Figures 4.2-4.8.

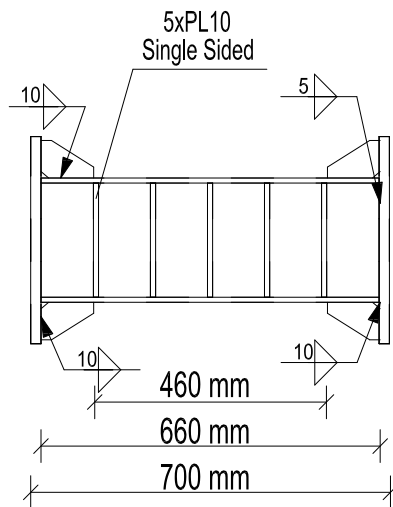


Figure 4.2. Technical drawings of specimens LCF1-LCF3

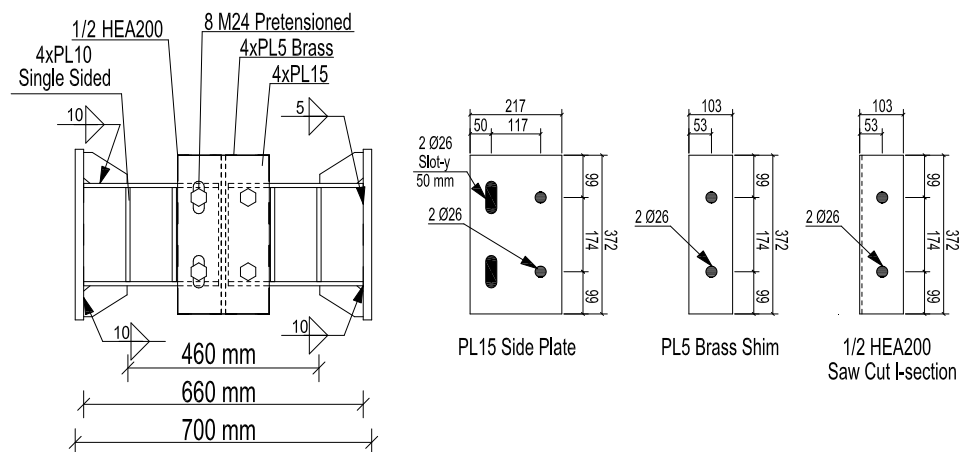


Figure 4.3. Technical drawings of specimens FR1 and FR2

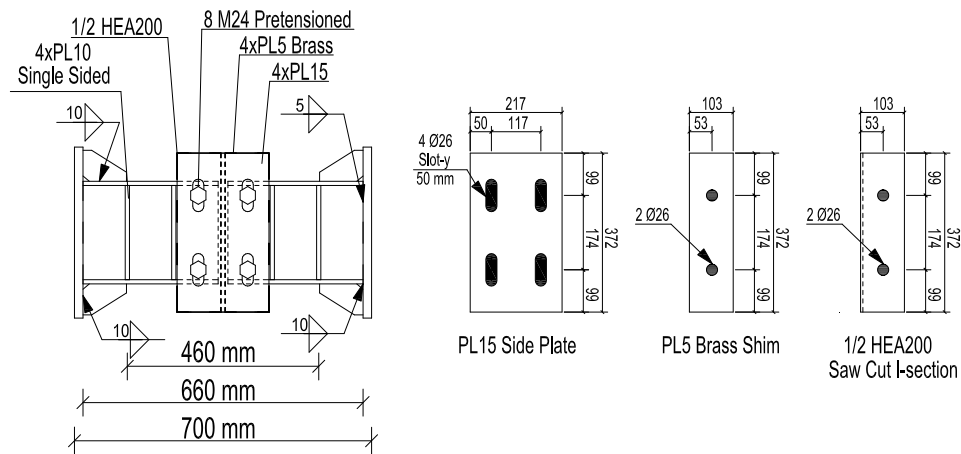


Figure 4.4. Technical drawings of specimens FR3 and FR4

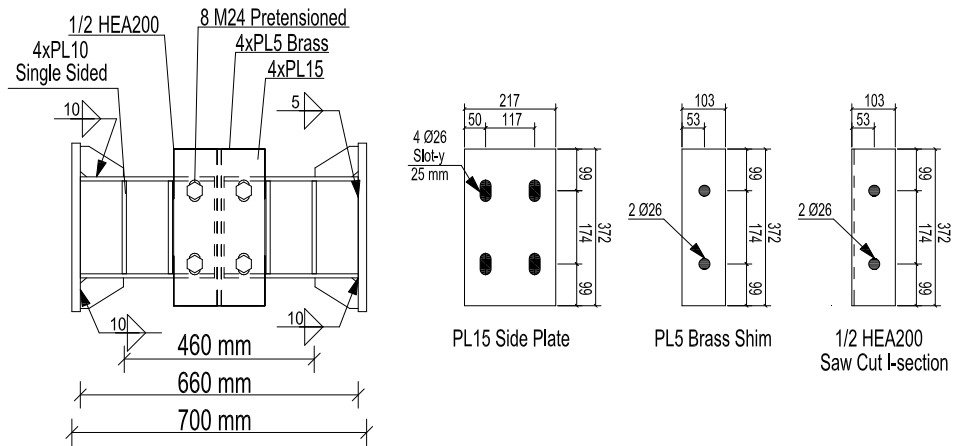


Figure 4.5. Technical drawings of specimens FR5

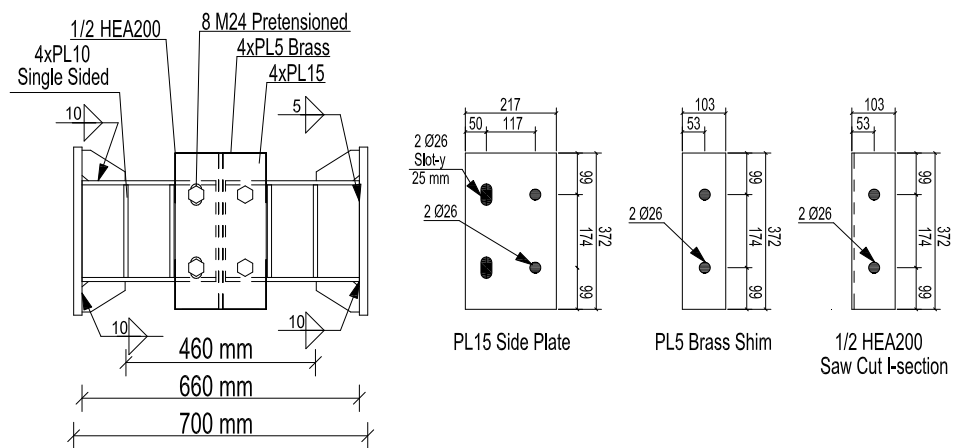


Figure 4.6. Technical drawings of specimens FR6

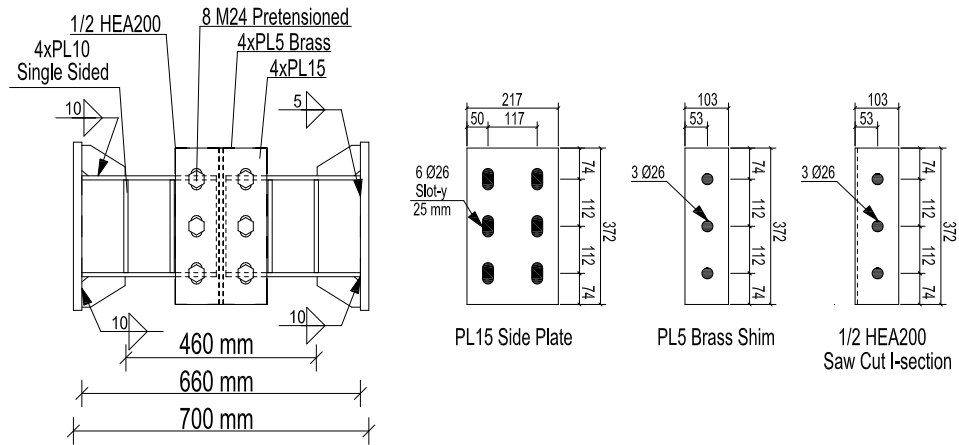


Figure 4.7. Technical drawings of specimens FR7

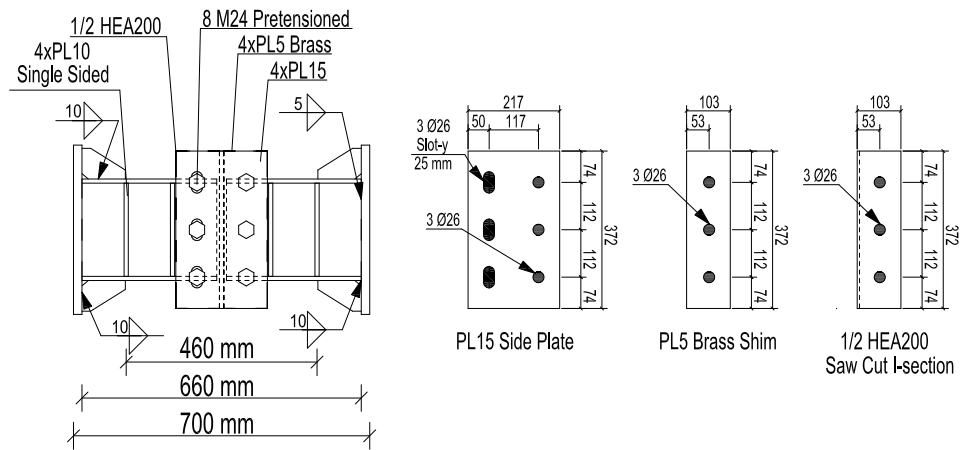


Figure 4.8. Technical drawings of specimens FR8

4.4 Experimental Results

The first three specimens (LCF1-LCF3) were tested under constant amplitude cycles in order to investigate low cycle fatigue behavior of the replaceable links with the extended end-plated connection. These specimens were subjected to constant amplitude cycles of 0.03, 0.09 and 0.15 rad rotation. Although the link with frictional mid-splice connection was subjected to constant cycles of 0.17 rad, for the specimen with extended end-plated connection 0.15 rad rotation was

selected. The reason for this is that the study conducted by Bozkurt et al. (2018) revealed that the link may not even be able to endure one cycle for large rotations. Therefore, the maximum cycle of 0.15 rotation was selected. Hysteretic responses of these specimens are depicted in Figure 4.9. These specimens failed due to web fracture (Figure 4.10). Table 4.5 summarizes the experimental results of these specimens in terms of maximum shear (V_{max}), total energy dissipation, maximum link rotation angle and the number of cycles successfully completed by the link. A link is considered to complete a cycle by reaching positive and negative displacements corresponding to the rotation value of the cycle. Overstrength values given in Table 4.5 indicate that all specimens exhibited more shear resistance than the plastic shear capacity of the link. Specimen LCF1 sustained 51 cycles at 0.03 rad up to failure while specimen LCF2 completed 6.5 cycles at 0.09 rad. On the other hand, specimen LCF3 endured only 2.5 cycles at 0.15 rad. It is seen that the number of cycles dramatically decreased as the severity of the rotation (cycle range) increases. Moreover, the total energy dissipated by specimens were 899.09 kN-m, 424.45 kN-m and 322.70 kN-m for LCF-1, LCF-2 and LCF-3, respectively. As the intensity of the constant amplitude decreases, the dissipated total energy increases. Furthermore, the results revealed that the link can fail at a few cycles of a large rotation or very low rotation with a large number of cycles. Therefore, it is crucial to increase the maximum rotation capacity as well as the number of cycles.

The number of cycles completed by the specimens are compared with the cycles calculated using the damage law proposed by Bozkurt et al. (2018). A generalized damage law for shear links was developed by Bozkurt et al. (2018) to predict the instant of fracture initiation. The required expressions to compute the generalized damage law is given in Eqns 4.1-4.4. According to proposed damage law, the experimented specimens of LCF1, LCF2 and LCF3 should sustain cycles of 58, 6.5 and 2.5, respectively. These results are very compatible with the experimental findings.

$$D = \bar{C} \sum_{i=1}^{\bar{N}} (\Delta\gamma_i)^{2.0} \quad (4.1)$$

where D is amount of damage, in the range 0 (undamaged) and 1 (full damage), \bar{N} is the number of damaging cycles, $\Delta\gamma_i$ is the range of the i^{th} cycle and \bar{C} , structural performance parameter, is calculated as follows:

$$\bar{C} = \begin{cases} \left(\frac{F_y}{E}\right) (20\gamma_u^{-2.16}) & \text{if } 0.035 \leq \gamma_u \leq 0.11 \\ \left(\frac{F_y}{E}\right) (2350) & \text{if } \gamma_u \geq 0.11 \end{cases} \quad (4.2)$$

where

$$2\gamma_u \approx \gamma_B = 8.7K_s(\alpha) \frac{1}{\beta^2} \quad (4.3)$$

where γ_u is rotation angle at which buckling is anticipated for the link web under cyclic loading, γ_B is link rotation angle measured from the farthest point of zero shear to the point of buckling, β is web slenderness (h/t_w), α is web panel aspect ratio a/h where a is the stiffener spacing, and K_s , the plate buckling coefficient, can be determined as follows considering clamped-end conditions for the link web:

$$K_s(\alpha) = \begin{cases} 8.98 + \left(\frac{5.60}{\alpha^2}\right) & \text{if } \alpha \geq 1 \\ 5.60 + \left(\frac{8.98}{\alpha^2}\right) & \text{if } \alpha \leq 1 \end{cases} \quad (4.4)$$

Table 4.5 Summary of experimental results of specimens LCF1-LCF3

Sp. #	V_p (kN)	V_{\max} (kN)	Overstrength	$N_f @ \gamma$ (rad)	TED (kN-m)
LCF1	346	447	1.29	51@0.03rad	899.09
LCF2	346	529	1.52	6.5@0.09rad	424.45
LCF3	346	577	1.67	2.5@0.15rad	322.70

TED: Total energy dissipation; N_f : Number of cycles

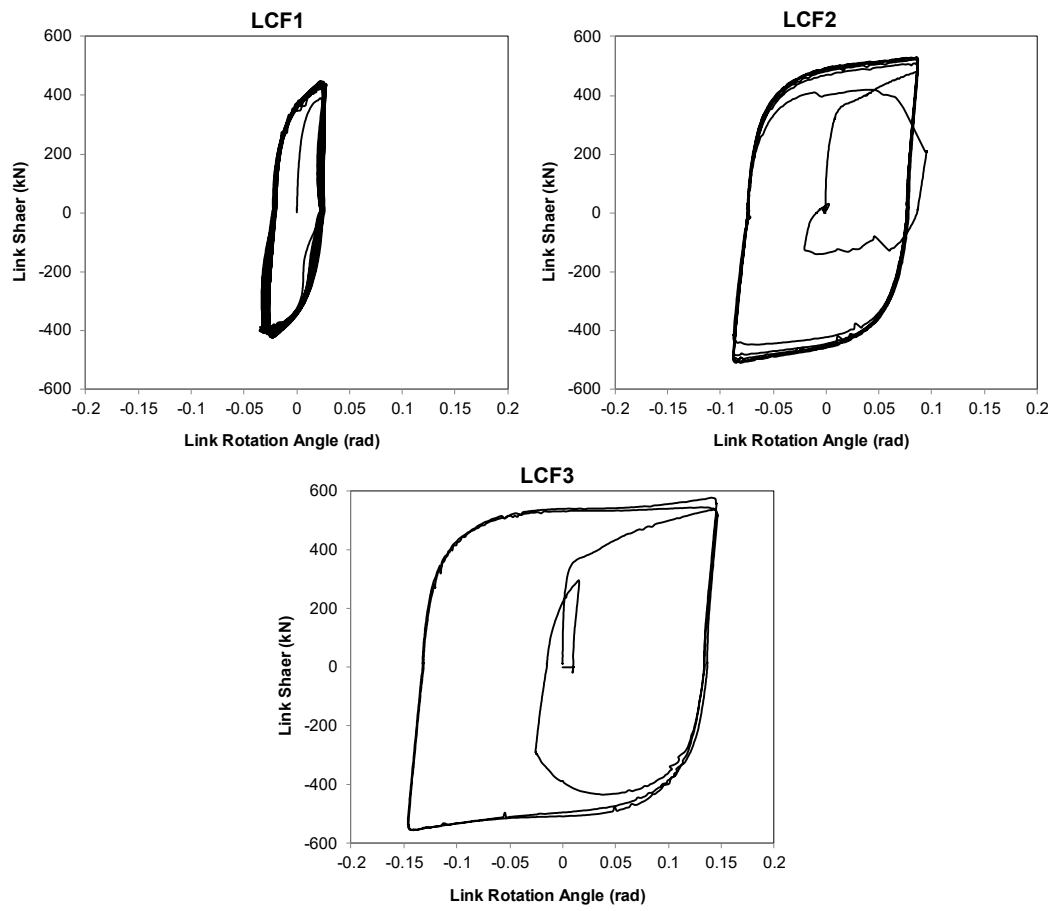


Figure 4.9. Hysteretic response of specimens LCF1-LCF3

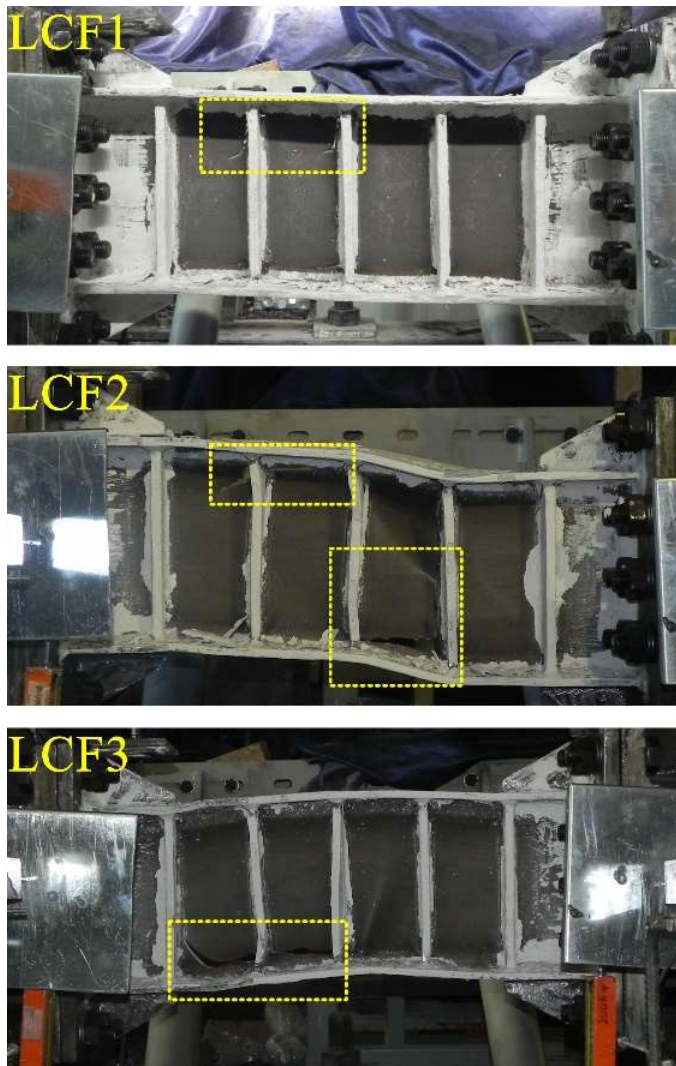


Figure 4.10. Failure modes of specimens LCF1-LCF3

The remaining experimented specimens were the ones with frictional mid-spliced connection (FR1-FR8). Specimens FR1 and FR3 were subjected to the loading protocol mandated by AISC up to 0.15 rad rotation and then a constant amplitude cycle of 0.17 rad was repeated. Specimen FR1 employing single sided slotted holes of 50 mm sustained 2.5 cycles of 0.17 rad whereas Specimen FR3 employing double sided slotted holes of 50 mm completed 9.5 cycles of 0.17 rad. Specimen FR2 employing single sided slotted holes of 50 mm endured 17 cycles of 0.17 rad. On the other hand, Specimen FR4 employing double sided slotted holes of 50 mm was subjected to constant amplitude cycles of 0.17, 0.2 and 0.23 rad. The specimen

sustained 43 cycles of 0.17 rad rotation without failure. After this point the rotation amplitude was increased to 0.2 rad and 0.23 rad to trigger fracture. The specimen endured additional 2 cycles of 0.2 rad followed by 4.5 cycles of 0.23 rad. In order to promote failure, the slot size was reduced from 50 mm to 25 mm for specimens FR5-FR8. Specimen FR5 employing double sided slotted holes sustained 8 cycles of 0.17 rad while specimen FR6 employing single sided slotted holes completed 5 cycles of 0.17 rad. The number of bolts was increased from 8 to 12 for specimens FR7 and FR8. Specimen FR7 employing double sided slotted holes sustained 12.5 cycles of 0.17 rad whereas specimen FR8 employing single sided slotted holes endured 5 cycles of 0.17 rad. Hysteretic responses of the specimens are given in Figures 4.11 and 4.12. A summary of the experimental results is given in Table 4.6. All specimens failed due to web fracture as shown in Figure 4.13 The damage was initiated at the bottom of the second panel of the left piece of the link in specimens FR5-FR8 while the damage was initiated in the upper part of the second panel of the right piece of the link in specimens FR1-FR4.

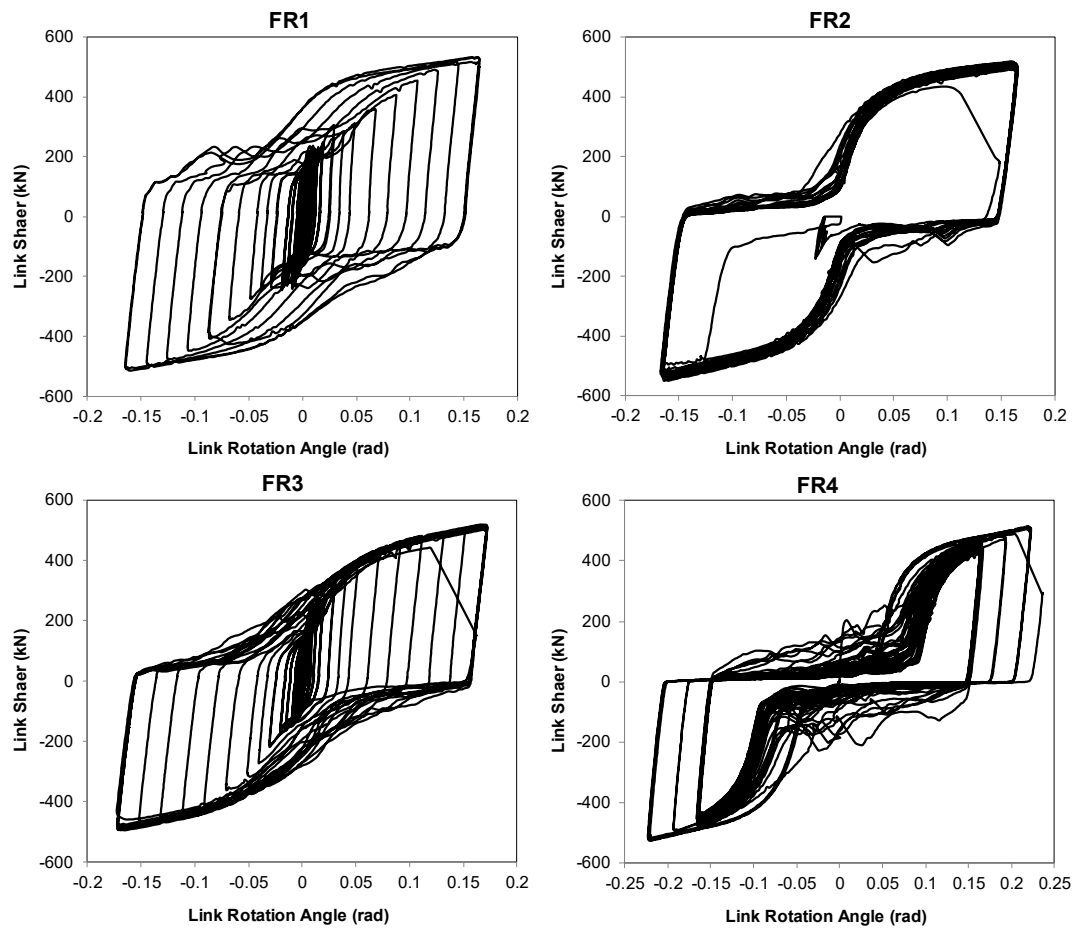


Figure 4.11. Hysteretic response of specimens FR1-FR4

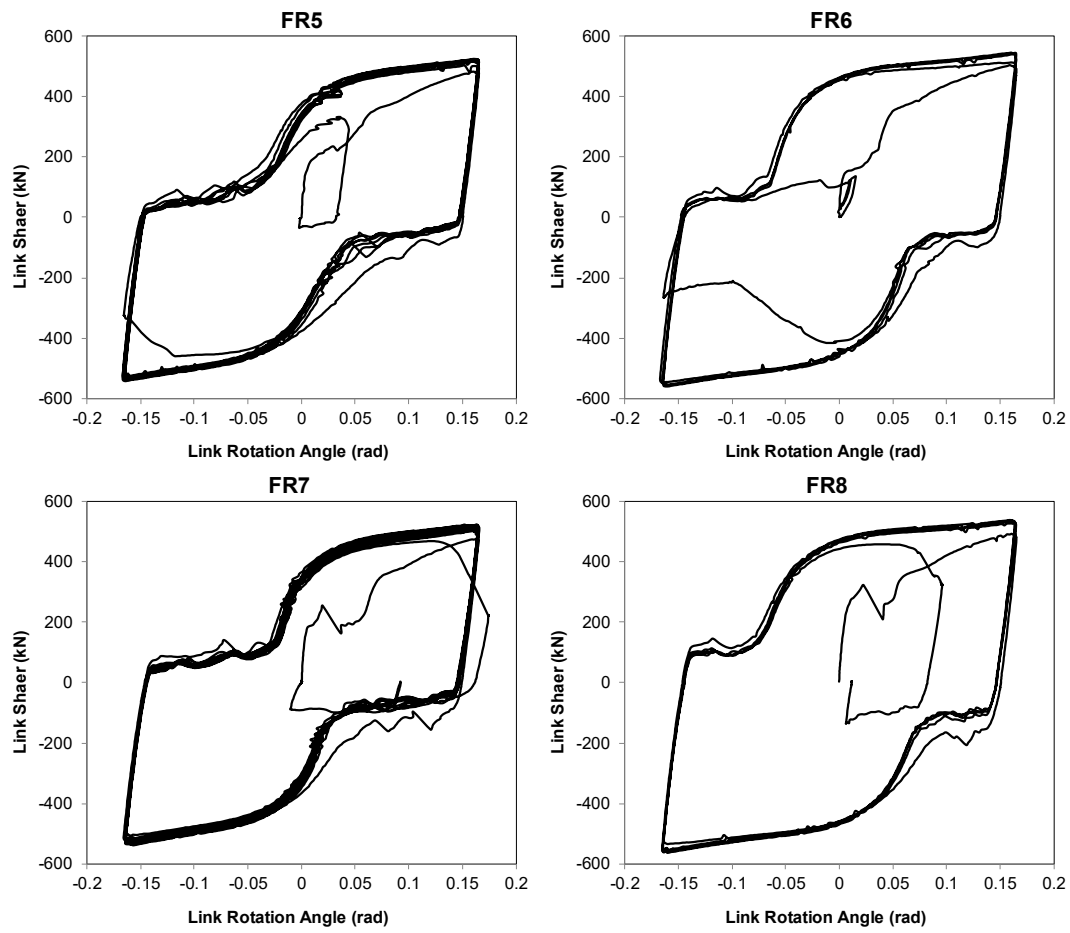


Figure 4.12. Hysteretic response of specimens FR5-FR8

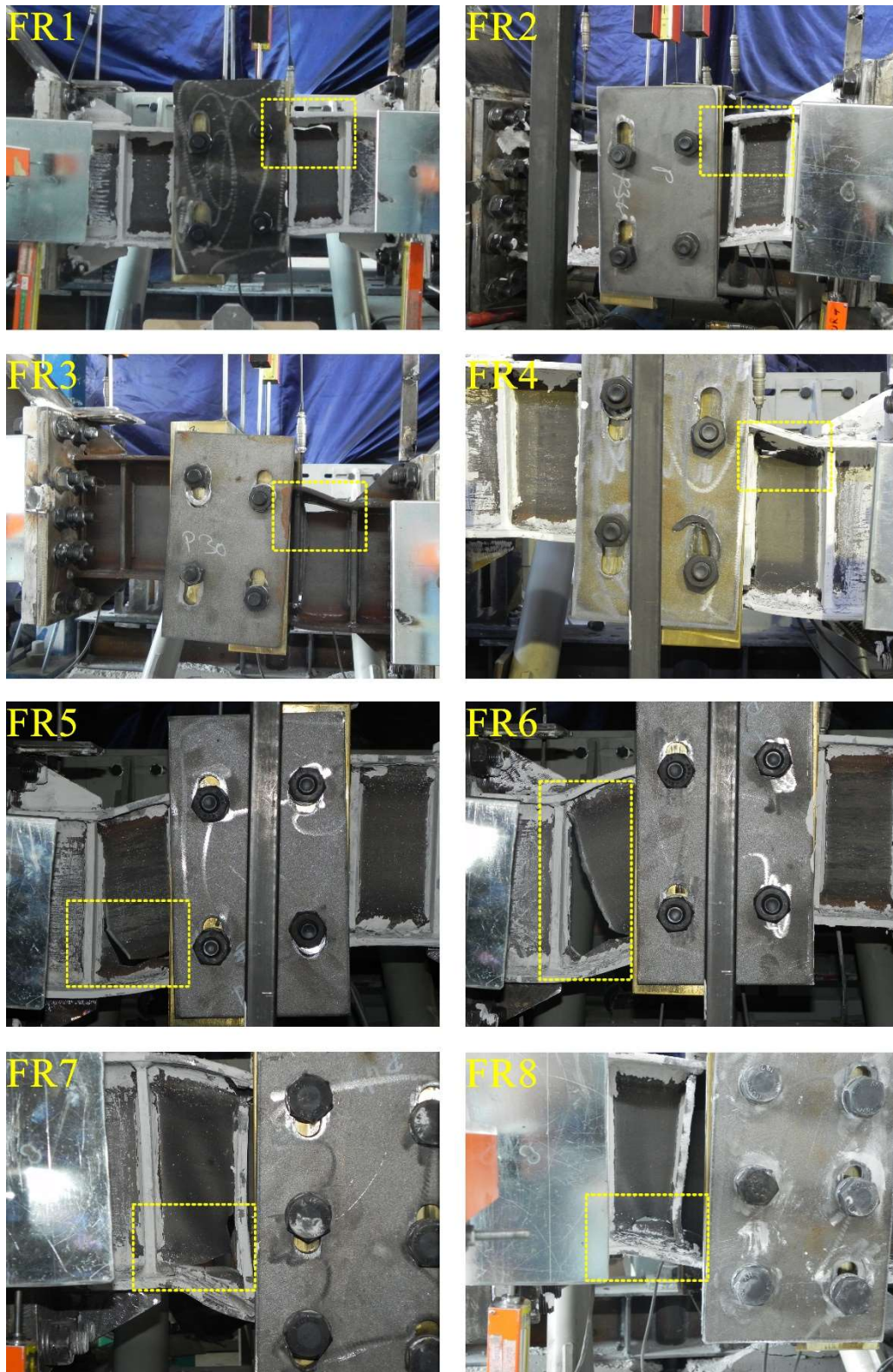


Figure 4.13. Failure modes of specimens

Table 4.6 Summary of experimental results of specimens FR1-FR8

Sp. #	V_p (kN)	V_{max} (kN)	Overstrength	γ (rad) @ N_f
FR1	346	533	1.54	AISC (0.15 rad) + 2.5@0.17rad
FR2	346	549	1.59	17@0.17rad
FR3	346	519	1.50	AISC (0.15 rad) + 9.5@0.17rad
FR4	346	528	1.53	43@0.17rad + 2@0.20rad + 4.5@0.23rad
FR5	346	542	1.57	8@0.17rad
FR6	346	561	1.62	5@0.17rad
FR7	346	541	1.56	12.5@0.17rad
FR8	346	564	1.63	5@0.17rad

Two types of wear were observed during the experiments. Abrasive and adhesive wear, which were reported for specimens FR2 and FR4 as shown in Figure 4.14. It is expected in abrasive wear that wear fragments are fractured and removed from faying surface which leads to a decrease in frictional surface resulting in a reduction in the friction resistance. On the other hand, some wear fragments may be removed from the faying surface; however, the majority of the wear fragments remain on the faying surface in adhesive wear. Adhesive wear is expected to occur in steel-brass surfaces while abrasive wear is expected to occur in steel-steel surfaces (Grigorian and Popov, 1994; Petty, 1999). It is seen from Figure 4.14 that voids formed on the side plates where the washers are clamped by the bolts on the side plates.

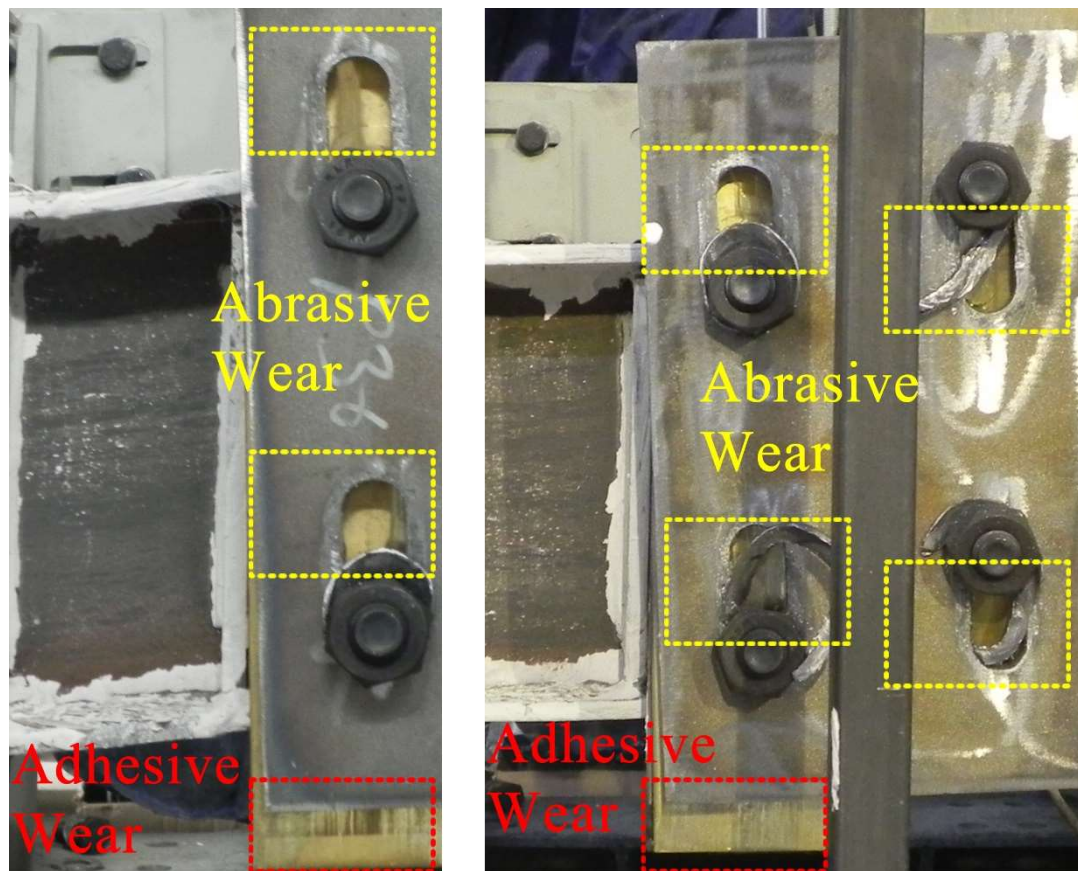


Figure 4.14. Abrasive and adhesive wear

Significant damages were observed on the washers during the experiments. Figure 4.15 shows the damage that occurred in the washers in Specimen FR3. The damages on the washer initiated with a slight bending of the washer. Then the washer deformed parallel to the direction of the slotted hole. With repeated cycles and friction forces, a part of the washer separated and fell down. Finally, after a few cycles the washer completely fell down. As the size of the slot increases, the damages occurred at the washer initiates in earlier cycles. Moreover, as the intensity of rotation increases, the damage development on the washer increases. The loss of washer leads to a significant reduction in pretension and friction forces that causes a significant reduction in energy dissipation.

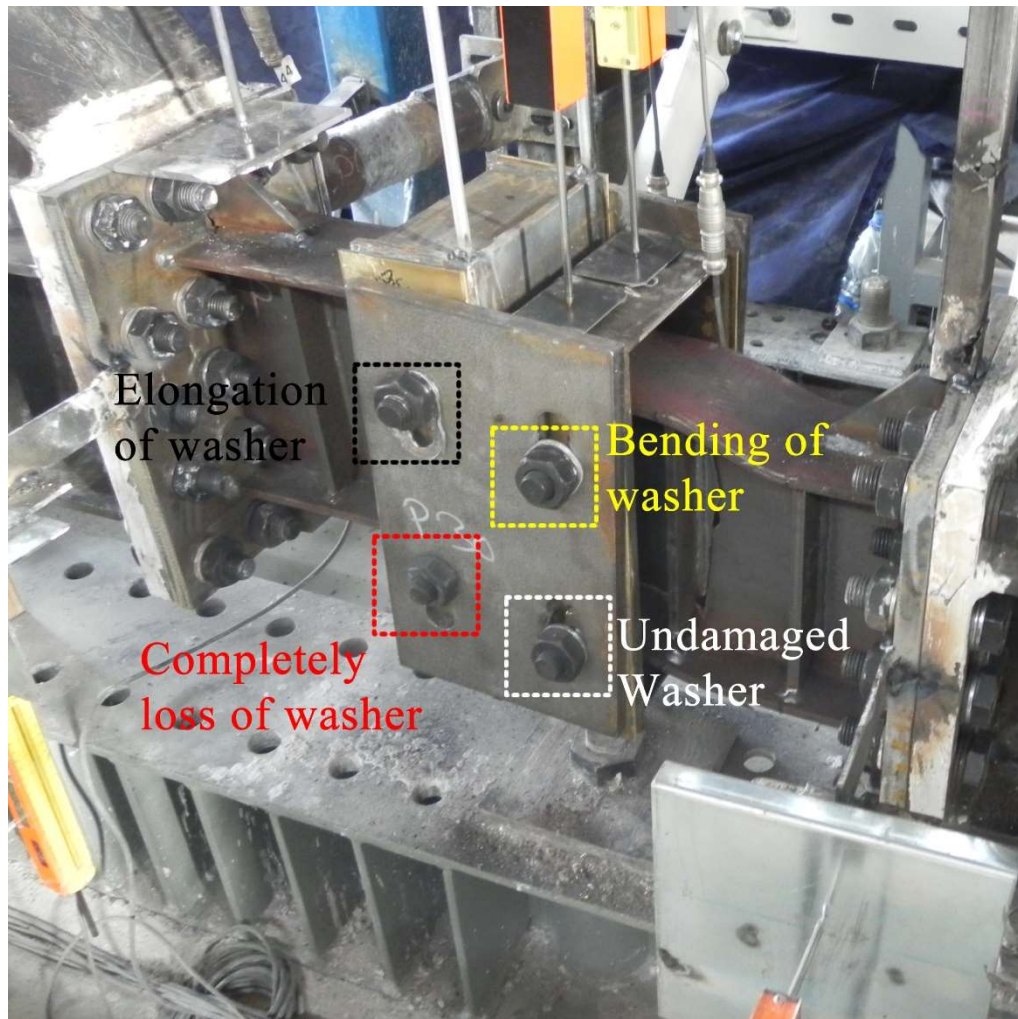


Figure 4.15. Damages on washers

Elongation of the bolt holes was observed at the saw cut I-section. Figure 4.16 demonstrates bolt hole elongation reported for Specimen FR2. The initial dimension of the bolt hole was measured as 25.6 mm. After the experiments, the bolt holes at the upper and lower part of the saw cut I-section were measured as 29.4 mm and 28.1 mm, respectively. This averagely 12% increase in the size of the bolt hole can correspond 0.005 rad rotation of the link.



Figure 4.16. Bolt hole elongation

During the experiments, the relative vertical movements between the pieces of the link were also recorded. The relative vertical movements for the specimens with 50 mm slot size given in Figures 4.17 indicate that the maximum relative movements are 34.5 mm and 41.73 for the specimens with single sided slotted holes while the maximum relative movements are 49.56 mm and 66.64 mm for the specimens with double slotted holes. On the other hand, The relative vertical movements for the specimens with 25 mm slot size given in Figure 4.18 indicate that the maximum relative movements are 34.3 mm and 24.0 for the specimens with single sided slotted holes while the maximum relative movements are 35.2 mm and 34.0 mm for the specimens with double slotted holes. The specimens dissipated energy via frictional surfaces through these relative movements. The effective link rotation experienced by the links were calculated to understand the maximum amount of rotation that the link experienced by yielding. Effective link rotation was obtained by extracting the rotation due to the relative movement from the total link rotation. The effective link rotation given in Figures 4.19 and 4.20 revealed that the links experienced a lower rotation compared to total link rotation angle. The effective link rotation for the specimen with the slot size of 50 mm depicted in Figures 4.19 indicated that the effective link rotations vary between 0.082 – 0.095 rad. It should be noted that these specimens were exposed to the maximum rotation of 0.17 rad (except specimen FR4) and the links were exposed to approximately half of the total rotation. On the other hand, the range of effective link rotations increased to 0.095 – 0.13 rad for the specimens with the slot size of 25 mm (Figure 4.20).

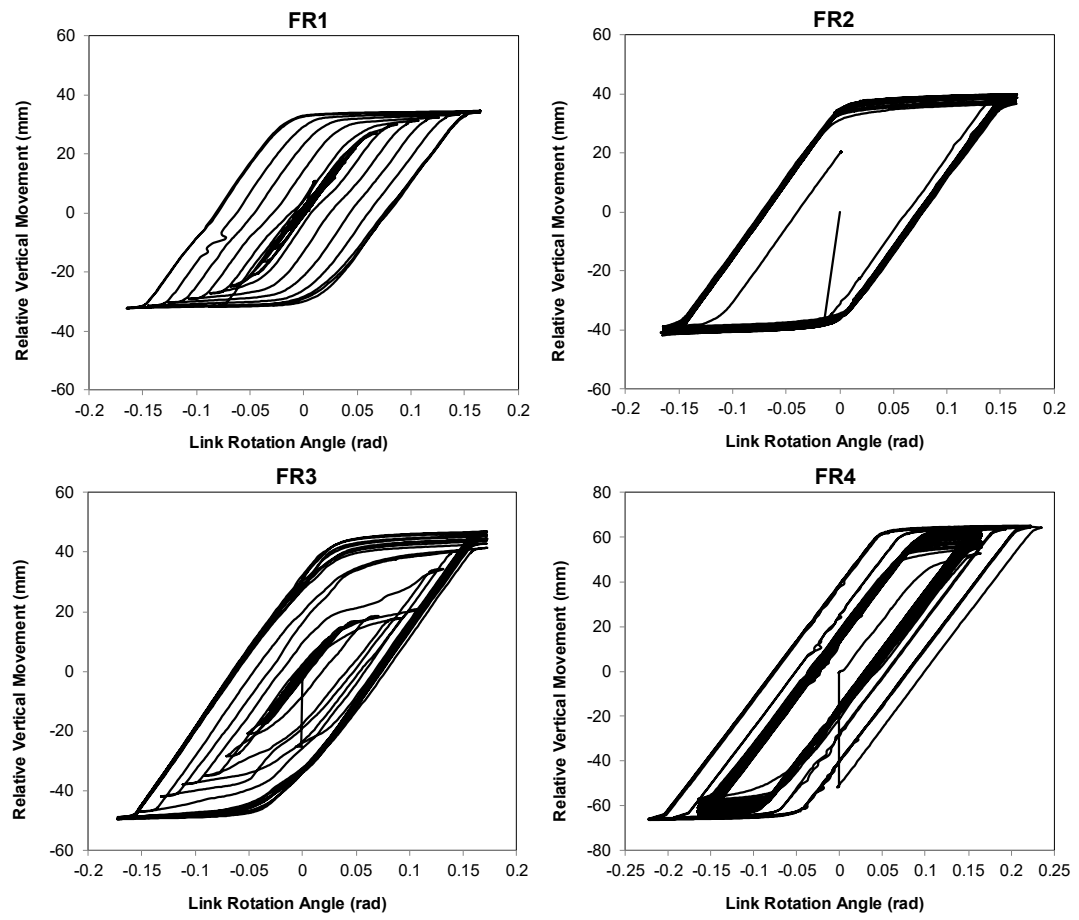


Figure 4.17. Relative vertical movement of specimens FR1-FR4

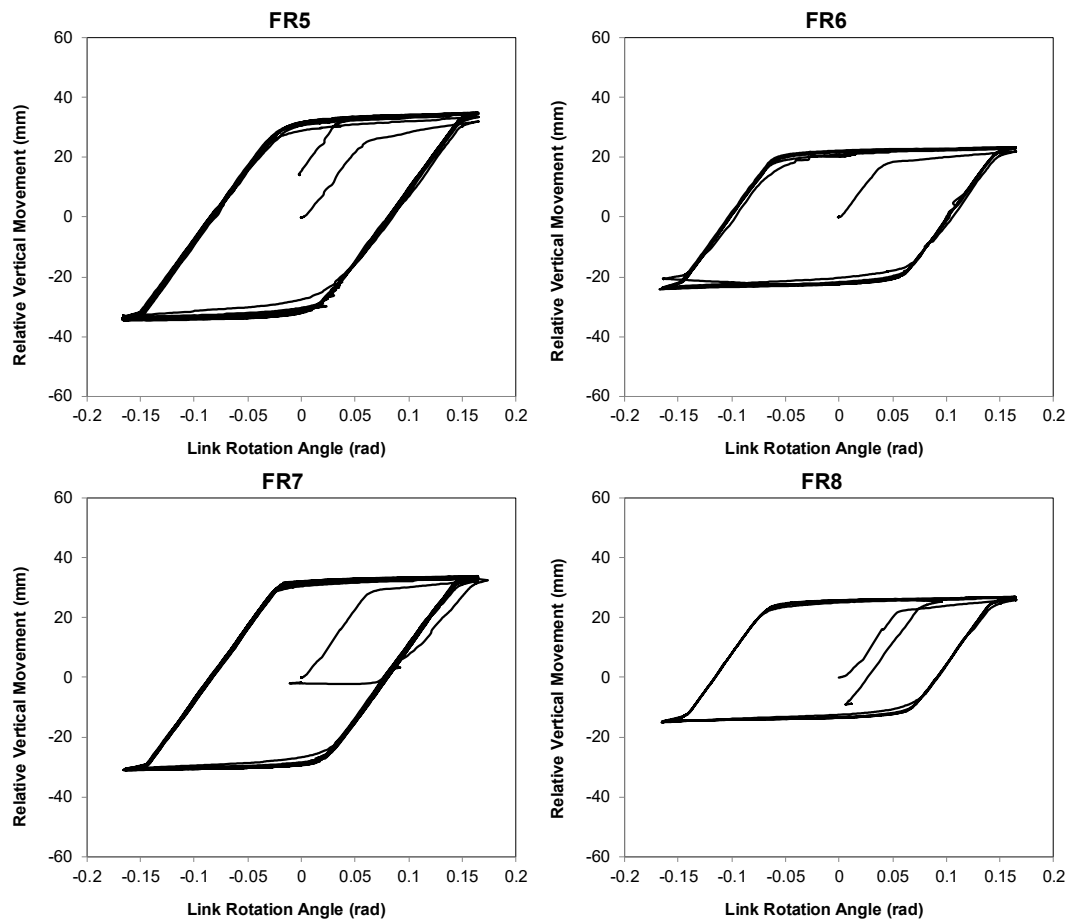


Figure 4.18. Relative vertical movement of specimens FR5-FR8

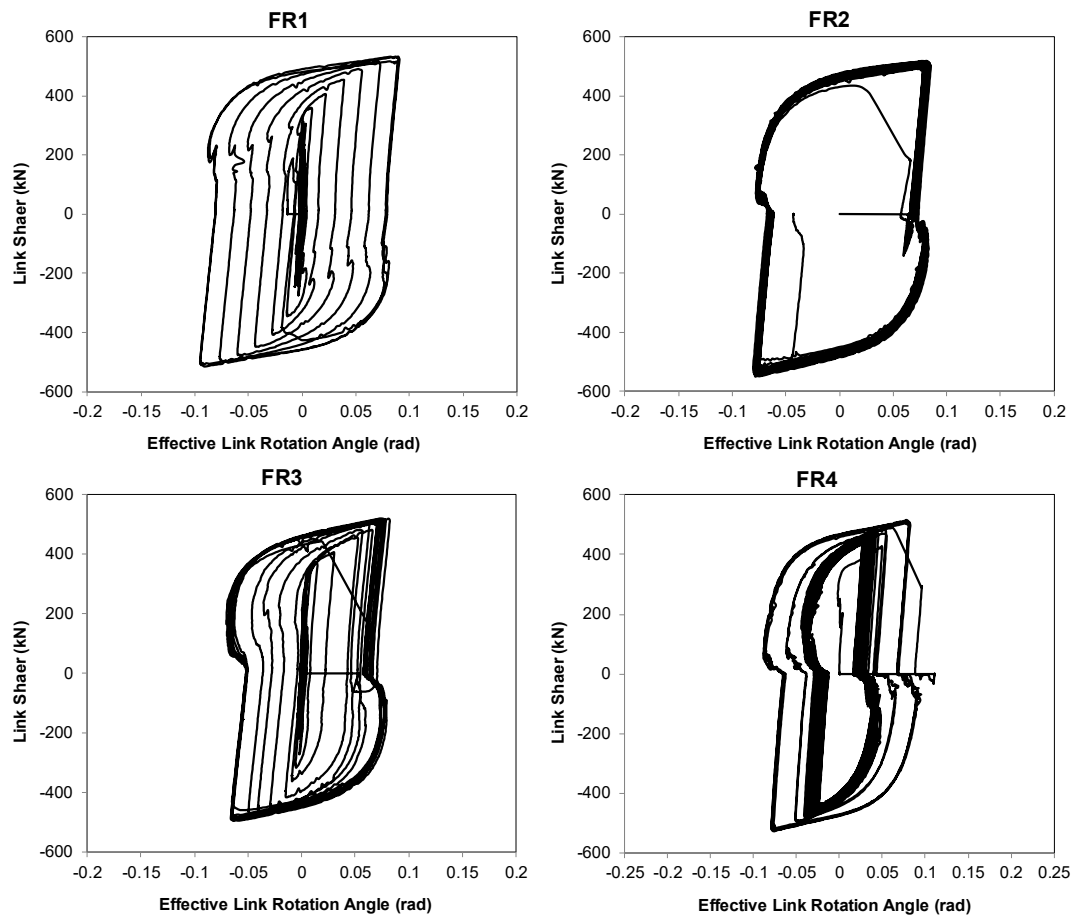


Figure 4.19. Link shear vs effective link rotation of specimens FR1-FR4

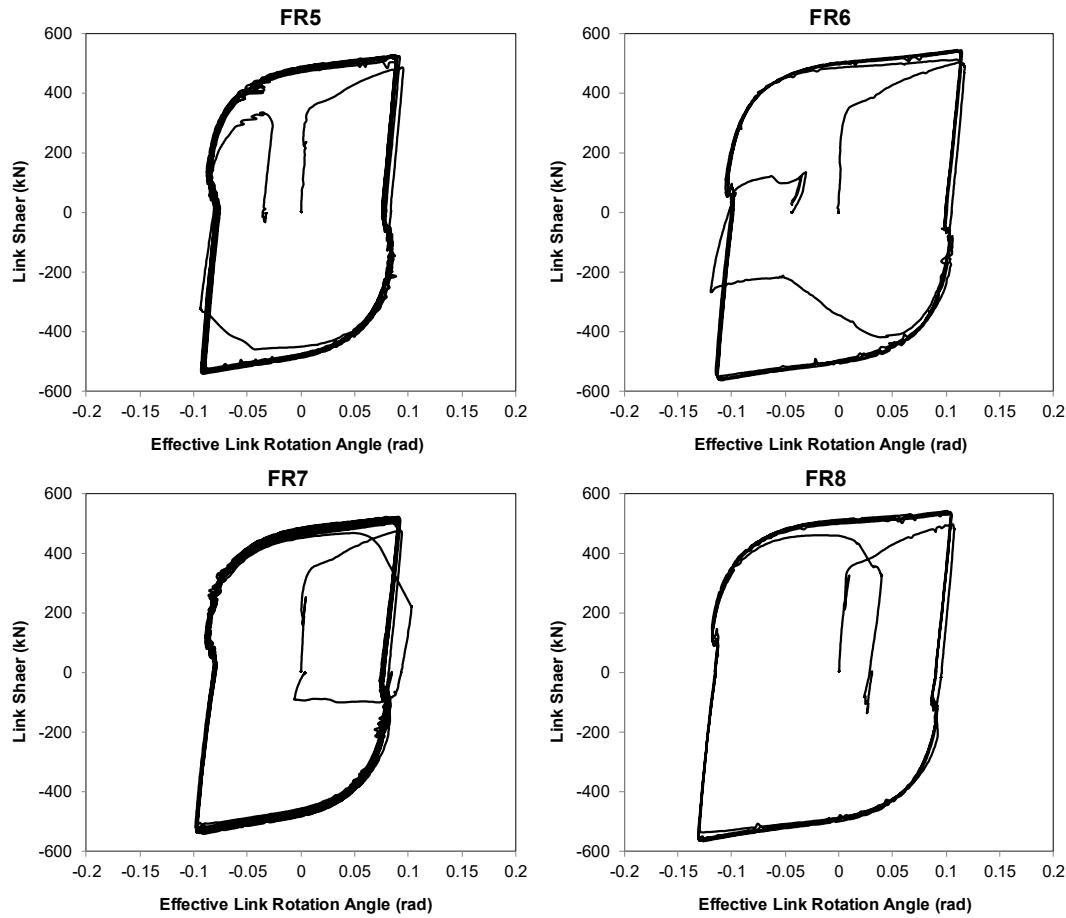


Figure 4.20. Link shear vs effective link rotation of specimens FR5-FR8

When the low-cycle fatigue life of the specimens is compared, it is clearly seen that the proposed frictional mid-spliced connection significantly extends the low-cycle fatigue life of the link. The replaceable link with extended end-plated connection barely sustained 2.5 cycles of 0.15 rad while the links with frictional mid-spliced connection endured between 5-17 cycles of 0.17 rad except that specimen FR4 completed 43 cycles of 0.17 rad, 2 cycles of 0.2 rad and 4.5 cycles of 0.23 rad. These results demonstrate that the proposed frictional mid-spliced connection increased the maximum rotation capacity as well as the number of cycles.

Table 4.7 demonstrates energy dissipated by the specimens. Total energy dissipation (TED) was calculated as the area under the whole hysteretic response. On the other hand, energy dissipated by link (EDL) was calculated as the area under the effective hysteretic response and energy dissipated by the friction (EDF) was computed by extracting EDL from TED. The ratios of EDL/TED vary between 61.75-87.33% for the specimens with 50 mm slot size while these ratios vary between 85.28-90.47% for the specimens with 25 mm slot size. The specimens with double slotted holes dissipated more energy via friction than the specimens with single slotted holes did. The main reason for the high ratio of EDL/TED is the loss of pretension caused by washer damage. The lowest EDL/TED ratios were observed at the specimens which were exposed to the AISC loading protocol. Since the severity of the AISC loading protocol up to 0.17 rad is significantly less than the constant amplitude of 0.17 rad, either washer damage was not observed or washer damage was observed at late cycles. On the other hand, the total energy dissipation can be enhanced by increasing the slot size. Specimen FR4 employing double sided slotted holes of 50 mm dissipated the highest total energy.

Table 4.7 Energy dissipated by specimens FR1-FR8

Sp. #	TED (kN-m)	EDL (kN-m)	EDF (kN-m)	EDL/TED (%)	EDF/TED (%)
FR1	657.02	405.73	251.29	61.75	38.25
FR2	1265.58	1105.24	160.35	87.33	12.67
FR3	1123.51	736.87	386.64	65.59	34.41
FR4	1328.305	946.19	382.12	71.23	28.77
FR5	740.18	631.23	108.95	85.28	14.72
FR6	506.12	457.87	48.25	90.47	9.53
FR7	1129.79	992.62	137.17	87.86	12.14
FR8	581.16	512.31	68.85	88.15	11.85

TED: Total energy dissipation; EDL: Energy dissipated by the link; EDF: Energy dissipated by the friction

The results of the specimen LCF3 which was subjected to a constant amplitude of 0.15 rad were compared with the specimens with the frictional mid-spliced connection. Total energy dissipation exhibited by specimens FR2, FR4-FR8 which were subjected to a constant amplitude of 0.17 rad (except FR4) was normalized with that of LCF3. Figure 4.21 indicates that the specimens with frictional mid-splice connection dissipated total energy 1.81-4.15 times higher than that of specimen LCF3. These results revealed that the proposed frictional mid-splice connection significantly enhances the energy dissipation of the link.

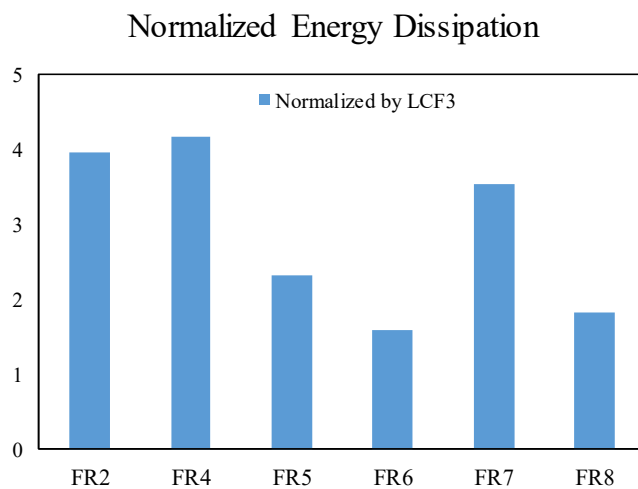
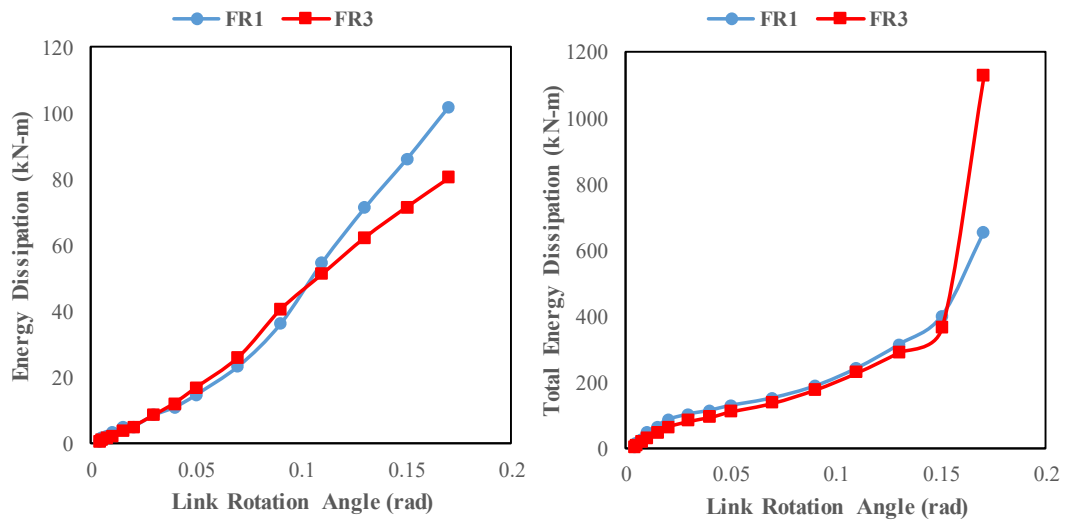


Figure 4.21. The comparison of normalized energy dissipation

Figure 4.22 demonstrates energy dissipated at each rotation cycle and cumulative energy dissipated for specimens FR1 and FR3. Both specimens completed the loading protocol of AISC up to 0.15 rad rotation. Later, specimen FR3 completed 9.5 cycles at 0.17 rad while specimen FR1 completed 3.5 cycles at 0.17 rad. Only difference is that specimen FR3 employed double sided slotted holes whereas specimen FR1 employed single sided slotted holes. According to the results, specimen FR1 dissipated less energy in earlier cycles than that of specimen FR3; however, this trend was reversed after 0.11 rad rotation. The reason is that washer damages were not observed in specimen FR1 up to failure. On the contrary, the

damage on washer started at 0.07 rad and partial separation of the washer was observed at 0.11 rad which leads to a decrease in the frictional forces. When total energy dissipation is examined, it is seen that up to 0.15 rad rotation both specimens dissipated almost similar total energy. However, specimen FR3 completed 6 more cycles of 0.17 rad rotation than that of Specimen FR1, which leads to 73% increase in total energy dissipation.



92.69 kN-m energy at each cycle while Specimen FR6 dissipated 101.76 kN-m energy at each cycle. Specimens FR7 and FR8 are also compared. These specimens employ 12 bolts and specimen FR7 employed double sided slotted holes of 25 mm whereas specimen FR8 employed single sided slotted holes of 25 mm. Specimens FR7 and FR8 dissipated a total of 1129.79 kN-m and 616.12 kN-m energy, respectively. Specimen FR5 dissipated 90.61 kN-m energy at each cycle while Specimen FR6 dissipated 122.67 kN-m energy at each cycle.

The results of specimen FR5-FR8 are compared in order to deeply understand the effects of the number of the bolts. Figure 4.23 demonstrates the comparison of energy dissipation of specimens FR5-FR8 having 25 mm slot size. The specimens with 12 bolts dissipated total energy 1.52 times higher than that of the specimens with eight bolts for the specimens with double slotted holes whereas the specimens with 12 bolts dissipated total energy 1.15 times higher than that of the specimens with eight bolts for the specimens with single slotted holes. These results indicate that the increase in the clamped area results in an increase in energy dissipation. Therefore, it can be recommended to use a high number of the bolts as long as the slip in faying surfaces is promoted. It can also be concluded that the specimens with double sided slotted holes dissipated total energy higher than that of the specimens with single sided slotted holes although energy dissipation at each cycle of 0.17 is higher in the latter.

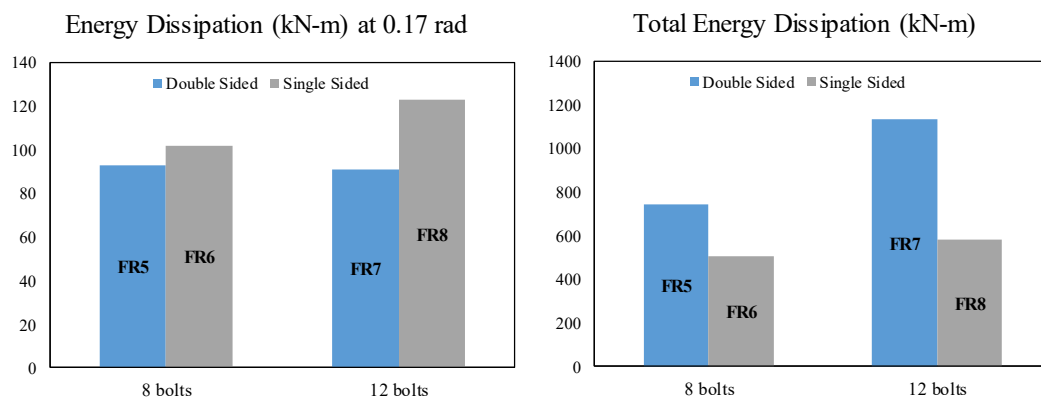


Figure 4.23. The comparison of energy dissipation of specimens FR5-FR8

Specimens FR2, FR4-FR6 are compared in order to investigate the effects of slot size. The comparison of energy dissipation of specimens FR2, FR4-FR6 is depicted in Figure 4.24. Although the specimens with 50 mm slot size dissipated less energy than that of the specimens with 25 mm slot size at 0.17 rad rotation, the total energy dissipation in the specimens with 50 mm slot size is significantly higher than that of the specimen with 25 mm slot size. Moreover, the specimens with double sided slotted holes dissipate total energy higher than that of the specimens with single sided slotted holes.

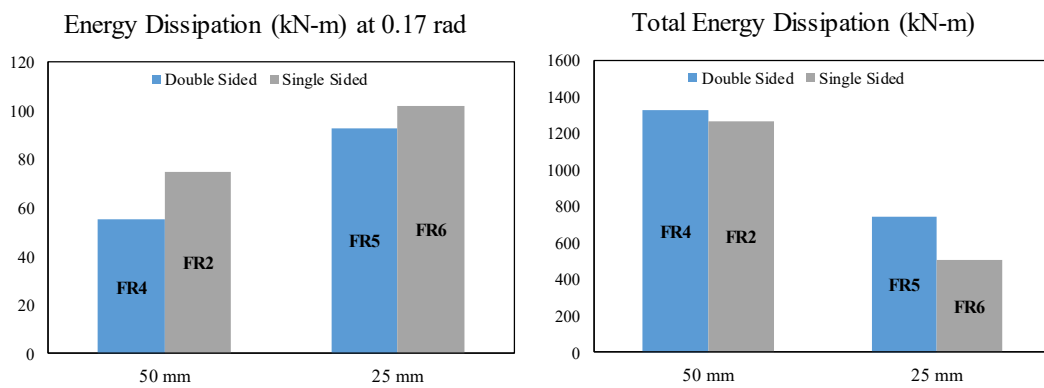


Figure 4.24. The comparison of energy dissipation of specimens FR2, FR4-FR6

The results of the specimens with different slot size, the number of bolts and the number of slots are compared in terms of low-cycle fatigue life and energy dissipation capacity. According to these results, the increase in the number of bolts leads to increases in both total energy dissipation and low-cycle fatigue life. Therefore, utilizing the highest number of bolts is recommended as long as the slip in faying surfaces is promoted. The same conclusion can be drawn for the slot size. As the slot size increases, low-cycle fatigue life and total energy dissipation of the link increase. Moreover, the specimens with double sided slots exhibited better performance than the specimens with single sided slots within the same size of slotted holes in terms of low-cycle fatigue life and total energy dissipation capacity. Therefore, selecting the largest slot size with double slotted holes is recommended.

The effective rotation expected from the link is recommended to be half of the maximum rotation as this is the limit for the experimented specimens.

CHAPTER 5

SUMMARY AND CONCLUSIONS

5.1 Summary

This thesis reports findings of a three-phase research program including experimental and numerical studies on replaceable links for eccentrically braced frames.

The first phase of research program investigated the performance of four-bolt extended unstiffened and stiffened end-plate connections used for replaceable shear links. To achieve this goal, a comprehensive experimental and numerical study has been undertaken. The current design guidelines and provisions were evaluated. Furthermore, a modification to AISC guidelines was recommended.

The second phase of research program developed a new mid-spliced end-plated detachable link which facilitates the replacement of the damaged links. The proposed link detail has been proven through an experimental and numerical study.

The third phase of research program developed a frictional mid-spliced replaceable link. In order to validate the proposed link detail, a comprehensive experimental study has been conducted.

5.2 Conclusions About Four-Bolt Extended End-Plate Connections for Replaceable Shear Links

End-plated connections for replaceable links were studied by making 10 nearly full-scale EBF tests. The width, thickness, and stiffening of the link were considered as the prime variables. The experimental study was complemented with

numerical analysis to investigate the strength of the end-plate as well as the bending strains. The following can be concluded from this study:

- The “thin” end-plate behavior can be adopted in the design of end-plates for replaceable shear links provided that the yielding of the end-plate is limited. Test results revealed that “thin” end plates are capable of showing satisfactory link rotation response.
- Finite element studies showed that the bending strains in the end-plates should be kept below $15\epsilon_y$ for satisfactory performance. The end-plate can fail through low-cycle fatigue in cases where the strains exceed this limit.
- The width of the end-plate has negligible influence on the strength when the width of the plate exceeds the flange width. Therefore, the width of the end-plate should be taken as the width of the flange plus 25.4 mm in calculations as recommended by the AISC Guideline DG16. European Provisions should be updated towards this end.
- The AISC Guidelines or the European Provisions can be used in the sizing of end-plates for replaceable shear links. Both the specifications provide conservative estimate of the end-plate capacity.
- The conservatism of design specifications is due to the use of longer lengths in yielding patterns than required. A set of modifications to the yield line mechanism parameter, Y , was proposed to more accurately determine the strength of end-plates.

The proposed expressions provide conservative estimates of the endplate strength for relatively thin (10 mm) end-plates. The study should be extended to reduce the conservatism in the proposed yield line mechanism parameter, Y . Cyclic strain hardening and the effect of washer and bolt head should be potential parameters to be considered. In addition, guidelines should be developed to distinguish between “thick” and “thin” end-plate behavior based on the proposed yield mechanisms. In the development process, the data from MRF and EBF tests should be considered.

5.3 Conclusions About Mid-Spliced End-Plated Replaceable Links

A replaceable link detail has been developed to enhance the performance of extended end-plated replaceable links. The proposed detail is based on splicing the link at mid-length and attaching the two pieces using a bolted connection between saw cut I-sections welded to the links and side plates. The proposed detail employs a gap between the webs of the saw cut I-sections that facilitates easy replacement. The bolted connection detail used to connect the two link pieces can be bearing type or slip-critical type. The proposed detail enables replacement of links under residual frame drift conditions. This can be accomplished by either using standard site drilled holes or slotted-holes drilled in the fabrication shop. The proposed link detail has been studied through proof-of-concept testing and numerical analysis. The following can be concluded based on the experimental and numerical investigations:

- The links studied as a part of the experimental program had rotation capacities that were significantly higher than the capacity required by AISC341. The experimental results validated the proposed replaceable link concept under different levels of residual frame drifts. The proposed design procedure for the mid-splice connections was validated with the experimental results as well.
- Bearing type and slip-critical type of mid-splice connections were found to provide adequate hysteretic response to replaceable links. A pinched hysteretic response was obtained when bearing type connections were used; however, the reduction in the energy dissipation was only 11% when compared with the slip-critical counterparts.
- The numerical modeling employing the finite element method has been validated with experimental results. The FE models were capable of simulating the global and local response of the specimens.
- The axial force produced in the mid-spliced links due to the restraining effects of the adjoining members was determined by a parametric numerical

study. An axial force equal to 10% of the axial yield force of the link (P_y) is recommended for a safe design.

- The webs of saw cut I-sections are subjected to significant bending effects due to the eccentricity of mid-splice connection. The distance (a) between the edge of the link flange and the outer face of the flange of saw cut I-section should be less than 75 mm to keep the principal strain less than $5 \times \epsilon_y$. The saw cut I-sections should be stiffened for eccentricities greater than 75 mm. Stiffeners can be placed in all designs regardless of the amount of eccentricity to safeguard against premature failure of saw-cut I-sections.
- Behavior of larger links was studied by calculating rupture index through numerical analysis. The results provided further validation of the proposed link detail.

The study concentrated on replaceable links without a concrete slab. Future research should concentrate on investigating the behavior of the proposed replaceable link concept when used with a composite slab.

5.4 Conclusions About Frictional Mid-Spliced End-Plated Replaceable Links

A comprehensive experimental study has been undertaken in order to enhance the low-cycle fatigue life of the replaceable links by friction dampers. A frictional mid-spliced connection has been developed for this purpose, where brass shims are placed between saw cut I-sections and side plates to promote stable friction behavior. The proposed connection employs a gap between saw cut I-sections which were connected with a bolted connection. The proposed connection is designed as bearing type and slotted holes are provided to side plates, which allow the slip in faying surfaces. Moreover, the proposed connection can be replaceable under residual drifts. The following conclusions can be drawn based on eleven specimens which were tested in the nearly full-scale frame under cyclic loading:

- The links with proposed connection details exhibited significantly higher rotation than the rotation capacity required by AISC 341.
- Low-cycle fatigue life of the link with the proposed connection was compared with that of the replaceable link with the extended end-plated connection. The results revealed that the proposed connection excessively extended the low-cycle fatigue life of the links.
- The proposed connection detail dissipated much higher energy than the replaceable link with the extended end-plated connection did.
- Utilizing the highest number of the bolts for mid-spliced connection is recommended to increase energy dissipation by friction.
- Double slotted holes are recommended to enhance both low-cycle fatigue life and total energy dissipation of the link.

Frictional energy dissipation of the proposed connection can be enhanced if the loss of pretension due to the washer is prevented. For further studies, the proposed connection can be improved by using spring or belleville washers.

REFERENCES

- ABAQUS 6.12-1 (2012) Documentation. Dassault Systèmes, Simulia, Providence, RI.
- AISC. (2016). Seismic Provisions for Structural Steel Buildings, ANSI/AISC 341-16. American Institute of Steel Construction, Chicago, IL.
- AISC. (2016b). Prequalified Connections for Special and Intermediate Steel Moment Frames for Seismic Applications, ANSI/AISC 358-16. American Institute of Steel Construction, Chicago, IL.
- American Institute of Steel Construction (AISC) (2010), Specification for Structural Steel Buildings, ANSI/AISC 360-16. Chicago.
- Ashikov A., Clifton G. C., and Belev B. (2017) “Experimental study on eccentrically braced frames with a new type of bolted replaceable active link,” in the 6th National Conference on earthquake engineering and the 2nd National Conference on earthquake engineering and seismology - 6CNIS & 2CNISS.
- Ashikov A., G. Clifton C., and Belev B. (2016) “Finite element analysis of eccentrically braced frames with a new type of bolted replaceable active link,” in New Zealand Society for Earthquake Engineering (NZSEE) Annual Technical Conference.
- Borgsmiller, J. (1995). Simplified method for design of moment end plate connections. M.S thesis, Virginia Polytechnic Institute and State University, Blacksburg, VA.
- Bozkurt M. B. and C. Topkaya (2017). “Replaceable links with direct brace attachments for eccentrically braced frames,” Earthquake Engineering and Structural Dynamics., vol. 46, pp. 2121–2139.

- Bozkurt M. B. and C. Topkaya (2018). "Replaceable links with gusseted brace joints for eccentrically braced frames," *Soil Dyn. Earthq. Eng.*, vol. 115, no. January, pp. 305–318.
- Bozkurt, M. B., Kazemzadeh Azad, S., & Topkaya, C. (2018). "Low-cycle fatigue testing of shear links and calibration of a damage law," *Journal of Structural Engineering*, 144(10), 04018189.
- Bozkurt M. B. (2017). "Developing replaceable members for steel lateral load resisting systems," Middle East Technical University.
- Bozkurt M. B., Kazemzadeh Azad S., and Topkaya C. (2019). "Development of detachable replaceable links for eccentrically braced frames," *Earthquake Engineering and Structural Dynamics*, vol. 48, no. 10.
- Brown, D., Iles, D., Brettle, M., Malik, A., & BCSA/SCI Connections Group. (2013). *Joints in Steel Construction: Moment-Resisting Joints to Eurocode 3 (P398)*.
- Bu, Y., Wang, Y., and Zhao, Y. (2019). "Study of stainless steel bolted extended end-plate joints under seismic loading." *Thin-Walled Structures*, 144(June), 106255.
- Clifton C., Bruneau M., MacRae G., Leon R., and Fussell A. (2011) "Steel structures damage from the Christchurch earthquake series of 2010 and 2011," *Bull. New Zeal. Soc. Earthq. Eng.*, vol. 44, no. 4, pp. 297–318.
- Clifton G. C., Nashid H., Ferguson G., Hodgson M., Seal C., and Macrae G. A. (2012). "Performance of Eccentrically Braced Framed Buildings In The Christchurch Earthquake Series of 2010 / 2011," *15 World Conf. Earthq. Eng.*, no. February.
- Della Corte, G., D'Aniello, M., & Landolfo, R. (2013). Analytical and numerical study of plastic overstrength of shear links. *Journal of Constructional Steel Research*, 82, 19-32.

- Dubina D., Stratan A., and Dinu F. (2011). "Re-centring capacity of dual-steel frames," *Steel Constr.*, vol. 4, no. 2, pp. 73–84.
- Dubina, D., Stratan, A., and Dinu, F. (2008). "Dual high-strength steel eccentrically braced frames with removable links." *Earthquake Engineering and Structural Dynamics*, 37(15), 1703-1720.
- Elkady, A. (2016), "Collapse risk assessment of steel moment resisting frames designed with deep wide-flange columns in seismic regions", Ph.D. dissertation, McGill University.
- ElSabbagh, A., Sharaf, T., Nagy, S., and ElGhandour, M. (2019). "Behavior of extended end-plate bolted connections subjected to monotonic and cyclic loads." *Engineering Structures*, 142–159.
- El-Tawil S., Vidarsson E., Mikesell T., and Kunnath S. K. (1999) "Inelastic Behavior And Design Of Steel Panel Zones," *Journal of Structural Engineering*, vol. 125, no. February, pp. 183–193.
- EN 10002. (2001). Tensile testing of metallic materials. Method of test at ambient temperature - EN 10002-1:2001. European Standard, Comité Européen de Normalisation, Brussels.
- Eurocode 3. (2005). Design of steel structures – Part 1-8: design of joints, EN 1993-1-8:2005. European Standard, Comité Européen de Normalisation, Brussels.
- Eurocode 8. (2004). Design of Structures for Earthquake Resistance - Part 1: General Rules, Seismic Actions and Rules for Buildings, EN 1998-1:2004. European Standard, Comité Européen de Normalisation, Brussels.
- Fujimoto, M., Aoyagi, T., Ukai, K., Wada, A., & Saito, K. (1972). Structural characteristics of eccentric k-braced frames. *Transactions AIJ*, (195).

- Gardiner S., Clifton G. C., and Macrae G. A. (2013). "Performance, Damage Assessment and Repair of a Multistorey Eccentrically Braced Framed Building Following the Christchurch Earthquake Series," no. February, pp. 1–16.
- Gardiner, G., Clifton, C., and MacRae, G. A. (2013). "Performance, damage assessment and repair of a multistorey eccentrically braced frame building following the Christchurch earthquake series." Proc., Steel Innovations Conference 2013, Christchurch, New Zealand.
- Ghobarah, A., Korol, R. M., Osman, A. (1992). "Cyclic behavior of extended end-plate joints." *Journal of Structural Engineering*, 118(5), 1333-1353.
- Grigorian, C. E., and Popov, E. P. (1994). "Energy dissipation with slotted bolted connections." Rep. No. UCB/EERC-94/02, Univ. of California, Berkeley, Calif.
- Ioan Chesoiu, A., Stratan, A., Dubina, D., Poljansek, M., Molina, F. J., Taucer, F., Pegon, P., Sabau, G. A. (2016). "Experimental validation of re-centring capability of eccentrically braced frames with removable links," *Engineering Structures*, vol. 113, pp. 335–346.
- Ji, X., Wang, Y., Ma, Q., and Okazaki, T. (2016). "Cyclic Behavior of Very Short Steel Shear Links." *Journal of Structural Engineering*, 142(2), 04015114.
- Kaufmann E.J., Metrovich B.R. and Pense A.W. (2001), "Characterization of cyclic inelastic strain behavior on properties of A572 Gr. 50 and A913 Gr. 50 rolled sections, ATLSS Report 01–13", National Center for Engineering Research on Advanced Technology for Large Structural Systems, Bethlehem.
- Kazemzadeh Azad, S., and Topkaya, C. (2017). "A review of research on steel eccentrically braced frames." *J. Constr. Steel Res.*, 128, 53-73.

- Krawinkler, H., Zohrei, M., Lashkari-Irvani, B., Cofie, N.G. and Hadidi-Tamjed, H. (1983). "Recommendations for experimental studies on the seismic behavior of steel components and materials, Report No. 61", The John A. Blume Earthquake Engineering Center, Stanford University, Stanford.
- Kennedy, N. A., Vinnakota, S., & Sherbourne, A. N. (1981). "The split-tee analogy in bolted splices and beam-column connections," *Joints in structural steelwork*, 2.
- Macrae G., Clifton G. C., Bruneau M., Kanvinde A., and Gardiner S. (2015). "Lessons from steel structures in Christchurch earthquakes," 8th Int. Conf. Behav. Steel Struct. Seism. Areas, July 1-3, no. February 2011, pp. 1474–1481.
- Manheim, D. N. (1983). *On the Design of Eccentrically Braced Frames*. University of California, Berkeley. Doctoral Thesis.
- Mansour N. (2010) "Eccentrically Braced Frames with Replaceable Shear Links," University of Toronto, Toronto, Ontario, Canada.
- Mansour N., Christopoulos C., and Tremblay R. (2011). "Experimental validation of replaceable shear links for eccentrically braced steel frames," *Journal of Structural Engineering*, vol. 137, no. 10, pp. 1141–1152.
- McCormick J., Aburano H., Ikenaga M., and Nakashima M. (2008) "Permissible Residual Deformation Levels for Building Structures Considering both Safety and Human Elements," 14th World Conf. Earthq. Eng., p. 8.
- Monir, H.S. and Zeynali K. (2013) "A modified friction damper for diagonal bracing of structures. " *Journal of Constructional Steel Research*, 87(0): p. 17-30.
- Morrison, M. L., Schweizer, D. Q., Quayyum, S., and Hassan, T. (2019). "An Unstiffened Eight-Bolt Extended End-Plate Moment Connection for Special and Intermediate Moment Frames." *Journal of Structural Engineering*, 145(7), 1–16.

- Murray, T. M., & Shoemaker, W. L. (2002). Steel Design Guide Series 16 Flush and extended multiple-row moment end-plate connections. American Institute of Steel Construction.
- Murray, T. M., & Sumner, E. A. (2003). Steel Design Guide Series 4 Extended end-plate moment connections seismic and wind applications. American Institute of Steel Construction.
- Özkılıç, Y. O. (2020) “A new replaceable fuse for moment resisting frames : Replaceable bolted reduced beam section connections,” Steel and Composite Structures, vol. 35, no. 3, pp. 353–370.
- Petty, G. D. (1999). “Evaluation of a friction component for a posttensioned steel connection.” MS thesis, Lehigh Univ., Bethlehem, Pa.
- Sabau, G. A., Poljansek, M., Taucer, F., Pegon, P., Molina, F. J., Tirelli, D., Viaccoz, B., Stratan, A., Ioan Chesoan, A. Dubina, D. (2014). Seismic engineering research infrastructures for European synergies: full-scale experimental validation of a dual eccentrically braced frame with removable links (DUAREM), Institute for the Protection and Security of the Citizen, Publications Office of the European Union, Luxembourg, Report EUR 27030
- Shi, G., Shi, Y., Wang, Y. (2007). “Behaviour of end-plate moment connections under earthquake loading.” Engineering Structures, 29, 703–716.
- Shi, Q., Yan, S., Wang, X., Sun, H., & Zhao, Y. (2020). “Seismic Behavior of the Removable Links in Eccentrically Braced Frames with Semirigid Connections. ” Advances in Civil Engineering.
- Song, Y., Uy, B., and Jia, W. (2019) “Numerical analysis of stainless steel-concrete composite beam-to-column joints with bolted flush endplates.” Steel Compos. Struct., vol. 33, no. 1, pp. 143–162.

- Srouji, R., Kukreti, A.R and Murray, T.M (1983). Yield-line analysis of end-plate connections with bolt force predictions. Research Report No. FSEL/MBMA 83-05, Fears Structural Engineering Laboratory, School of Civil Engineering and Environmental Science, University of Oklahoma, Norman, Oklahoma.
- Stephens, M. T., Dusicka, P., & Lewis, G. (2018). “End web stiffeners for connecting ductile replaceable links.” *Journal of Constructional Steel Research*, 150, 405-414.
- Stratan A. and Dubina D. (2004). “Bolted Links for Eccentrically Braced Steel Frames,” in *Proceedings of the 5th AISC/ECCS International Workshop: Connections in Steel Structures V. Behaviour, Strength and Design*, pp. 223–332.
- Stratan A., Dubina D., and Dinu F. (2003). “Control of global performance of seismic resistant EBF with removable link,” in *International speciality conference; 4th, Behaviour of steel structures in seismic areas* , pp. 455–462.
- Sumner, E. A., and Murray, T. M. (2002). “Behavior of extended end-plate moment connections subject to cyclic loading.” *Journal of Structural Engineering*, 128(4), 501–508.
- Tartaglia, R., D’Aniello, M., and Landolfo, R. (2018a). “The influence of rib stiffeners on the response of extended end-plate joints.” *Journal of Constructional Steel Research*, 148, 669–690.
- Tartaglia, R., D’Aniello, M., and Rassati, G. A. (2019). “Proposal of AISC-compliant seismic design criteria for ductile partially-restrained end-plate bolted joints.” *Journal of Constructional Steel Research*, 159, 364–383.
- Tartaglia, R., D’Aniello, M., Rassati, G. A., Swanson, J. A., and Landolfo, R. (2018b). “Full strength extended stiffened end-plate joints: AISC vs recent European design criteria.” *Engineering Structures*, 159, 155–171.

- Tremblay, R. (1993). Seismic behavior and design of friction concentrically braced frames for steel buildings, University of British Columbia.
- Tsai, K.-C., and Popov, E. P. (1990). "Cyclic behavior of end-plate moment connections." *Journal of Structural Engineering*, 116(11), 2917–2930.
- Yin, Z., Huang, Z., Zhang, H., & Feng, D. (2019). "Experimental Study on Energy Dissipation Performance and Failure Mode of Web-Connected Replaceable Energy Dissipation Link." *Applied Sciences*, 9(15), 3200.
- Zimbru, M., D'Aniello, M., Stratan, A., & Dubina, D. (2017). "Finite element modelling of detachable short links." *Proceedings of COMPDYN*.
- Zimbru, M., D'Aniello, M., Stratan, A., Landolfo, R., & Dubină, D. (2018). "Finite element analysis of composite replaceable short links. " In *Key Engineering Materials* (Vol. 763, pp. 576-583).

CURRICULUM VITAE

PERSONAL INFORMATION

Surname, Name: Özkılıç, Yasin Onuralp
Nationality: Turkish (TC)
Date and Place of Birth: 16 October 1990, Konya
Marital Status: Married
Phone: +90 506 263 98 08
email: yoozkilic@gmail.com

EDUCATION

Degree	Institution	Year of Graduation
MS	METU Civil Engineering	2014
BS	METU Civil Engineering	2016

WORK EXPERIENCE

Year	Place	Enrollment
2018-Present	Necmettin Erbakan University	Research Assistant
2014-2017	Middle East Technical University	Research Assistant
2014	Promer Engineering	Structural Designer

FOREIGN LANGUAGES

Advanced English

JOURNAL PUBLICATIONS

1. Özkılıç Y. O. (2020). A new replaceable fuse for moment resisting frames: Replaceable bolted reduced beam section connections. Steel and Composite Structures, 35(3), 353-370., Doi: 10.12989/scs.2020.35.3.353
2. Aksoylu C., Özkılıç Y. O., Arslan M. H. (2020). Damages on Prefabricated Concrete Dapped-End Purlins due to Snow Loads and a Novel Reinforcement Detail. Engineering Structures.
3. Aksoylu C., Yazman Ş., Özkılıç Y. O., Gemi L., Arslan M. H. (2020). Experimental analysis of reinforced concrete shear deficient beams with circular

web openings strengthened by CFRP composite. *Composite Structures*, 112561, Doi: <https://doi.org/10.1016/j.compstruct.2020.112561>

4. Madenci E., Özkılıç Y. O., Gemi L. (2020). Experimental and Theoretical Investigation on Flexure Performance of Pultruded GFRP Composite Beams with Damage Analyses. *Composite Structures*, 112162

5. Madenci E., Özkılıç Y. O., Gemi L. (2020). Buckling and Free Vibration Analyses of Pultruded GFRP Laminated Composites: Experimental, Numerical and Analytical Investigations. *Composite Structures*, 112806.

6. Gemi L., Aksoylu C., Yazman Ş., Özkılıç Y. O., Arslan M. H. (2019). Experimental investigation of shear capacity and damage analysis of thinned end prefabricated concrete purlins strengthened by CFRP composite. *Composite Structures*, 229, 111399, Doi: [10.1016/j.compstruct.2019.111399](https://doi.org/10.1016/j.compstruct.2019.111399)

7. Özkılıç Y. O., Bozkurt M. B., Topkaya, C. (2018). Evaluation of seismic response factors for BRBFs using FEMA P695 methodology. *Journal of Constructional Steel Research*, 151, 41-57., Doi: [10.1016/j.jcsr.2018.09.015](https://doi.org/10.1016/j.jcsr.2018.09.015)

8. Özkılıç Y. O., Madenci E., Gemi L. (2020). Tensile and compressive behaviors of the pultruded GRFP lamina. *Turkish Journal of Engineering*, 4(4), 169-175.

9. Gemi L., Madenci E., Özkılıç Y. O. (2020) Çelik, Cam FRP ve Hibrit Donatılı Betonarme Kirişlerin Eğilme Performansının İncelenmesi. *Düzce Üniversitesi Bilim ve Teknoloji Dergisi*, 8(2), 1470-1483.

10. Madenci E., Gemi L., Özkılıç Y. O. (2020) Theoretical Investigation on Static Analysis of Pultruded GFRP Composite Beams. *Academic Platform Journal of Engineering and Science*, 8(3), 483-489

RESEARCH PROJECTS

1. Investigation of Mechanical Behavior of Pultruded Glass Fiber Reinforced Composite Profiles Under Seismic, Elevated Temperature and Service Loads, Funded by Necmettin Erbakan University, Project Number: 201219004, 2020-..., Project Budget: 65000 TL

2. Replaceable Reduced Beam Sections in Moment Resisting Frames, Funded by Necmettin Erbakan University, Project Number: 181219006, 2018-..., Project Budget: 30000 TL

3. The Investigation of the Replaceable Links with End-plated Connections for Eccentrically Braced Frames, Funded by Middle East Technical University, Project Number: GAP-303-2018-2858, 2018, Project Budget: 10000 TL

4. The Investigation of the Behavior of Eccentrically Braced Frames under Low-cycle Fatigue, Funded by Middle East Technical University, Project Number: BAP- 03-03-2017-004, 2017, Project Budget: 10500 TL

PROCEEDINGS

1. Özkılıç Y. O., Aksoylu C., Arslan M. H. (2019). Farklı Açılı Yerleştirilen Kesme Donatısının Kiriş Davranışı Üzerine Etkisinin Numerik Olarak Araştırılması. 2nd International Conference on Technology and Science (Energy - Environment -Economics), Techno-Science.
2. Özkılıç Y. O., Aksoylu C., Arslan M. H. (2019). Kesme Donatısı Yetersiz Betonarme Kirişler İçin Farklı Kesme Donatısı Yerleşiminin Numerik Olarak İncelenmesi. 2nd International Conference on Technology and Science (Energy - Environment -Economics), Techno-Science, 2, 1029-1034.
3. Aksoylu C., Özkılıç Y. O., Arslan M. H. (2019). Farklı Kesme Açıklığına Sahip Basit Mesnetli Betonarme Kirişlerin Davranışlarını İncelemek Üzere Numerik Çalışma. 2nd International Conference on Technology and Science (Energy - Environment -Economics), Techno-Science, 2, 699-704.
4. Özkılıç Y. O. (2019). The Effects of Stiffener Configurations on Long Link in Eccentrically Braced Frames. 8th International Steel Structures Symposium
5. Özkılıç Y. O. (2019). Numerical Study of Replaceable Reduced Beam Section with Beam Splice Connection. 8th International Steel Structures Symposium
6. Madenci E., Gemi L., Özkılıç Y. O. (2019). An Investigation on Flexure Behavior of Pultruded Glass Fiber Reinforced Polymer Composite Beams. International Symposium on Innovations in Civil Engineering and Technology (Iciviltch 2019)
7. Madenci E., Özkılıç Y. O., Gemi L. (2019). The Effects of Length to Depth Ratio on the Reinforced Concrete Pultruded GFRP Beams. International Symposium on Innovations in Civil Engineering and Technology (Iciviltch 2019)
8. Gemi L., Madenci E., Özkılıç Y. O. (2019). Investigation of Reinforced Concrete-Filled Pultruded Beams Strengthened by GFRP Composite. The International Aluminium-Themed Engineering and Natural Sciences Conference
9. Gemi L., Özkılıç Y. O., Madenci E. (2019). An Experimental Investigation on Buckling Behavior of the Pultruded GFRP Beam. The International Aluminium-Themed Engineering and Natural Sciences Conference
10. Aksoylu C., Özkılıç Y. O., Yazman Ş., Gemi L., Arslan M. H. (2019). The Effects of the Number of CFRP Layers in the Prefabricated Purlins. The International Aluminium-Themed Engineering and Natural Sciences Conference in Seydişehir/Turkey (Iatens'19), 285-290.
11. Özkılıç Y. O., Aksoylu C., Yazman Ş., Gemi L., Arslan M. H. (2019). The Effects of Ply Orientation on Prestressed Prefabricated Purlins Strengthened by CFRP. The International Aluminium-Themed Engineering and Natural Sciences Conference in Seydişehir/Turkey (Iatens'19), 279-284.

12. Gemi L., Madenci E., Özkılıç Y. O. (2019). An Investigation on Effect of Steel/Glass Fiber Bars in Concrete Beams. VI. International Earthquake Symposium
13. Gemi L., Özkılıç Y. O., Madenci E. (2019). Reinforced Concrete-Filled Glass Fiber Reinforced Polymer Pultruded Beams Strengthened by Fiber Reinforced Polymer. VI. International Earthquake Symposium
14. Gemi L., Özkılıç Y. O., Madenci E. (2019). Investigation Of Flexural Behavior of FRP Wrapped And Concrete Filled GFRP Box Profile Beams. VI. International Earthquake Symposium
15. Özkılıç Y. O., Madenci E., Gemi L. (2019). Performance of Pultruded Glass Fiber Reinforced Polymer Composite Beams under Quasistatic Load. 5th International Conference on Engineering Sciences: Proceedings of the ICES2019
16. Özkılıç Y. O., Gemi L., Madenci E. (2019). Hybrid Reinforced Concrete Filled Pultruded GFRP Beams Strengthened by GFRP Composites. 5th International Conference on Engineering Sciences: Proceedings of the ICES2019
17. Arslan Musa Hakan, Aksoylu C., Gemi L., Yazman Ş., Özkılıç Y. O. (2019). Effect of Circular Holes in Shear Region on the Behavior of CFRP Strengthened RC Beams. 4th Eurasian Conference on Civil and Environmental Engineering (ECOCEE), 860-865.
18. Aksoylu C., Özkılıç Y. O., Yazman Ş., Gemi L., Arslan M. H. (2019). The Numerical Study of the Effects of Steel Reinforcement Ratio to Behavior of Prefabricated Purlins. 2th International Congress on Engineering and Architecture, 1761-1767.
19. Yazman Ş., Aksoylu C., Özkılıç Y. O., Gemi L., Arslan M. H. (2019). Experimental and Numerical Investigation of Prefabricated Thinned Ended Purlins with and without CFRP Composites. 2th International Congress on Engineering and Architecture, 577-581.
20. Özkılıç Y. O., Aksoylu C., Yazman Ş., Gemi L., Arslan M. H. (2019). The Effects of Material Properties and Pretension to Behavior of Prefabricated Purlins. 2th International Congress on Engineering and Architecture, 1756-1760.
21. Aksoylu C., Yazman Ş., Özkılıç Y. O., Gemi L., Arslan M. H. (2019). İnceltilmiş Uçlu Betonarme Prefabrik Aşıkların Kesme Kapasitelerinin CFRP Uygulaması ile Artırılması. International Science and Academic Congress, 285-291.
22. Özkılıç Y. O., Aksoylu C., Yazman Ş., Gemi L., Arslan M. H. (2019). Prefabriğe İnceltilmiş Aşık Uçlarının Deneysel ve Numerik Sonlu Eleman Analizlerinin Karşılaştırılması. International Science and Academic Congress, 299-307.

23. Yazman Ş., Aksoylu C., Özkılıç Y. O., Gemi L., Arslan M. H. (2019). Sanayi Yapılarında Kullanılan Betonarme Prefabrike Öngerilmeli Aşıkların Kesme ve Eğilme Kapasitelerini Artırmaya Yönelik CFRP Uygulaması. International Science and Academic Congress, 292-298.
24. Özkılıç Y. O. and Köroğlu M. A. (2018). Finite Element Parametric Study of Drilled Flange Reduced Beam Section. International Eurasian Conference on Science, Engineering and Technology
25. Özkılıç Y. O. and Köroğlu M. A. (2018). Using Trapezoidal Web for Link Element. International Eurasian Conference on Science, Engineering and Technology
26. Özkılıç Y. O. (2018). Replaceable Link-to-Column Bolted End-Plate Connections for EBFs. International Congress on Engineering and Architecture
27. Özkılıç Y. O. (2018). The Effects of Stiffener Configurations on Short Links. International Congress on Engineering and Architecture
28. Özkılıç Y. O. and Köroğlu M. A. (2018). Finite Element Analysis of Steel Beams with Corrugated Webs under Bending Moment. International Congress on Engineering and Architecture
29. Özkılıç Y. O. and Köroğlu M. A. (2018). Finite Element Analysis of Reduced Beam Sections. International Congress on Engineering and Architecture
30. Özkılıç Y. O. (2018). Link with Sinusoidal Web in Eccentrically Braced Frames. International Congress on Engineering and Architecture
31. Özkılıç Y. O. and Köroğlu M. A. (2018). Effect of Sea Water on Mechanical Properties of Concrete with Recycled Waste Rubber Steel Wires. International Congress on Engineering and Architecture
32. Bozkurt M. B., Özkılıç Y. O., Topkaya C. (2018). Effect of Different Bracing Configuration On Global Response Of Buckling Restrained Braced Frames. 13th International Congress on Advances in Civil Engineering
33. Bozkurt M. B., Özkılıç Y. O., Topkaya C. (2018). Investigation on Connection Details for Welded Overlap Core Steel Encased Buckling Restrained Braces. 13th International Congress on Advances in Civil Engineering
34. Bozkurt M. B., Özkılıç Y. O., Topkaya C. (2017). Evaluation of Seismic Performance Factors for Chevron Buckling Restrained Braced Frames. 4th International Conference on Earthquake Engineering and Seismology
35. Bozkurt M. B., Özkılıç Y. O., Topkaya C. (2017). Evaluation of Seismic Performance Factors for Chevron Buckling Restrained Braced Frames. 4th International Conference on Earthquake Engineering and Seismology

36. Bozkurt M. B., Özkılıç Y. O., Topkaya C. (2017). Effects of Different Core Plate Properties on Global Response Of Buckling Restrained Braced Frames. 9th Hellenic National Conference of Steel Structures, Larisa, Greece
37. Bozkurt M. B., Özkılıç Y. O., Topkaya C. (2017). Determination of Displacement Amplification Factors for Chevron BRBFs. 9th Hellenic National Conference of Steel Structures, Larisa, Greece
38. Bozkurt M. B., Özkılıç Y. O., Topkaya C. (2017). Determination of Displacement Amplification Factors for Chevron BRBFs. 9th Hellenic Conference of Steel Structures
39. Bozkurt M. B., Özkılıç Y. O., Topkaya C. (2017). Effects of Different Core Plate Properties on Global Response of BRBFs. 9th Hellenic Conference on Steel Structures
40. Bozkurt M. B., Özkılıç Y. O., Topkaya C. (2016). Evaluation of Displacement Amplification Factors for Steel Buckling Restrained Braced Frames. 8th International Conference on Steel and Aluminium Structures
41. Bozkurt M. B., Özkılıç Y. O., Topkaya C. (2016). Response of Buckling Restrained Braced Frames with Different Yield Strength and Yielding Length. 12th International Congress on Advances in Civil Engineering